Analytical and Computational Studies on Liquid Behaviour in a Zero Gravity Environment

Wei Yan

A Thesis

in

The Department

of

Mechanical Engineering

Presented in Partial Fulfillment of the Requirements

for the Degree of Master of Applied Science at

Concordia University

Montreal, Quebec, Canada

September 1991

ISBN 0-315-80981 7

ABSTRACT

Analytical and Computational Studies on Liquid Behaviour in a Zero Gravity Environment

Wei Yan

Analytical and numerical investigations regarding the behaviour of a mechanical system that is comprised by a liquid-vapor-solid vessel in a zero gravity environment are presented.

The analytical results focus on the static states assumed by the system when all the body and frame forces, except the surface tension forces, are removed. It is shown that the stationary state of the system with the smallest vapor-liquid interface is also the state of absolute minimum of the global potential energy. A new variable, the critical depth, that demarcates the transition from one static state to another with different characteristics, along with the interface configuration ratio, are used to describe the phenomenon.

The dynamic effects are analyzed through the solutions of continuity, momenta and the free-surface kinematic equations, and the Laplace-Young and Dupré-Young conditions. Simulations show the dynamic response of the system during transitions from one to zero gravity static states under the

influence of various physical and geometric conditions. As expected, the results demonstrate that the nulled gravity stationary state is approached asymptotically as the dynamic effects diminish due to the action of the viscous dissipation. The interface formation time is shown to increase with the Reynolds number and the contact angle. Finally, transitions from one stationary state to another where the global potential energy attains its absolute minimum value are confirmed numerically.

DEDICATION

To my parents, Xu Shi Yan and Liu Qin Zhuang;

and to my wife, Xiu Tao Zhang.

ACKNOWLEDGEMENTS

My sincerest gratitude goes out to my thesis advisors, Dr.G.H.Vatistas and Dr.T.S.Sankar for their help, guidance and encouragement. A special debt of thanks is owed to Mr.V. Kozel for his assistance in the numerical part.

I wish to thank the Concordia University for the Graduate Fellowship and the International Student Tuition Fee Remission. I also wish to thank the Canadian and Quebec governments for the financial support through NSERC and FCAR grants to Drs. T.S.Sankar and G.H.Vatistas respectively.

The thesis could not have been created without all of the encouragement and support from my family and friends. I would like to thank my wife, Xiu Tao Zhang, for her unwavering support, patience and understanding.

TABLE OF CONTENTS

LIST OF FIGURES

NOMENCLATURE

A	liquid-vapor interface surface area
D	divergence
f	function of the fractional volume of fluid
f_n	function symbol
F	force
g	the universal constant of the terrestrial gravity
A_x	body acceleration at x-direction
A_y	body acceleration at y-direction
E	potential energy
E_i	potential energy in configurations i, i = a or b
H	height of a tank
H_c	liquid depth which is the interface height from the bottom of a tank at the central line under 0-g gravity
$H_{c,max}$	maximum liquid depth at the central line under 0-g gravity
H_L	liquid distance between higher plane along walls and the bottom of a tank under 0-g gravity
H_o	liquid height at the central line under 1-g gravity
ΔH	liquid distance between lower plane and higher plane
L	half width or radius of a tank
p	pressure
P_n	pressure inside the fluid
P_s	surface pressure
r	radial coordinate

R	radius of curvature of a spherical surface
Re	Reynolds number
sgn	sign of velocity component
S_{ls}	area of liquid-solid
S_{vl}	area of vapor-liquid
S_{vs}	area of vapor-solid
t	time
t_o	characteristic time
$t_{0.5}$	time required for the liquid-vapor interface oscillations to decay to 0.5% of their original amplitude
Δt	time increment
u	velocity component in x-direction or r-direction
V	liquid volume
v	velocity component in y-direction or z-direction
x	coordinate in the horizontal direction
X(y)	interface function
X_c	liquid wetting length on a side wall of a cylindrical tank
X_r	liquid wetting length on a side of a rectangular tank wall
Δx	cell width
y	coordinate in the vertical direction
Y(x)	interface function
y(x)	liquid-vapor interface curve function of x
Δy	cell height
z	axial coordinate

Greek Letters

α	contact angle
β	angle
γ	liquid critical depth
γ_c	liquid critical depth in a cylindrical tank
γ_r	liquid critical depth in a rectangular tank
δ	distance of the vertex at the central line at 0-g from the original level at 1-g
δ_{rect}	dimensionless distance of the vertex at the central line under 0-g from the original level in a rectangular tank
δ_{cyl}	dimensionless distance of the vertex at the central line under 0-g from the original level in a cylindrical tank
ε	coordinate index, $\varepsilon = 0$ or 1 for Cartesian or cylindrical coordinate, respectively
ζ	distance parameter
η	ratio of distance between the cell centers and the distance between the free surface and the center of the interpolation cell
θ	interface configuration ratio
θ_{ci}	interface configuration ratio of configuration system i in a cylindrical tank, i = 3 and 4
$\theta_{ci,max}$	maximum interface configuration ratio of configuration system i in a cylindrical tank, i = 3 and 4
$\theta_{ci,min}$	minimum interface configuration ratio of configuration system i in a cylindrical tank, i = 3 and 4
θ_{ri}	interface configuration ratio of configuration system i in a rectangular tank, i = 1, 2, 5 and 6

$\theta_{ri,max}$	maximum interface configuration ratio of configuration system i in a rectangular tank, i = 1, 2, 5 and 6
$\theta_{ri,min}$	minimum interface configuration ratio of configuration system i in a rectangular tank, i = 1, 2, 5 and 6
$\Delta\theta_a$	difference between minimum interface configuration ratios of system 1 and 2
$\Delta\theta_b$	difference between maximum interface configuration ratio of system 1 and minimum interface configuration ratio of system 2
ν	kinematic viscosity
ξ	distance parameter
Π	force potential
π_i	dimensionless parameter, i=1, 2 and 3
ρ	density of liquid
ρ_c	density of other material, such as vapor
σ	surface tension
σ_{vs}	surface tension at vapor-solid interface
σ_{ls}	surface tension at liquid-solid interface
σ_{vl}	surface tension at vapor-liquid interface
τ	interface formation time, equal to $t_{0.5}/t_o$
Ψ	upstream differencing parameter
ω	over-relaxation factor

Superscripts

-	dimensionless
n+1	a quantity evaluated at time $(n+1)\Delta t$

Subscripts

i	number of cell in x-direction
j	number of cell in y-direction

CHAPTER 1

INTRODUCTION

1.1 General

The study of liquids in near zero gravity environment has been strongly motivated by the recent activities in space technology. The increasing sophistication of space vehicles and their missions, has brought forth serious attention to the problems associated with the behavior of fluids under reduced gravitational conditions.

Microgravity science deals with phenomena taking place under the influence of exceedingly low gravitational acceleration. These conditions can be produced in an aircraft flying through a parabolic trajectory, in drop towers, in sounding rockets and in spacecrafts during planetary orbit or in transit to other planets. The deployment of the space shuttle and the agreement to build the International Space Station, Freedom (ISSF), which will be inhabited permanently by humans, has intensified research activities in the field of microgravity science and technology. Beginning in 1996, the ISSF is to be built up by carrying components of the space station into orbit by space shuttles (Canadian Press, 1991).

In Canada, one of the international partners in ISSF, microgravity related research projects have been financially supported by the Canadian

Space Agency since 1984. Many of them have been experiments in drop towers, some of them have been performed using aircrafts such as the KC-135 and others are being prepared for the early 1990's available through the NASA Space Shuttle programme. The experimental capabilities and scope will be significantly advanced with the launching of the ISSF where longer test durations become available.

Problems related with liquids stored in space vehicle tanks under zero-gravity environment are currently under investigation. The present work is devoted to liquid behavior under static and dynamic conditions. The analysis is carried out using analytical and computational methods.

1.2 The Problem

A liquid and a vapor contained in a solid vessel are in contact with each other and are separated by an interface that behaves as though it consists of two homogeneous fluids separated by a uniformly stretched membrane of infinitesimal thickness (Young, 1805). The surface tension of a liquid is defined as the surface potential energy per unit area of surface. A fluid particle located near the surface of a liquid is subjected to a resultant force directed back into the liquid. A particle at the surface can thus be considered as having potential energy greater than that of a particle inside the liquid. The value of the potential energy is equal to the work that has been expended against the resultant force in bringing the molecule from the interior to the surface. The surface potential energy is proportional to its surface area. Surface tension strives to make the surface as small as possible. Thus the surface tends to

form a shape of minimum area, which therefore has minimum potential energy, the condition for stable equilibrium. For example, a drop of liquid tends to become spherical, since a sphere has minimum surface area for a given volume.

A schematic diagram illustrating how these surface tension forces act at the solid-liquid-vapor interfaces in a capillary dominated environment is presented in Figs.1.2.1 and 1.2.2. The free surface energies at the solid-liquid-vapor interfaces may be visualized in the forms of the surface tension forces acting in the direction of the surface, denoted by σ. The contact angle is the angle between the tangential planes to the solid-liquid and liquid-vapor interfaces at the line of contact with the solid. A wetting liquid is the one with the contact angles lying between 0^o and 90^o, as shown in Fig.1.2.1. An example of this is water in contact with glass. Moreover, most propellants to be considered are wetting liquids. Non-wetting liquids form contact angles between 90^o and 180^o, as shown in Fig.1.2.2, the best example being mercury in contact with a glass. The wettability between the liquid and the container defines whether the spherical surface encloses the liquid or the vapor.

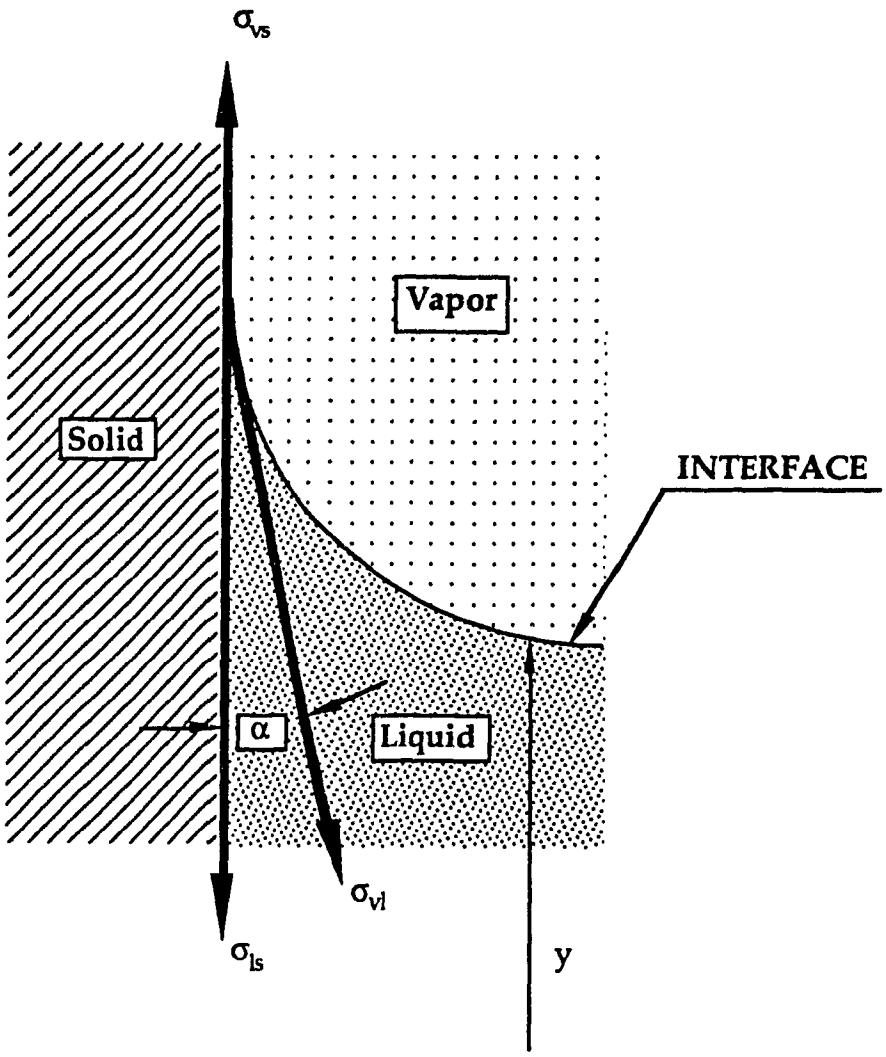

Fig.1.2.1. Surface tension and contact angle of wetting liquid in zero-gravity.

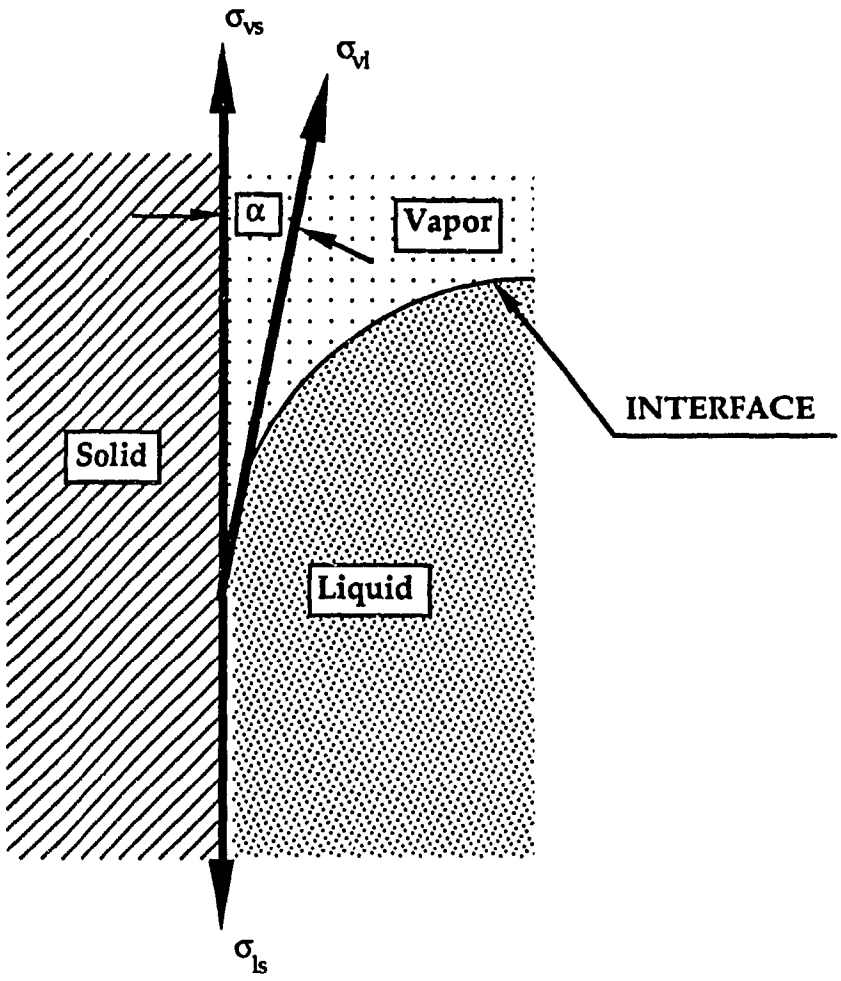

Fig.1.2.2. Surface tension and contact angle of non-wetting liquid in zero-gravity.

It is observed that the contact angle depends entirely on the nature of the solid-liquid-vapor interfacial surfaces. The contact angle has a definite value when the states of the interfaces are fixed. Laplace's second law of capillarity indicates the constancy of the contact angle in a given system, that is, the contact angle remains constant in any gravity field because the intermolecular forces are independent of the level of the gravitational field.

In general, a liquid is under the influence of inertial and intermolecular forces that are represented in the form of surface tension forces. In a normal gravitational field the inertial forces dominate and the surface tension forces are suppressed becoming only significant in very small fluid systems. Thus, the development of the liquid interface and the pressure is mainly due to inertial forces. In orbit, the actual value of gravitational constant does not decrease substantially. Inside the spacecraft, however, almost 0-g conditions are present since the centrifugal acceleration balances the gravitational acceleration. The forces arising due to non-uniformity of the earth's gravitational field, solar activity, aerodynamic deceleration, internal gravitation, forces generated due to the interaction of the electric charge of the apparatus with earth's magnetic field and solar pressure are extremely small. Therefore, in a microgravity environment surface tension may become comparable to inertial forces and hence exert a great influence in the development of the liquid-vapor interface. In the present thesis zero gravity environment will imply that the effective body force is zero and all the other extraneous forces are neglected.

Future space activities will require the handling and storage of a large amount of liquids. These will include fuel for control motors and refueling of

smaller vehicles, water, atmospheric gases in liquid form, cryogens and other types of liquids used in experiments or industrial processes. There are many problems associated with liquid behavior in a microgravity environment. A typical example can be found in the propellant tanks of space vehicles. Improper positioning of the liquid (away from the draining outlets) may cause ingestion of gas bubbles, resulting in changing flow rates and mixture ratios and adversely affect engine performance. Vortexing during propellant draining enhances the severity of the problem. Similar difficulties are also encountered during liquid filling. The liquid may be forced by external disturbances to oscillate. If it happens that the forcing frequency is proximal to the liquid mass natural frequency, attitude control difficulties and in severe cases structural damage may result. Although many of the problems associated with the physics of liquid motion in microgravity, such as liquid positioning, sloshing, draining and refilling, have been solved in the past by practical means, they, however, have generated additional difficulties. Knowledge of the liquid-vapor interface dynamic behavior and the final equilibrium liquid configuration is essential to solve the problems of effective tank volume and effective liquid storage, pump inlet design, positioning of tank inlets and outlets, and the orientation control of space vehicle. Therefore, a better understanding of the physics of solid-liquid-vapor systems is required.

1.3 Previous Work

Study on surface tension phenomena can be traced as far back as Leonardo da Vinci and Sir Issac Newton. It was Young who first established the theory by demonstrating how the principles of surface tension and contact angle can be used to explain many capillary phenomena. The theory was represented on a mathematical formula by Laplace. Gauss obtained the equation of the free surface and the conditions of the contact angle by applying the principle of conservation of energy to the system. Dupre and Gibbs utilized soap bubbles and other devices, and determined the equilibrium configuration of liquids.

Although work on capillary-dominated fluid motions started early in the 19th century, serious attention to problems of liquid setting and interface dynamics as related to liquid storage and management at spacecrafts under microgravity conditions began around the end of 1950s and the early 1960s. Extensive research was carried out during that period. The status of zero-gravity technology at that time was surveyed by Unterberg et al (1962). A comprehensive review by Otto (1966) also summarized the fruitful results during that time.

Benedikt (1959, 1961) studied the hydrostatic behavior of liquids in microgravity environment, while liquid deformations due to surface tension forces were taken into account. He indicated that there is a transition period between the time when gravity is removed and the time when an equilibrium is established.

Several researchers have analytically investigated the configuration of the liquid-vapor interface under zero-gravity conditions. Solutions for the configuration of the interface between parallel plates was presented as a function of the gravity field by Reynolds (1961). These formulations and the principles have inferred the configuration of the interface in other geometries. Li (1961, 1962) predicted the interface configuration in many geometries by applying the minimum energy principle. He showed conclusively that the configurations are primarily dependent on the tank geometry, the contact angle, the ullage, and the gravitational level. The equilibrium interface in a cylindrical container of a general cross-section was calculated by Concus (1986). Their analytical approach was valid in predicting the steady state case with large liquid heights.

Several types of zero-gravity facilities, such as drop towers, airplanes, ballistic rockets and orbiting vehicles, have been used to conduct experiments in the past. Each of them involves the use of free fall, or force equilibrium with the local gravitational field. Among these, the drop tower, the aircraft flying on a parabolic trajectory, and the ballistic rocket have been the most popular.

A number of experiments have been carried out in drop towers. Reynolds (1959) examined wetting and non-wetting liquid placed in a transparent container with different ullage by means of still and motion picture photography during a 1-second free-fall in the drop test. The results of his study indicate that wetting liquids in spherical tanks will crawl around the container walls, leaving a vapor pocket in the center. Non-wetting fluids coalesced as a globe in the center of a container, with a complete vapor

blanket between the globe and the walls. Experimental studies concerning the interface dynamic response to changes in gravity levels were conducted in the NASA Lewis Research Center 2.3 seconds drop tower facility. The observations verified the analytically predicted free-surface configurations (Petrash, et al, 1962, 1963). These experiments were conducted in various geometrical containers at several filling ratios using liquids forming three different contact angles (0, 40, 125 degrees) with the solid wall. The experimental work was confirmed and extended by Clodfelter (1963) who reported on the end boundary effects in flat-bottom cylinders at the 1.85 second drop facility. A free-fall experiment in a drop tower with a capillary tube geometry verified the contention that the solid-liquid-vapor system tends to a configuration in which the free surface energies are minimal (Petrash, Jan., 1963). This energy minimization process can significantly alter the liquid-vapor interface configuration depending on the geometry employed. Experimental studies of the behavior of liquids under various conditions under the absence of gravity forces were also conducted by Siegel (1961).

The zero-gravity test bed on aircrafts has been used for the experiments of Clodfelter et al (1961), Neiner (1959) and Trusela et al (1960). It was found that the time required for damping out interface oscillations increased with the decrease in viscosity. Non-wetting liquids tended to form a sphere removed from the tank wall, as did the gas ullage with wetting liquids.

An analytical method to predict the time required for a liquid-vapor system in a spherical container partially filled with a totally wetting liquid to deform from a gravity dominated condition to that of a nulled gravity

equilibrium state was presented by Paynter (1964). A dimensionless time parameter was proposed to estimate zero-gravity liquid deformation rates at different tank radii. A free-fall experimental study was conducted to determine the time required for the liquid-vapor interface to reach equilibrium in spherical, cylindrical, and annular tanks by Siegert (1964). The dependence of the time to reach equilibrium as a function of the pertinent liquid parameters and system dimensions was obtained.

Although experiments under zero-gravity can provide real information on the liquid behavior, a number of factors affect adversely the results. The short time durations (2 to 3 seconds) of microgravity conditions is the major disadvantage of drop towers. It was reported that complete stability or equilibrium of liquid were not achieved in all test drops. Furthermore, the undesirable influence of initial disturbance created while releasing the container becomes quite significant. Thus, such experiments are not suitable for investigating liquid dynamic processes leading to steady-state or equilibrium states, since the liquid dynamic motion usually does not really reach the state of rest within a few seconds. Alternatively, microgravity conditions can be maintained for about 25 seconds by an aircraft flying a parabolic trajectory. The inaccuracies in the flight trajectory due to pilot error and side gusts, and the long dead time required, reduces significantly the effectiveness of the method. Another disadvantage is that the experiments have to be carried out in batches.

Liquid dynamic behavior of the free surface during a step transition from terrestrial field to zero gravity in rectangular and cylindrical tanks have been investigated numerically by Vatistas et al (1990, 1991).

1.4 Thesis Outline

Since experimental tests are still prohibitively expensive and most often impossible, the present work is devoted mainly to analytical and numerical methods with the aim to study aspects of the mechanics of liquid interface under zero gravity. More specifically, the present investigations deal with (a) the liquid static shapes under zero gravity conditions, and (b) the dynamic response of the free-surface during a step transition from one gravity to zero gravity. The zero gravity stationary states are obtained using analytical methods, which is confirmed by the computational approach, while the transient response is accomplished via numerical methods.

The analytical part of the thesis concentrates on liquid free-surface characterization under hydrostatic conditions in a nulled gravity environment. This is achieved based on the minimum potential energy principle, resulting in two new dimensionless parameters: the interface configuration ratio and the liquid critical depth. The latter parameter represents the condition (critical height) under which the free-surface splits into two fluid bodies in search of the most preferable equilibrium condition (global potential energy extremum). The stationary interface configuration for containers given the contact angle and ullage volume can be predicted by the value of the critical depth.

The numerical results are obtained using a modified version of the code previously developed by Nichols et al, (1980). Simulations concerning

the liquid interface dynamics in rectangular and cylindrical containers are accomplished solving simultaneously continuity, the Navier-Stokes equations, the kinematic free-surface condition, and the Laplace-Young equation. Time required for the static free-surface formation as a function of the Reynolds number and the contact angle is of primary importance. The new hypothesis concerning the most preferable equilibrium condition (for liquid heights smaller than the critical depth) is confirmed by the numerical results. The numerically obtained steady-state interface configuration is found to be in conformity with the analytical results as well as the limited visualization experiment reported by Petrash et al (1963).

In this chapter, fluid problems under microgravity and discussions concerning the methods employed to solve the problems are introduced. Chapter 2 deals in detail with the interface shape and location, as well as liquid distribution at the equilibrium state by introducing and discussing interface configuration ratios and critical depths. Chapter 3 is concerned with the dynamic behavior of liquids during the transition from the terrestrial to weightlessness conditions by the computational technique. The finite difference method is presented. Chapter 4 considers the dynamic responses to the transitions and variations between analytic and numerical analyses. Chapter 5 provides the important conclusions.

CHAPTER 2

LIQUIDS IN STATIC EQUILIBRIUM

2.1 Liquids at Equilibrium State

The purpose of the analytical investigations is to determine the static liquid-vapor interface shape under zero gravity conditions. Two dimensional rectangular and cylindrical geometries are to be considered. Liquids forming a variety of contact angles with the containing walls will be investigated.

A rigid tank partially filled with an incompressible and homogeneous wetting liquid is subjected to zero-gravity, shown in Fig.2.1.1. In a normal gravitational field, the fluid mass develops a pressure gradient. This arises from the fact that the fluid on the lower layers must support the weight of the liquid above. Hence, on the Earth, for relatively large containers, the capillary effects are suppressed and result in a distorted, flat and free liquid surface. In space, particularly in the zero gravity environment, the free surface shape will be the results of surface tension and wall adhesion forces since other forces and accelerations are negligibly small though they may not completely vanish.

Using variational principles Myshkis et al (1987) proved that the potential energy, E, for the mechanical system consisting of a liquid, its vapor and a rigid containing vessel,

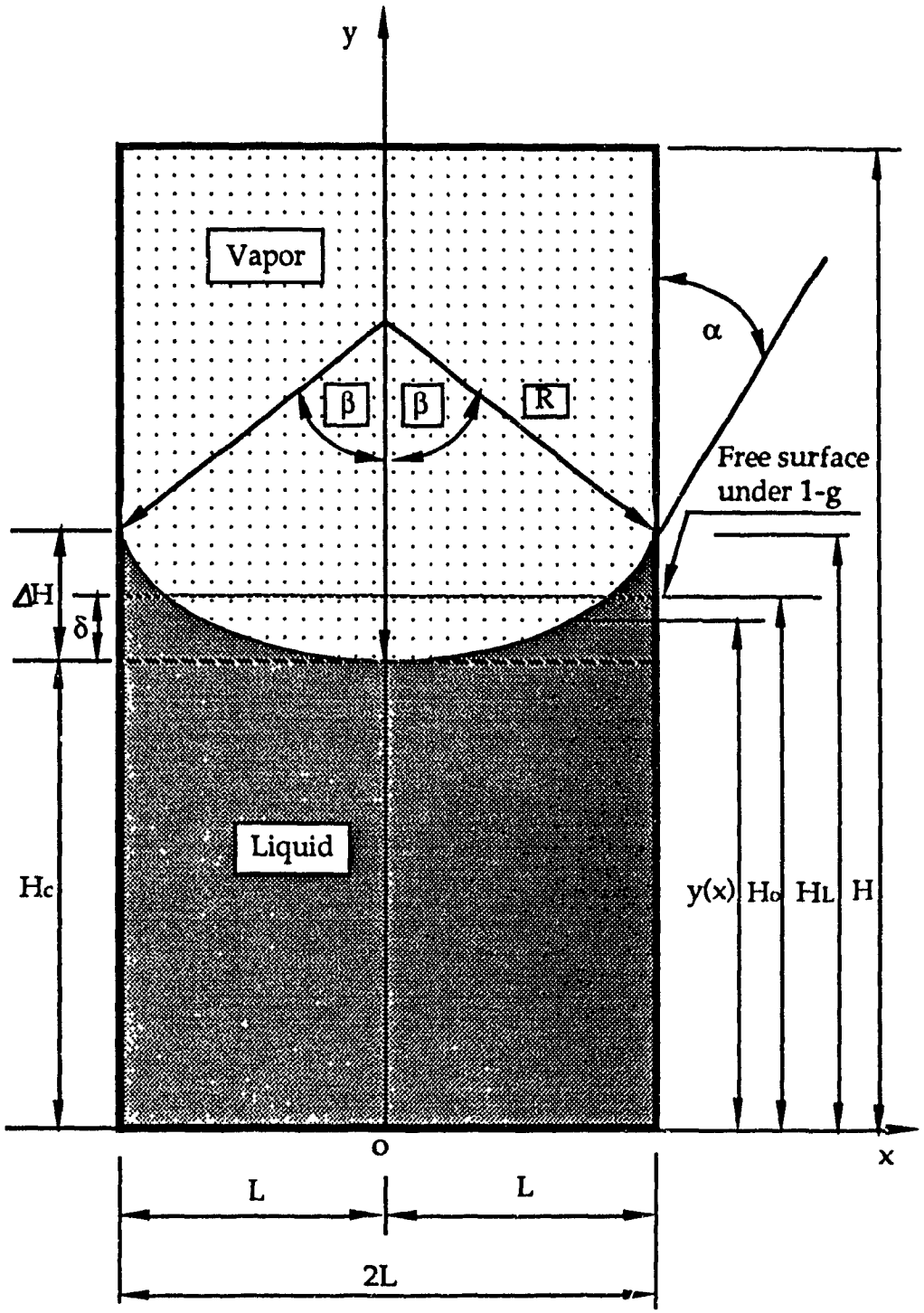

Fig.2.1.1 Schematic of liquid in a rigid tank under zero-gravity

$$E = \sigma_{vl}|S_{vl}| + \sigma_{ls}|S_{ls}| + \sigma_{vs}|S_{vs}| + \rho\int_V \Pi\, dV \qquad (2.1.1)$$

where S_{vl}, S_{ls} and S_{vs} are the areas of the vapor-liquid, liquid-solid and vapor-solid interfaces, respectively, and σ_{vl}, σ_{ls} and σ_{vs} are the surface tension at these interfaces; Π is the force potential ($\vec{F} = -\vec{\nabla}\Pi$) and V is the total liquid volume, will attain minima for all variations of S_{vl} respecting the constraint

$$\delta\int_V dV = 0 \qquad (2.1.2)$$

provided the following necessary and sufficient conditions:

Dupre-Young condition

$$\sigma_{vs} = \sigma_{ls} + \sigma_{vl}\cos(\alpha) \qquad (2.1.3)$$

Laplace-Young condition

$$\sigma\left\{\frac{d}{dx}\left[\frac{\frac{dy}{dx}}{\sqrt{1+\left(\frac{dy}{dx}\right)^2}}\right] + \frac{\varepsilon}{x}\left[\frac{\frac{dy}{dx}}{\sqrt{1+\left(\frac{dy}{dx}\right)^2}}\right]\right\} = \rho\,\Pi + \text{constant} \qquad (2.1.4)$$

are satisfied, where ε=0 or 1 indicates Cartesian or cylindrical coordinate, respectively, and y=y(x) is the location of the interface. In zero gravity where no extraneous forces exist (Π = 0), equation (2.1.4) simplifies to:

$$\sigma\left\{\frac{d}{dx}\left[\frac{\frac{dy}{dx}}{\sqrt{1+\left(\frac{dy}{dx}\right)^2}}\right]+\frac{\varepsilon}{x}\left[\frac{\frac{dy}{dx}}{\sqrt{1+\left(\frac{dy}{dx}\right)^2}}\right]\right\} = \text{constant} \qquad (2.1.5)$$

From equation.(2.1.5), both the rectangular and the cylindrical tank configurations of Fig.2.1.1 give the general free surface equation:

$$\frac{1}{R} = \text{constant} \qquad (2.1.6)$$

Hence, in a weightless environment, the equilibrium liquid configuration will deform reaching a constant curvature free surface.

The contact angle requirement indicates that:

$$\frac{dy}{dx}_{(x=L)} = \cot(\alpha) \qquad (2.1.7)$$

The surface radius is then

$$R = \frac{L}{\cos(\alpha)} \qquad (2.1.8)$$

Under the condition that the liquid-vapor interface curve passes through the point $(0, H_c)$, the equation of the interface is given by

$$x^2+[(H_c+R)-y]^2 = R^2 \qquad (0 \le x \le L) \qquad (2.1.9)$$

for concave down as wetting liquid and

$$x^2+[(R-H_c)+y]^2=R^2 \qquad (0\le x\le L) \tag{2.1.10}$$

for concave up as non-wetting liquid, respectively.

Solving for y from equations (2.1.9) and (2.1.10), yield

$$y = R + H_c - \sqrt{R^2 - x^2} \tag{2.1.11}$$

$$y = H_c - R + \sqrt{R^2 - x^2} \tag{2.1.12}$$

for wetting and non-wetting liquid, respectively.

From the above equations,

$$\Delta H = |H_L - H_c| = \left|R - \sqrt{R^2 - L^2}\right| \tag{2.1.13}$$

or

$$H_c = H_L \pm \Delta H \tag{2.1.14}$$

The distances of the vertex at the central line from the original one-g liquid level in rectangular or cylindrical tanks are given by

$$\delta_{rect} = \frac{L}{2\cos^2(\alpha)}\left|\cos(\alpha)\,[2-\sin(\alpha)] - \left(\frac{\pi}{2}-\alpha\right)\right| \tag{2.1.15}$$

$$\delta_{cyl} = \frac{L}{\cos(\alpha)}\left\{1 - \frac{2}{3}\frac{[1 - \sin^3(\alpha)]}{\cos^2(\alpha)}\right\} \qquad (2.1.16)$$

respectively.

If equations (2.1.15) and (2.1.16) are divided by L, their dimensionless form is obtained:

$$\bar{\delta}_{rect} = \frac{1}{2\cos^2(\alpha)}\left\{\cos(\alpha)\,[2 - \sin(\alpha)] - \left(\frac{\pi}{2} - \alpha\right)\right\} \qquad (2.1.17)$$

$$\bar{\delta}_{cyl} = \frac{1}{\cos(\alpha)}\left\{1 - \frac{2}{3}\frac{[1 - \sin^3(\alpha)]}{\cos^2(\alpha)}\right\} \qquad (2.1.18)$$

for rectangular and cylindrical geometries, respectively.

2.2 Interface Configuration Ratio

The potential energy of a mechanical system consisting of a liquid, its vapor and a solid container under zero gravity, when all the extraneous forces have been removed is:

$$E = \sigma_{vl}|S_{vl}| + \sigma_{ls}|S_{ls}| + \sigma_{vs}|S_{vs}| \qquad (2.2.1)$$

It is assumed that there are two liquid configurations, (a) and (b), where the energy is minimum. The variation of E is then given by:

$$\delta E = \sigma_{vl}\,\delta|S_{vl}| + \sigma_{ls}\,\delta|S_{ls}| + \sigma_{vs}\,\delta|S_{vs}| \tag{2.2.2}$$

Since

$$\delta|S_{ls}| = -\,\delta|S_{vs}| \tag{2.2.3}$$

then

$$\delta E = \sigma_{vl}\left\{\delta|S_{vl}| + \cos(\alpha)\,\delta|S_{vs}|\right\} \tag{2.2.4}$$

If assuming that S_{vl} for (b) is less than that for (a), then $\delta|S_{vl}| < 0$. For this case $\delta|S_{ls}| > 0$, which implies that $\delta|S_{vs}| < 0$. Therefore,

$$\delta E < 0 \quad \text{or} \quad E_b < E_a \tag{2.2.5}$$

The latter suggests that the state with the smallest vapor-liquid interface is the one with the absolute minimum potential energy. If the interface area is not initially at a minimum, will become so through a dynamic process. If on the other hand it is at a local minimum then given a disturbance of an appropriate magnitude it might degenerate to the the absolute minimum state. Hence, for a given amount of liquid, the system with the smallest liquid-vapor interface area will be the preferable state. The symbol θ is defined here as the interface configuration ratio, which is represented by the ratio of a liquid-vapor surface area to the liquid volume in a tank in the static equilibrium state. Mathematically

$$\theta = \frac{A}{V} \qquad (2.2.6)$$

where A is liquid-vapor interface area and V is liquid volume. In certain situations the free-surface might have several configurations (bifurcating solutions) that satisfy Laplace's equation and the contact angle requirements. In this situation the system will tend to the state with an absolute free-surface energy minimum. The smaller the normalized interface configuration ratio $\bar{\theta}$ ($\bar{\theta} = \theta L$) the smaller the free surface energy since V/L^3 remains constant. This type of the configuration is more stable and more likely to be formed for certain amounts of liquid while maintaining the same contact angles.

2.3 Wetting Liquid Interface Configurations and Location of Liquid in Rectangular Tanks

Two cases of wetting liquids (contact angle between 0^o and 90^o) in containers in a zero gravity environment are introduced here. One of them is under the condition that the liquid volume is sufficient to cover the base of the containing vessel in all cases. The other is that the volume of a liquid may not be enough to cover the base of the container.

2.3.1. Configuration System 1

Consider a wetting liquid in a rigid rectangular tank in the zero gravity environment, given in Fig.2.3.1. The interface area and the liquid volume enclosed by the interface and tank walls of the configuration system 1 are

obtained by the liquid surface area and volume integrals, respectively. Thus, the interface configuration ratio of the liquid-vapor interface area to liquid volume in the system 1, θ_{r1} is

$$\theta_{r1} = \frac{\beta_1}{\cos(\alpha)\left\{H_c + L\left[\frac{1-\sin(\alpha)}{\cos(\alpha)} - \frac{\beta_1}{2\cos^2(\alpha)} + \frac{1}{2}\tan(\alpha)\right]\right\}} \qquad (2.3.1)$$

$$\left(0 \le \alpha < \frac{\pi}{2}\right)$$

Where α is the contact angle, H_c is the liquid depth which is the interface height from the bottom of a tank at the central line, L is the half width of the tank, and

$$\beta_1 = \frac{\pi}{2} - \alpha. \qquad (2.3.2)$$

The dimensionless $\bar{\theta}_{r1}$ is obtained by multiplying with L on both sides of the equation (2.3.1).

$$\bar{\theta}_{r1} = \frac{\beta_1}{\cos(\alpha)\left\{\bar{H}_c + \frac{1-\sin(\alpha)}{\cos(\alpha)} - \frac{\beta_1}{2\cos^2(\alpha)} + \frac{1}{2}\tan(\alpha)\right\}} \qquad (2.3.3)$$

$$\left(0 \le \alpha < \frac{\pi}{2}\right)$$

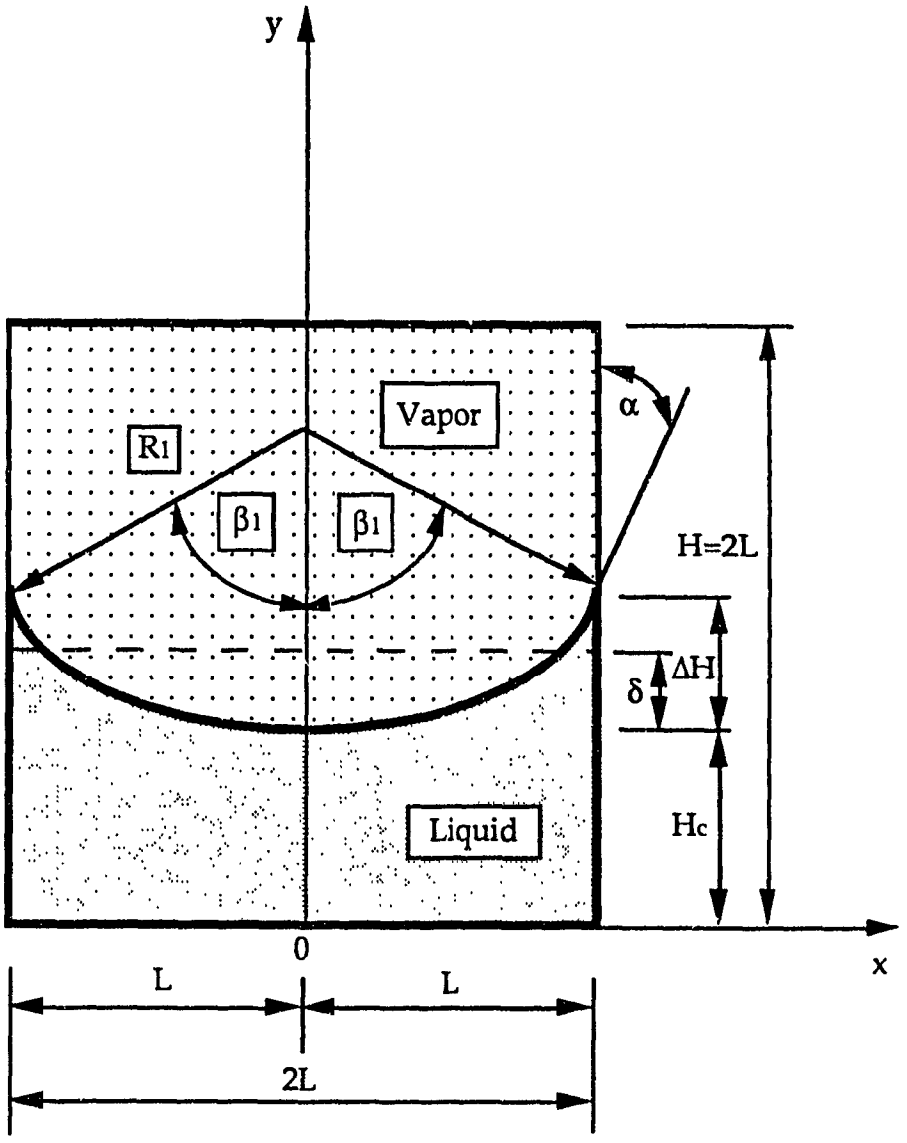

Fig.2.3.1 Wetting liquid configuration system 1
in a rectangular tank under zero-gravity

where dimensionless $\overline{H}_c$ is

$$\overline{H}_c = \frac{H_c}{L} \tag{2.3.4}$$

The distance between the liquid surface at the center and along the solid walls ΔH, in dimensionless form is:

$$\Delta\overline{H} = \frac{1 - \sin(\alpha)}{\cos(\alpha)} \tag{2.3.5}$$

Figure.2.3.2 shows that $\Delta\overline{H}$ decreases with the contact angle.

The maximum value of $\overline{H}_c$ is reached when the liquid-vapor interface approaches the top of a tank, mathematically,

$$\overline{H}_{c,\,max} = \frac{H}{L} - \Delta\overline{H} = \frac{2\cos(\alpha) + \sin(\alpha) - 1}{\cos(\alpha)} \tag{2.3.6}$$

In Fig.2.3.3, the results of the equation (2.3.6) reveal that $\overline{H}_{c,\,max}$ is the function of contact angles, rising almost linearly with the contact angle.

The configuration ratios decrease with increasing liquid depth $\overline{H}_c$ for different contact angles are shown in Fig.2.3.4. It indicates that the configuration ratio is monotonically decreasing with $\overline{H}_c$ for different contact angles.

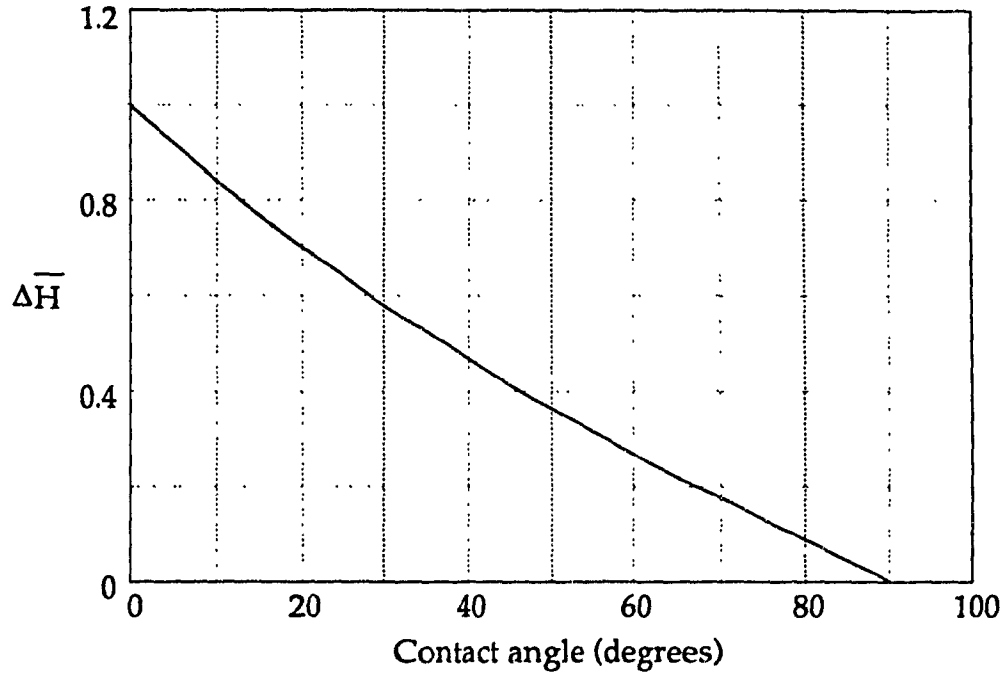

Fig.2.3.2 Dimensionless $\Delta\overline{H}$ versus contact angles

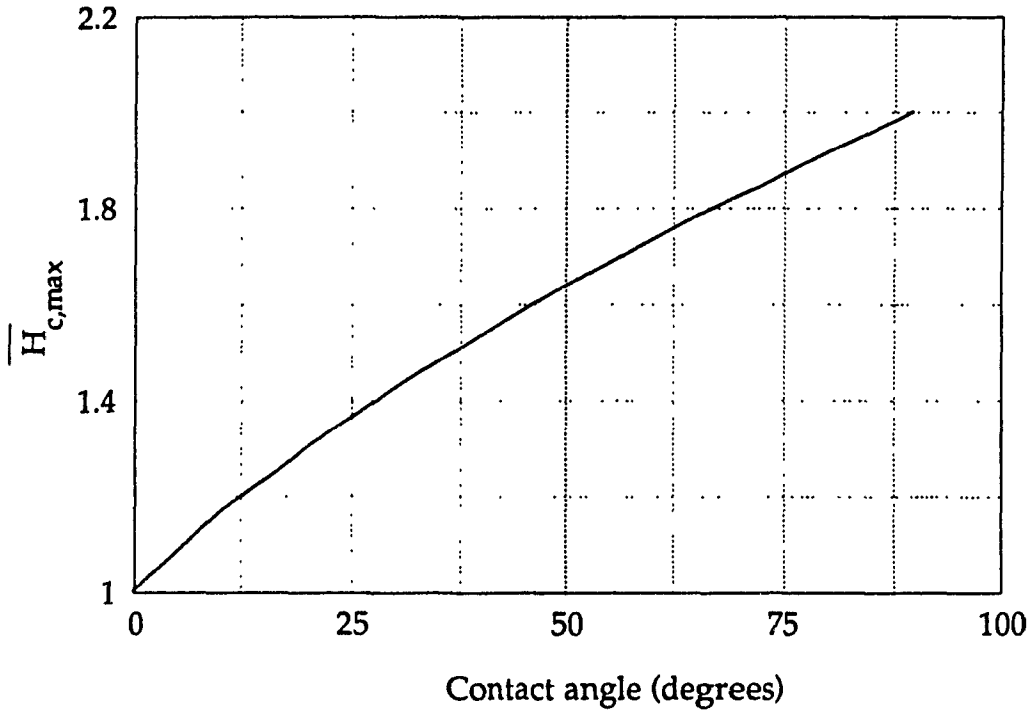

Fig.2.3.3 Dimensionless $\overline{H}_{c,max}$ versus contact angles

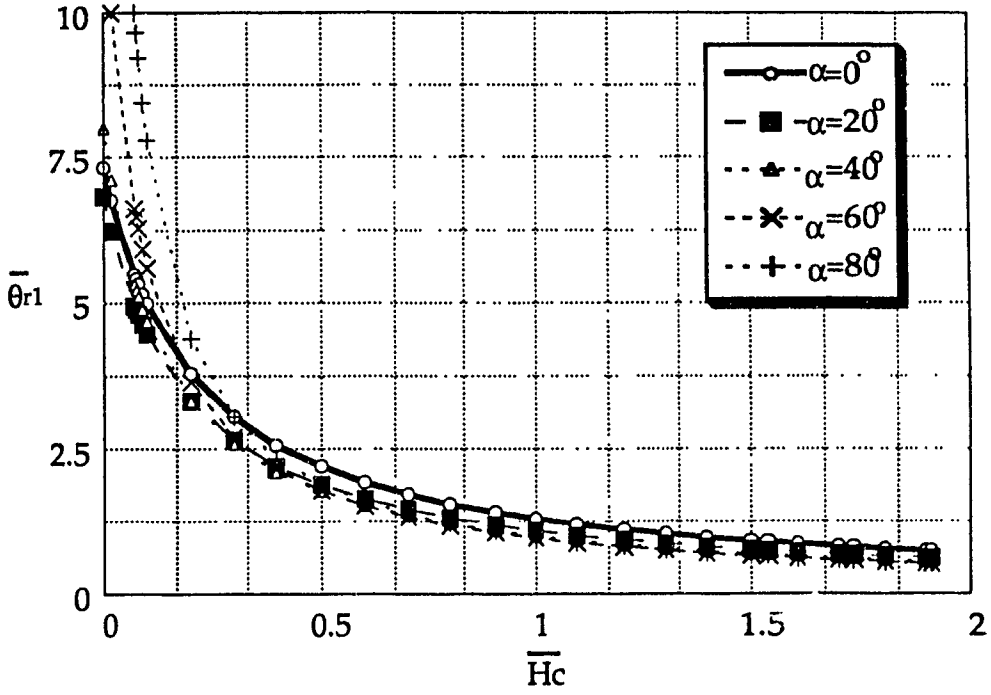

Fig.2.3.4 Dimensionless configuration ratio $\overline{\theta}_{r1}$ versus liquid depth $\overline{H}_c$ at different contact angles

Equation (2.3.3) suggests that the dimensionless ratio $\bar{\theta}_{r1}$ is a function of the liquid depth $\bar{H}_c$ and the contact angle α. The dependence of liquid depth with respect to the contact angle has been discussed above. The smaller liquid depth $\bar{H}_c$, the larger the $\bar{\theta}_{r1}$. The minimum value of $\bar{\theta}_{r1,min}$ will be obtained when the interface along container walls reaches the top of the tank, that is $H_c = H_{c,max}$, (see Fig.2.3.5). The minimum configuration ratio in dimensionless form is given by:

$$\bar{\theta}_{r1,\,min} = \frac{4\,\beta_1 \cos(\alpha)}{4 - \pi + 2\,\alpha + 4\cos(2\alpha) + \sin(2\,\alpha)} \qquad (2.3.7)$$

As shown in Fig.2.3.6, H_c appears to approach zero as maximum $\theta_{r1,max}$ is reached.

$$\bar{\theta}_{r1,\,max} = \frac{4\,\beta_1 \cos(\alpha)}{4\cos(\alpha) - \sin(2\alpha) - \pi + 2\,\alpha} \qquad (2.3.8)$$

However, this phenomenon may not be true, it will be discussed in detail in section 3.4.

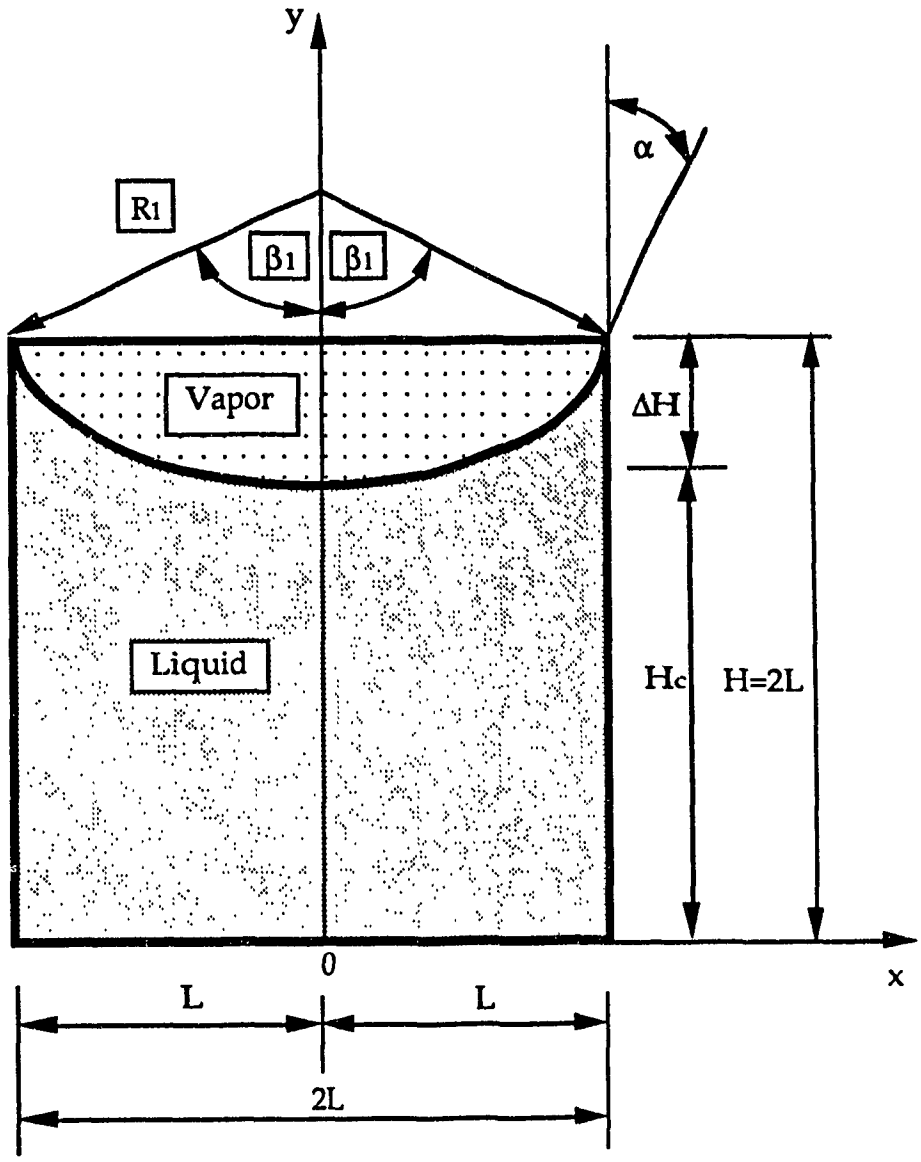

Fig.2.3.5 Minimum interface configuration ratio of system 1 in a rectangular tank when $H_c = H_{c,max}$ under zero-gravity

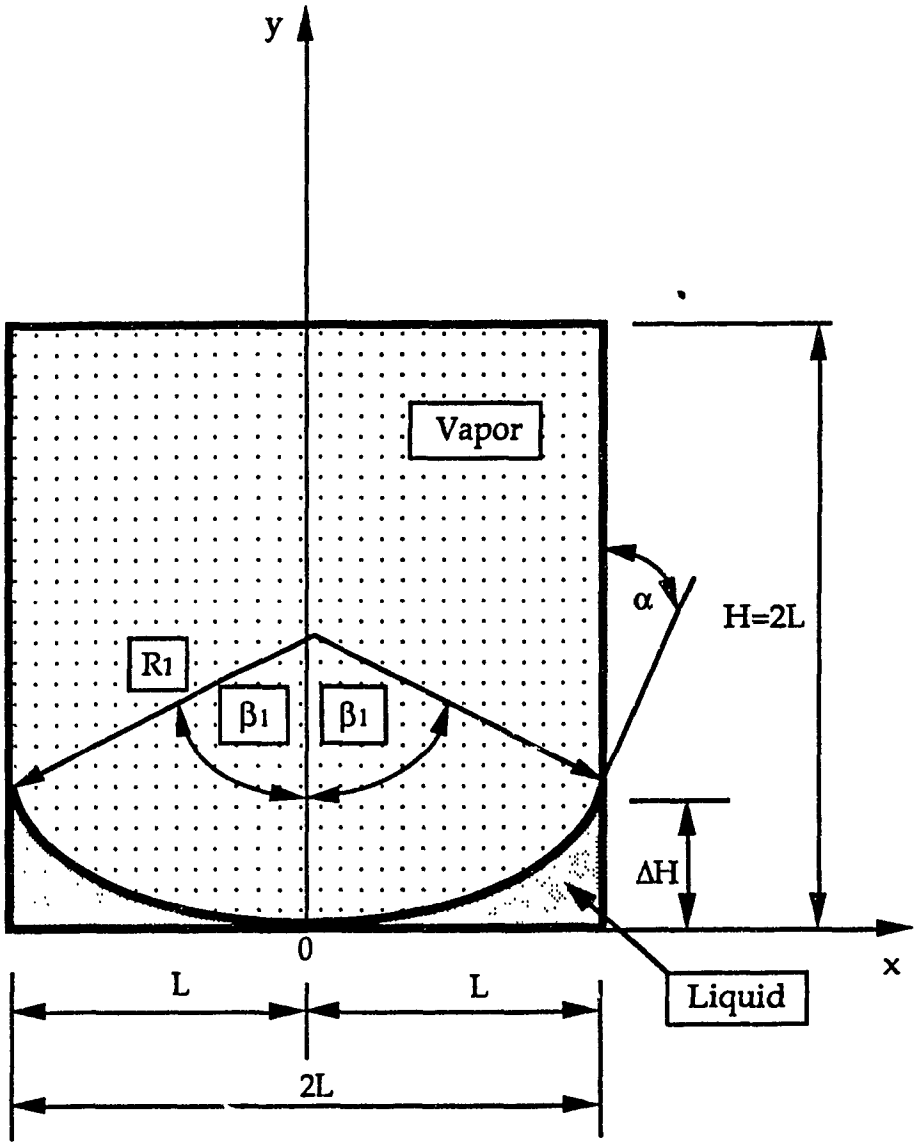

Fig.2.3.6 Maximum interface configuration ratio of system 1 in a rectangular tank when $H_c = 0$ under zero-gravity

2.3.2. Configuration System 2

The other possible interface configuration for system 2 is shown in Figs.2.3.7 and 2.3.8 for contact angle α less and more than 45 degrees, respectively. The interface configuration ratio θ is given

$$\theta_{r2} = \frac{2\sqrt{2}\,\beta_2 \sin\beta_2}{X_r\left(\sin^2\beta_2 + \sin\beta_2\cos\beta_2 - \beta_2\right)} \qquad \left(0 \le \alpha < \frac{\pi}{4}\right) \tag{2.3.9}$$

$$\theta_{r2} = \frac{2\sqrt{2}\,\beta_2 \sin\beta_2}{X_r\left(\sin^2\beta_2 - \sin\beta_2\cos\beta_2 + \beta_2\right)} \qquad \left(\frac{\pi}{4} < \alpha < \frac{\pi}{2}\right) \tag{2.3.10}$$

where X_r is liquid wetting length on a side of the tank wall, and

$$\beta_2 = \left|\frac{\pi}{4} - \alpha\right| \tag{2.3.11}$$

The value of the minimum $\theta_{r2,min}$ for this separate symmetrical system is obtained when $X_r \rightarrow L$, as shown in Figs.2.3.9 and 2.3.10. Equations (2.3.9) and (2.3.10) become the followings at the non-dimensional form.

$$\bar{\theta}_{r2,min} = \frac{2\sqrt{2}\,\beta_2 \sin\beta_2}{\sin^2\beta_2 + \sin\beta_2\cos\beta_2 - \beta_2} \qquad \left(0 \le \alpha < \frac{\pi}{4}\right) \tag{2.3.12}$$

$$\bar{\theta}_{r2,min} = \frac{2\sqrt{2}\,\beta_2 \sin\beta_2}{\sin^2\beta_2 - \sin\beta_2\cos\beta_2 + \beta_2} \qquad \left(\frac{\pi}{4} < \alpha < \frac{\pi}{2}\right) \tag{2.3.13}$$

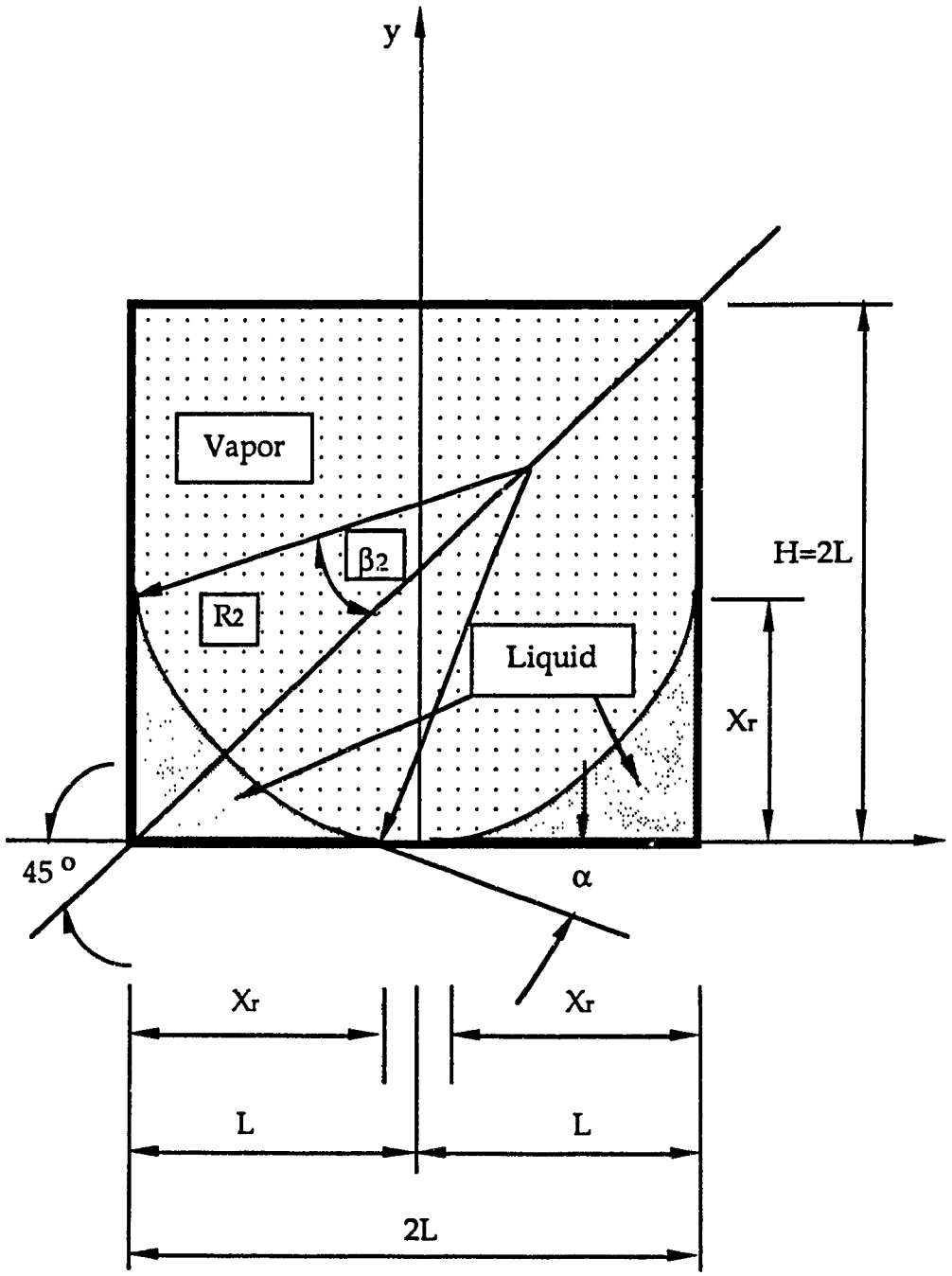

Fig.2.3.7 Wetting liquid configuration system 2 ($0^o \leq \alpha < 45^o$)

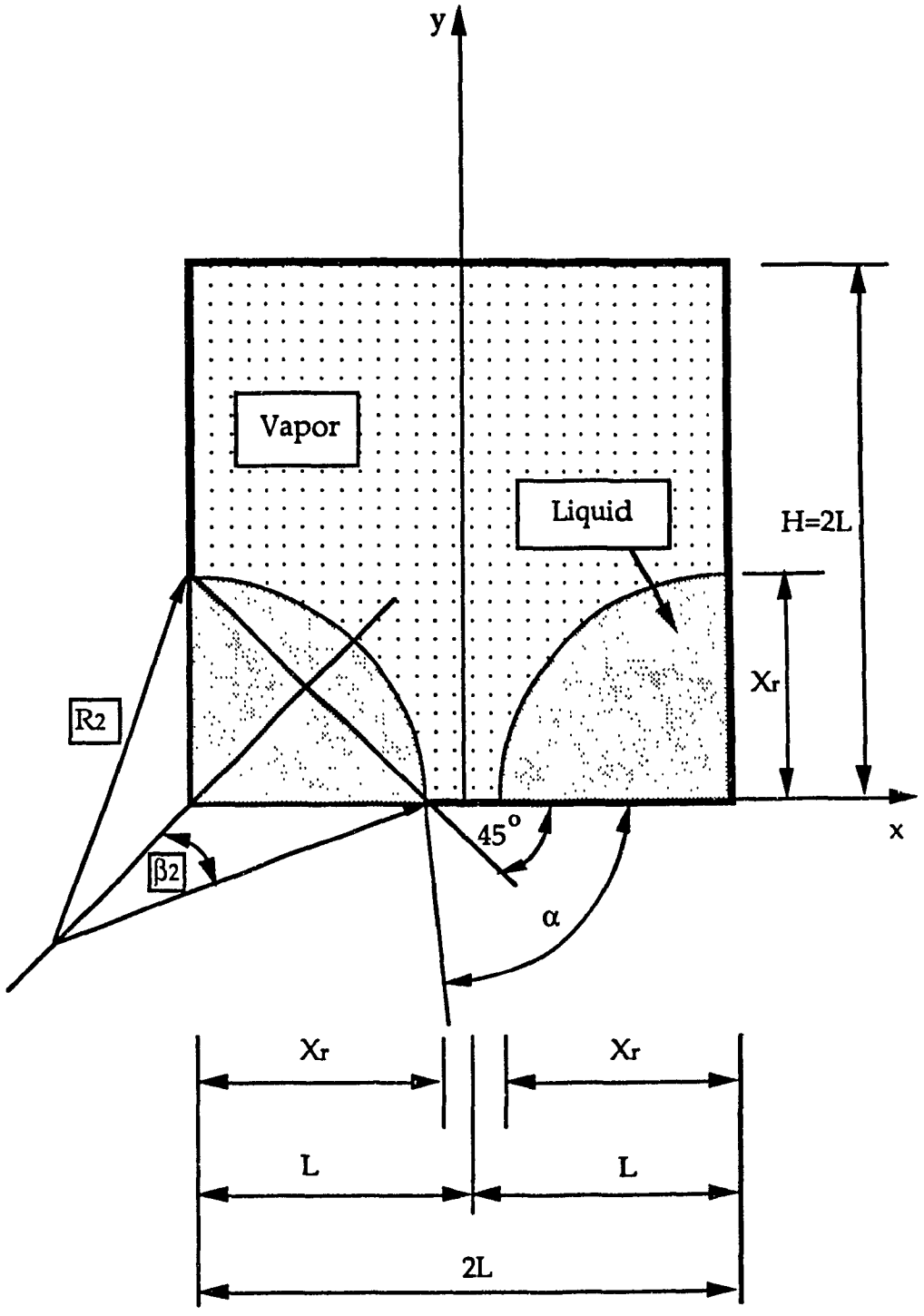

Fig.2.3.8 Wetting liquid configuration system 2 ($45^o < \alpha < 90^o$)

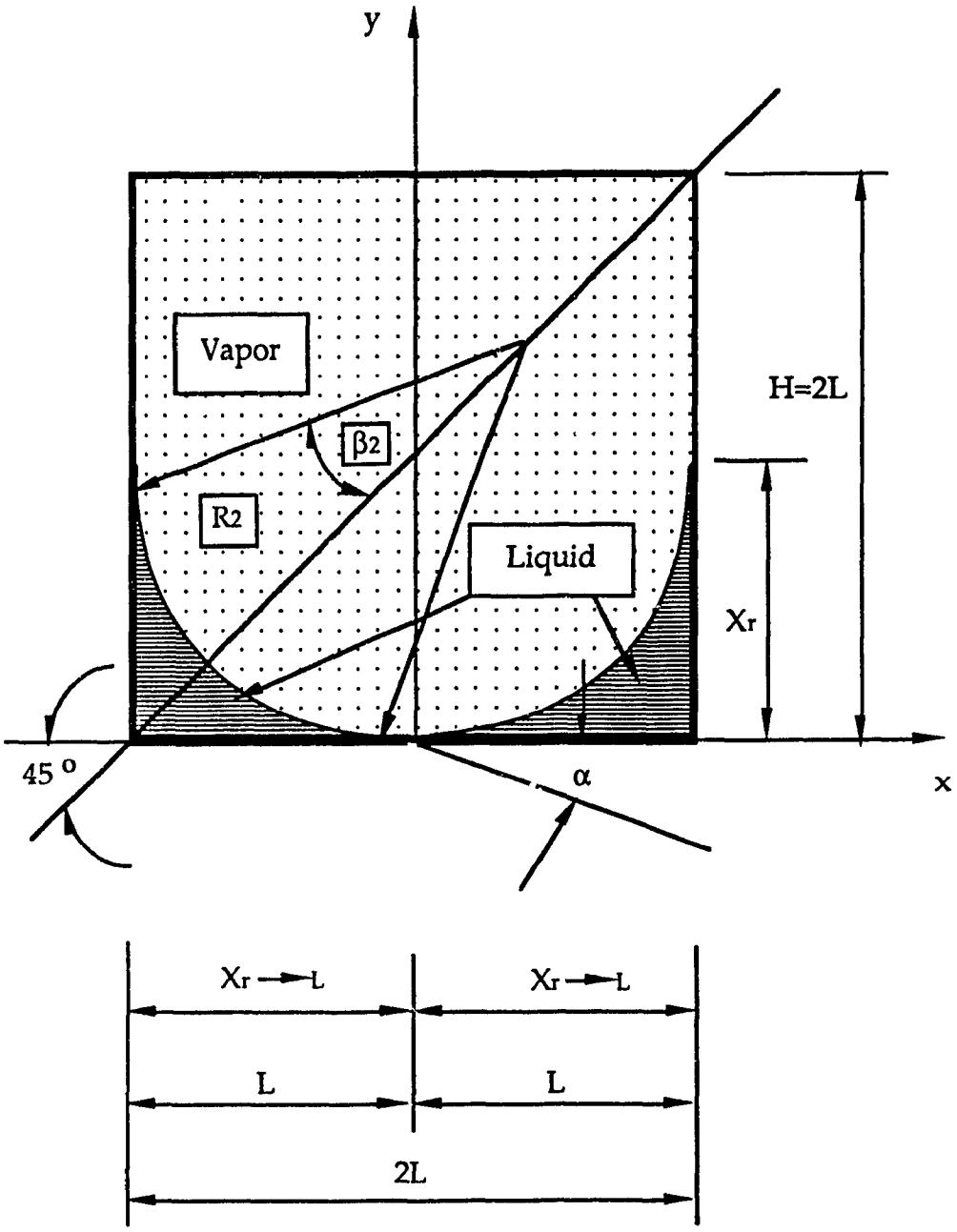

Fig.2.3.9 Minimum interface configuration ratio of wetting liquid at system 2 ($0^o \leq \alpha < 45^o$)

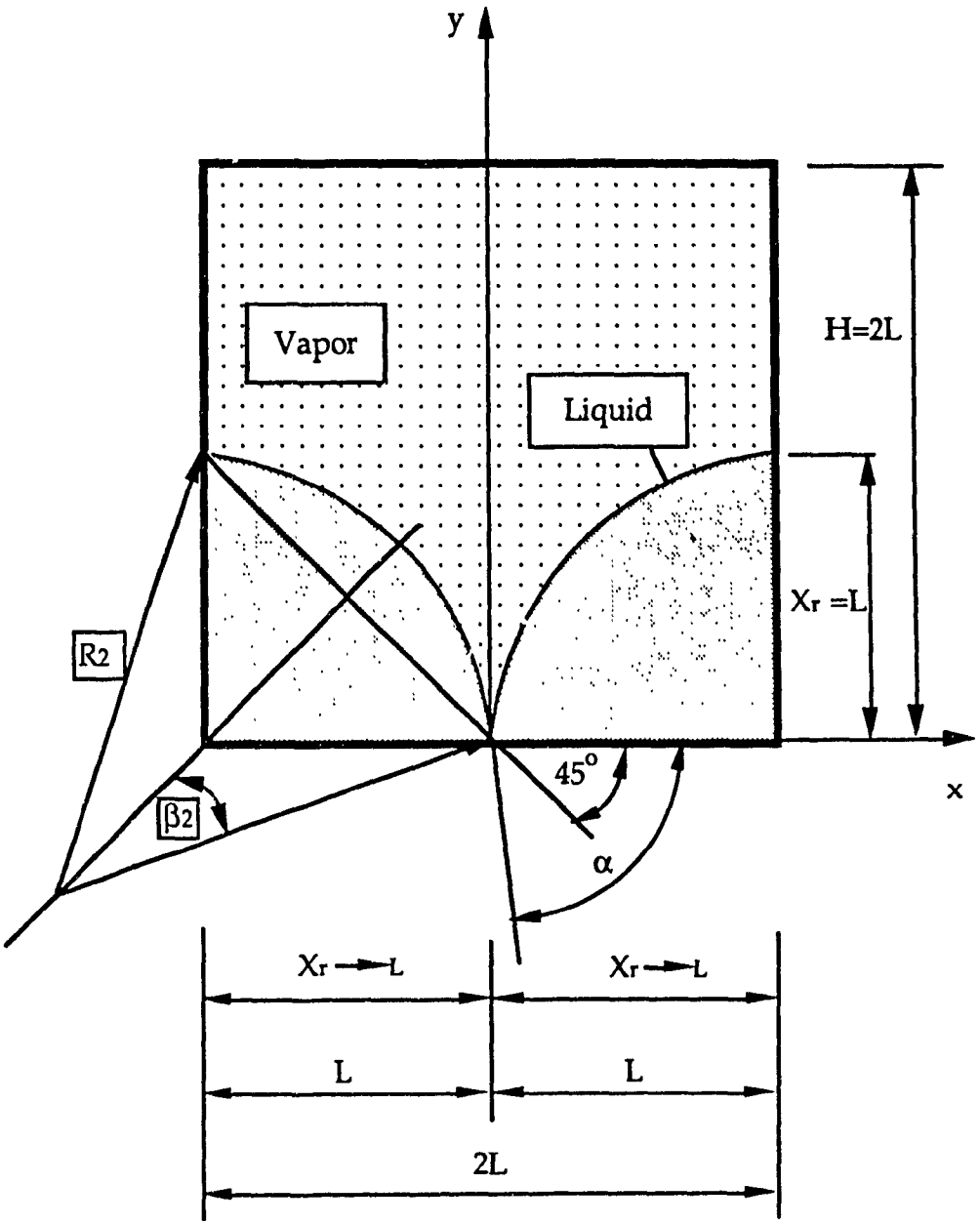

Fig.2.3.10 Minimum interface configuration ratio of wetting liquid at system 2 ($45^o < \alpha < 90^o$)

2.4 Comparison Between configuration Systems 1 and 2 in Rectangular Tanks

Consideration is given to systems with configurations 1 and 2 in a rectangular tank. Here, extermination of the free energy principle is reflected by the minimum interface configuration ratio $\bar{\theta}$. The smaller $\bar{\theta}$ obtained from one of the systems is the most stable configuration for a given amount of liquid.

2.4.1 Minimum Ratio of System 1 and Minimum Ratio of system 2

The configuration system 1 with the minimum interface configuration ratio $\bar{\theta}_{r1,min}$ is shown in Fig.2.3.5 while the system 2 with $\bar{\theta}_{r2,min}$ is shown in Figs.2.3.9 or 2.3.10 depending on the contact angle. The difference of interface configuration ratios between system 1 and system 2 is presented as follows:

$$\Delta\bar{\theta}_{ra} = \bar{\theta}_{r2,min} - \bar{\theta}_{r1,min}$$

$$= \frac{2\sqrt{2}\,\beta_2 \sin\beta_2}{\sin^2\beta_2 + \sin\beta_2\cos\beta_2 - \beta_2} - \frac{4\left(\frac{\pi}{2} - \alpha\right)\cos(\alpha)}{4 - \pi + 2\alpha + 4\cos(2\alpha) + \sin(2\alpha)} \qquad (2.4.1)$$

$$\left(0 \le \alpha < \frac{\pi}{4}\right)$$

$$\Delta\bar{\theta}_{ra} = \bar{\theta}_{r2,min} - \bar{\theta}_{r1,min}$$

$$= \frac{2\sqrt{2}\,\beta_2 \sin\beta_2}{\sin^2\beta_2 - \sin\beta_2\cos\beta_2 + \beta_2} - \frac{4\left(\frac{\pi}{2} - \alpha\right)\cos(\alpha)}{4 - \pi + 2\alpha + 4\cos(2\alpha) + \sin(2\alpha)} \qquad (2.4.2)$$

$$\left(\frac{\pi}{4} < \alpha < \frac{\pi}{2}\right)$$

The equations (2.4.1) and (2.4.2) are plotted in Figs.2.4.1 and Fig.2.4.2, respectively. The solutions are

$$\Delta\bar{\theta}_{ra} = \bar{\theta}_{r2,min} - \bar{\theta}_{r1,min} > 0 \qquad (2.4.3)$$

The graphs show that the ratio difference $\Delta\bar{\theta}_{ra}$ has all positive values, which means that configuration system 2 has a larger θ value than that of system 1. Therefore, the interface at the zero gravity is shown in the configuration of system 1 when the liquid level is high enough.

2.4.2 Maximum Ratio of System 1 and Minimum Ratio of system 2

Consider the maximum interface configuration ratio $\bar{\theta}_{r1,max}$ of system 1 shown in Fig.2.3.6 compared with the minimum interface configuration ratio $\bar{\theta}_{r2,min}$ of system 2 shown in Figs.2.3.9 and 2.3.10.

$$\Delta\bar{\theta}_{rb} = \bar{\theta}_{r2,min} - \bar{\theta}_{r1,max}$$

$$= \frac{2\sqrt{2}\,\beta_2 \sin\beta_2}{\sin^2\beta_2 + \sin\beta_2\cos\beta_2 - \beta_2} - \frac{4\left(\frac{\pi}{2} - \alpha\right)\cos(\alpha)}{4\cos(\alpha) - \sin(2\alpha) - \pi + 2\alpha} \qquad (2.4.4)$$

$$\left(0 \le \alpha < \frac{\pi}{4}\right)$$

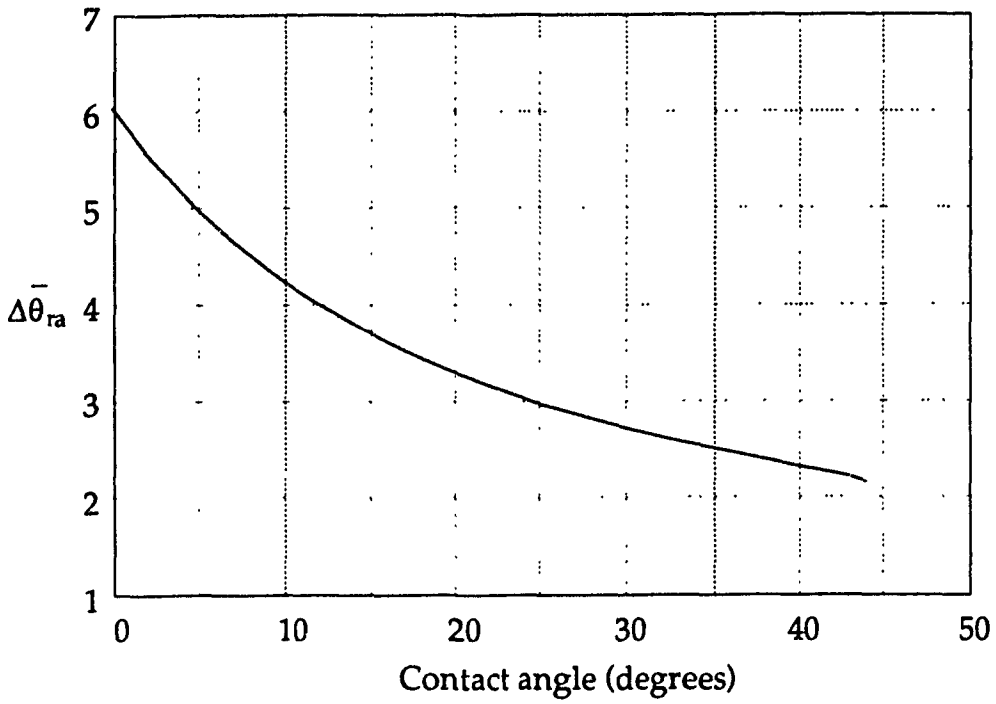

Fig.2.4.1 Comparison minimum interface configuration ratios between configuration systems 1 and 2 at contact angle ($0^o \leq \alpha < 45^o$)

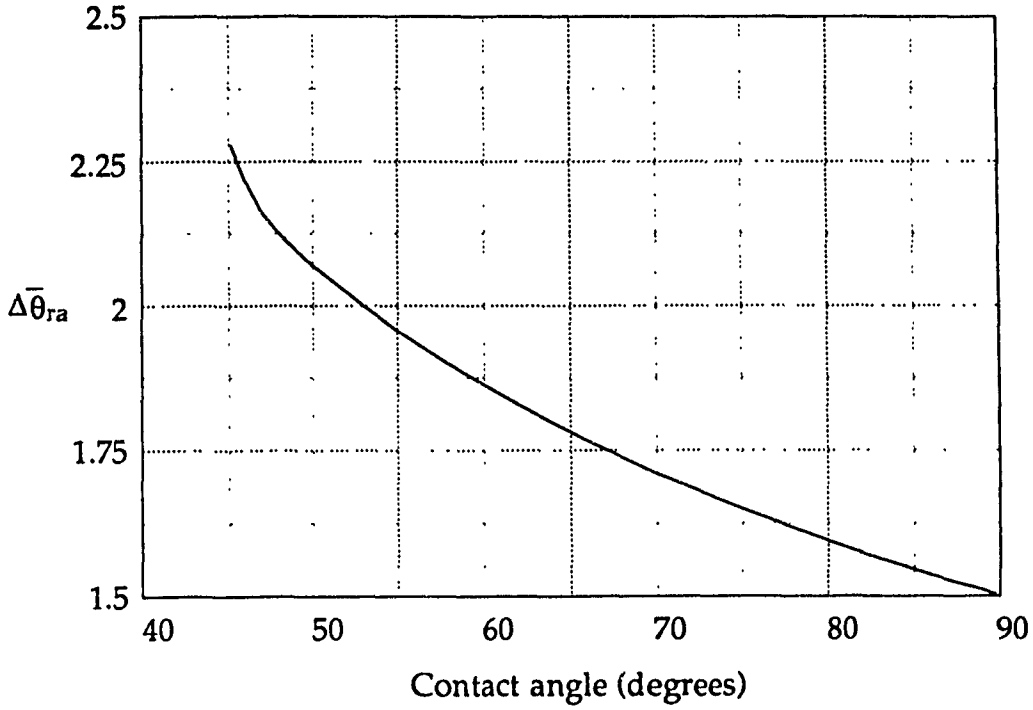

Fig.2.4.2 Comparison minimum interface configuration ratios between configuration systems 1 and 2 at contact angle ($45^o < \alpha < 90^o$)

$$\Delta\bar{\theta}_{rb} = \bar{\theta}_{r2,min} - \bar{\theta}_{r1,max}$$

$$= \frac{2\sqrt{2}\,\beta_2 \sin\beta_2}{\sin^2\beta_2 - \sin\beta_2\cos\beta_2 + \beta_2} - \frac{4\left(\frac{\pi}{2} - \alpha\right)\cos(\alpha)}{4\cos(\alpha) - \sin(2\alpha) - \pi + 2\alpha} \qquad (2.4.5)$$

$$\left(\frac{\pi}{4} < \alpha < \frac{\pi}{2}\right)$$

From Figs.2.4.3 and 2.4.4 the following is apparent

$$\Delta\bar{\theta}_{rb} = \bar{\theta}_{r2,min} - \bar{\theta}_{r1,max} \le 0 \qquad (2.4.6)$$

The results show that the obtained values are negative, which means the minimum ratio $\bar{\theta}_{r2,min}$ of system 2 is smaller than the assumed maximum $\bar{\theta}_{r1,max}$ of system 1. The configuration of system 2 given in Fig.2.3.9 or Fig.2.3.10 exists in a zero gravity only if the liquid level is low.

From above discussion, the assumed maximum ratio $\bar{\theta}_{r1,max}$ of system 1 will not be presented at the zero gravity even if the liquid is enough to cover the base of the tank bottom under 1-g gravity because the configuration of system 1 will change to system 2 when the liquid depth decreases, before liquid touches the bottom which is the condition of $\bar{\theta}_{r1,max}$. Figures.2.4.5 and 2.4.6 illustrate the conclusion. Suppose the liquid depth is originally at $\bar{H}_{c,max}$, the interface configuration ratio is $\bar{\theta}_{r1,min}$. When the liquid depth decreases, the configuration ratio increases. When the ratio is more than that of system 2, the configuration will be changed from the previous system 1 to system 2.

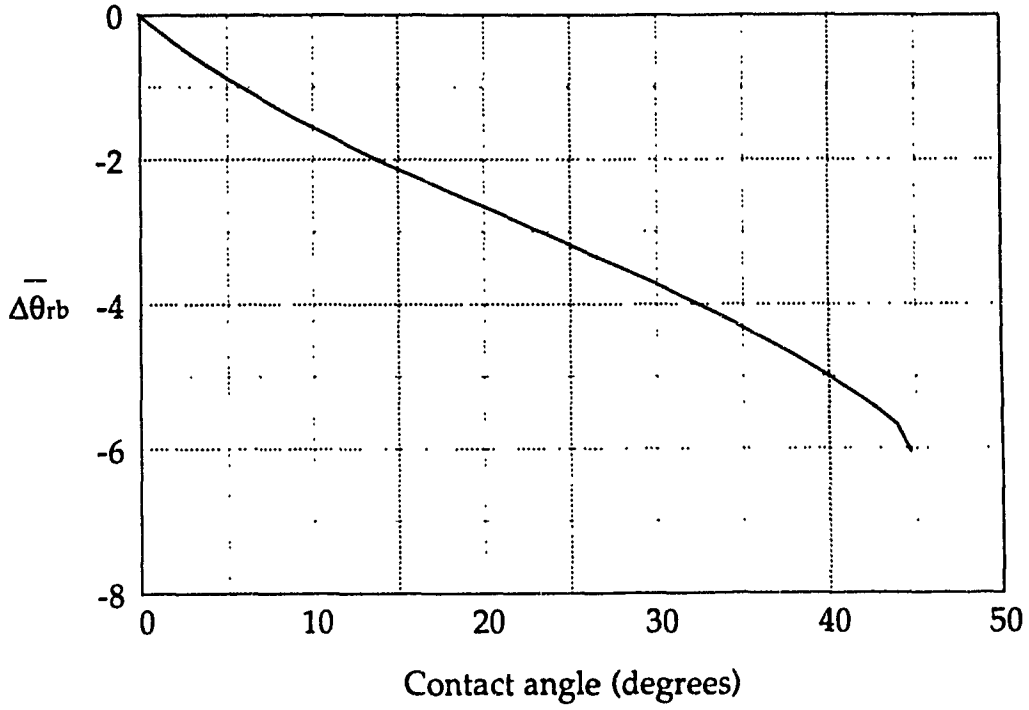

Fig.2.4.3 Comparison of the maximum interface configuration ratios of system 1 with the minimum interface configuration ratios of system 2 at $0^o \leq \alpha < 45^o$

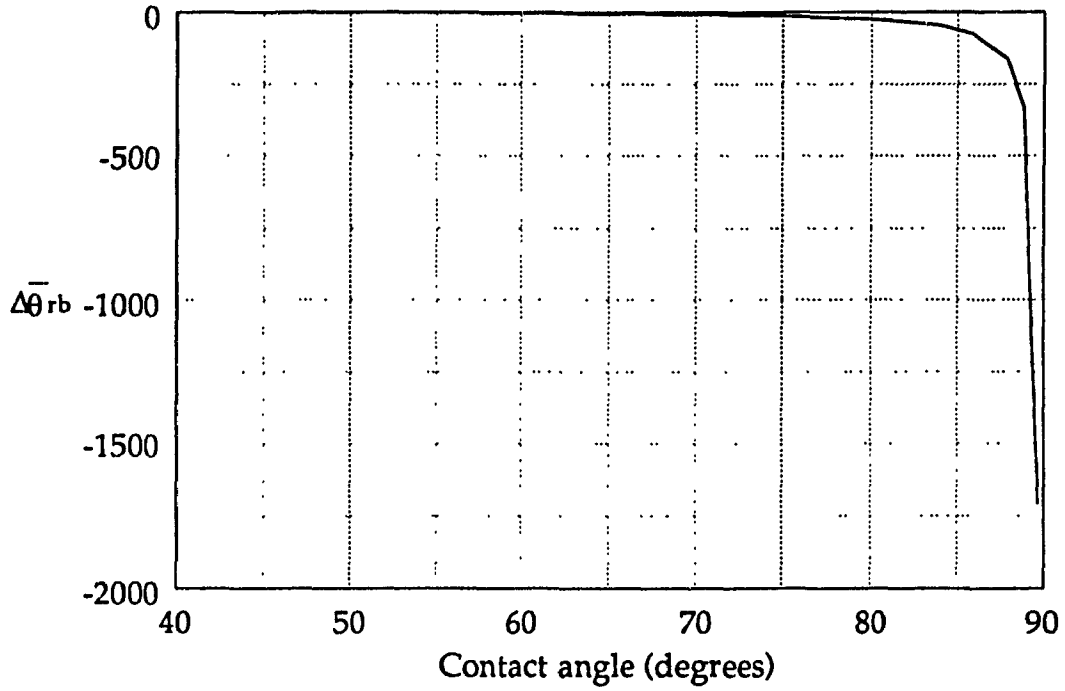

Fig.2.4.4 Comparison of the maximum interface configuration ratios of system 1 with the minimum interface configuration ratios of system 2 at $45^o < \alpha < 90^o$

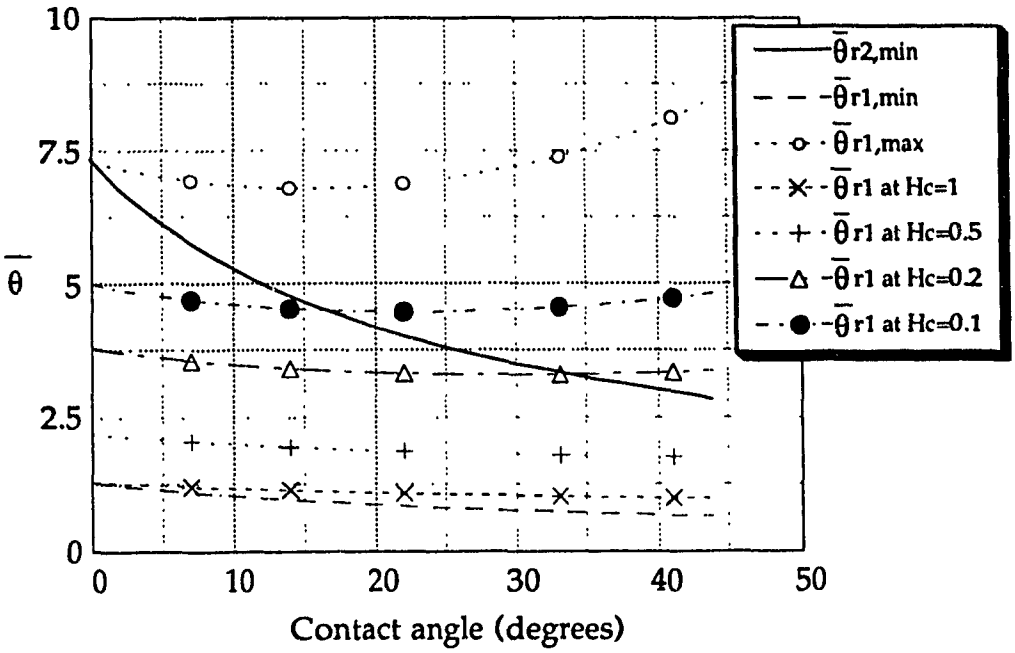

Fig.2.4.5 Interface configuration ratio changes of system 1 due to liquid depth Hc changing, compared with interface configuration ratio of system 2 at $0^o \leq \alpha < 45^o$

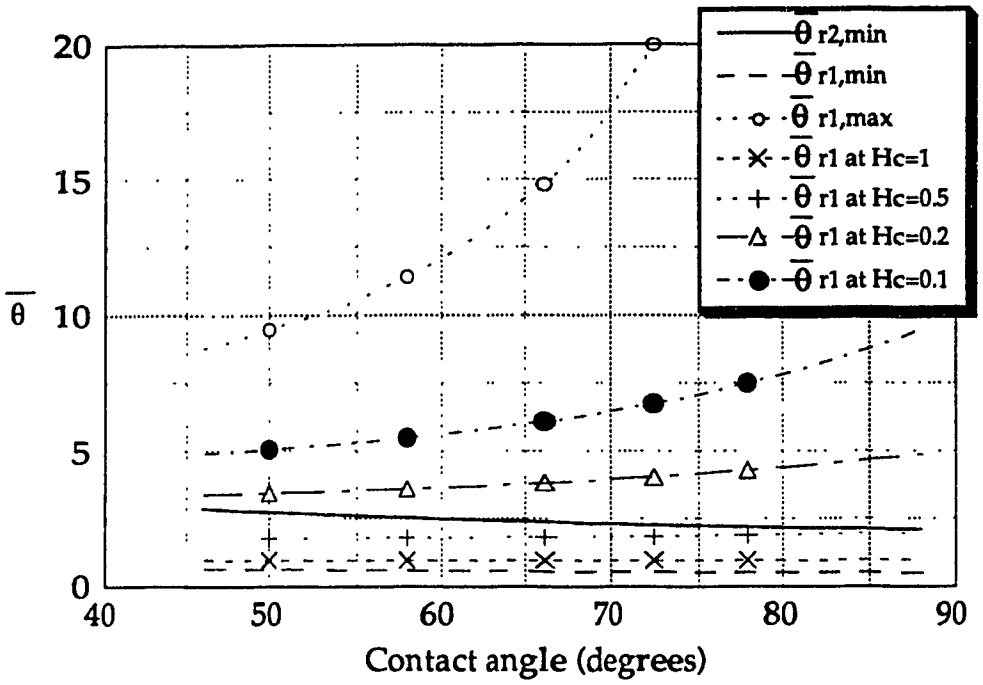

Fig.2.4.6 Interface configuration ratio changes of system 1 due to liquid depth Hc changing, compared with interface configuration ratio of system 2 at $45^{o} < \alpha < 90^{o}$

It is interesting to notice that the liquid depth required to change the configuration system is dependant on the contact angle. For example, the liquid with a contact angle less than approximately 16° at a liquid depth of 0.1 still retains configuration of system 1, while the liquid with more than 16° acquires the configuration of system 2. As for the mathematical formula, the configuration ratio goes to singularity when the contact angle reaches 45°.

2.5 Wetting Liquid Interface Configuration and Location of Liquid in Cylindrical Tanks

Similar to the analysis of rectangular tanks, two configuration systems of wetting liquid placed in a flat-bottom circular cylindrical tank in the zero gravity environment are introduced here. One of which is with the sufficient liquid volume. The other is with not enough volume of liquid to cover the base of the container under the conditions to be investigated.

2.5.1 Configuration system 3

Consider a liquid-vapor configuration system 3 of a cylindrical tank shown in Fig.2.5.1. Following the same procedure as in the rectangular tank, the interface configuration ratio θ_{c3} of surface area to liquid volume is defined by

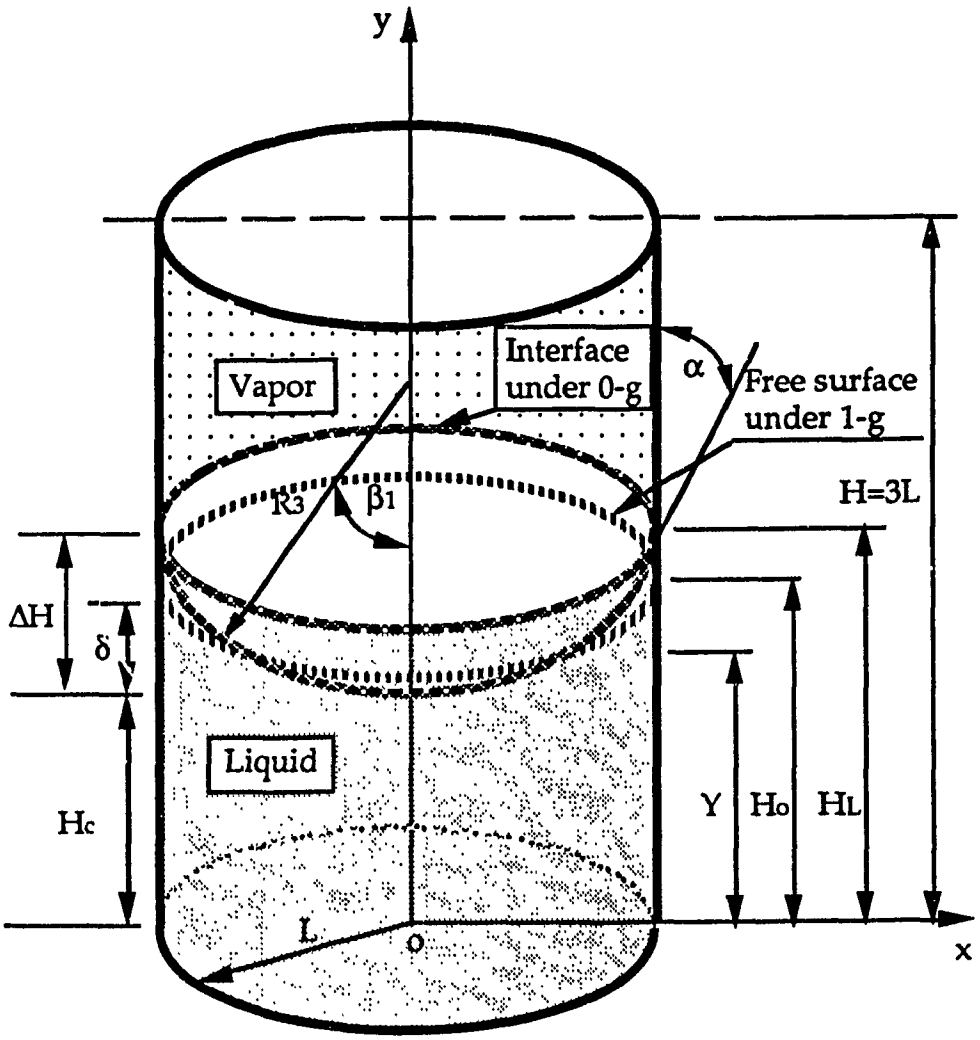

Fig.2.5.1 Wetting liquid configuration system 3 in a cylindrical tank with contact angle $0^o \leq \alpha < 90^o$ at zero-gravity

$$\theta_{c3} = \frac{2[1-\sin(\alpha)]}{\cos^2(\alpha)\left\{\frac{L[1-\sin(\alpha)][2\cos^2(\alpha)-1+\sin(\alpha)]}{3\cos^3(\alpha)} + H_c\right\}} \qquad (2.5.1)$$

$$\left(0 \le \alpha < \frac{\pi}{2}\right)$$

or in the dimensionless form

$$\bar{\theta}_{c3} = \frac{2[1-\sin(\alpha)]}{\cos^2(\alpha)\left\{\frac{[1-\sin(\alpha)][2\cos^2(\alpha)-1+\sin(\alpha)]}{3\cos^3(\alpha)} + \bar{H}_c\right\}} \qquad (2.5.2)$$

$$\left(0 \le \alpha < \frac{\pi}{2}\right)$$

In Fig.2.5.2, the result of the equation (2.5.2) shows that the configuration ratio is the function of contact angles and liquid depth.

The minimum value of $\bar{\theta}_{c3}$ will be obtained when the interface on the container wall reaches the top of a tank;

$$\bar{\theta}_{c3,min} = \frac{6\cos(\alpha)[1-\sin(\alpha)]}{3\cos^3(\alpha)+2\sin(\alpha)-2\sin^2(\alpha)-\sin(\alpha)\cos^2(\alpha)} \qquad (2.5.3)$$

while the maximum will be obtained from;

$$\bar{\theta}_{c3,max} = \frac{6\cos(\alpha)}{\cos^2(\alpha)-\sin^2(\alpha)+\sin(\alpha)} \qquad (2.5.4)$$

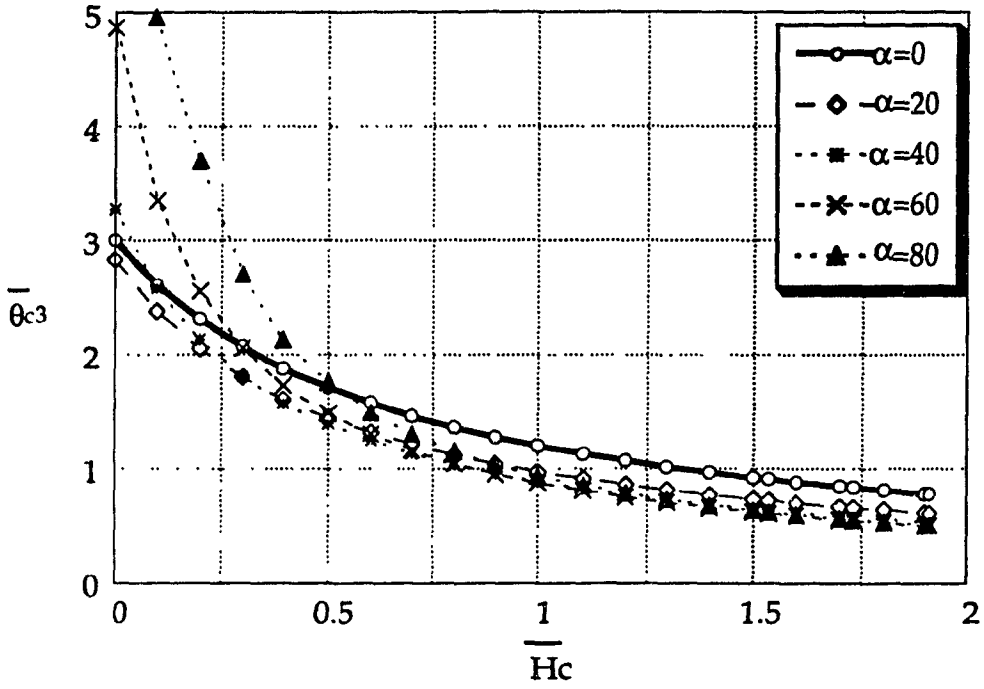

Fig.2.5.2 Interface configuration ratios versus liquid depth at different contact angles

2.5.2 Configuration system 4

The alternate interface configuration of system 4 for a cylindrical tank is presented in Figs.2.5.3 and 2.5.4 for contact angle α smaller or greater than 45°. The volume of the liquid is obtained by the integral disc method. The free surface area is calculated by revolving the liquid-vapor interface curve about the y axis. The configuration ratio θ_{c4} derived from the volume and the area is simply expressed by

$$\theta_{c4} = \frac{2 R_4 (L - h_4 \beta_3)}{\frac{4}{3}L^3 + h_4 L^2 - R_1^2 (L - h_4 \beta_3)} \qquad \left(0 \le \alpha < \frac{\pi}{4}\right) \qquad (2.5.5)$$

$$\theta_{c4} = \frac{6 R_4 \left[(h_4 + L) \beta_3 - L\right]}{L^3 - 3 R_4^2 L - 3 h_4 L^2 + 3 (h_4 + L) R_4^2 \beta_3} \qquad \left(\frac{\pi}{4} < \alpha < \frac{\pi}{2}\right) \qquad (2.5.6)$$

where

$$R_4 = \frac{\sqrt{2}\, X_c}{2 \sin \beta_2} \qquad (2.5.7)$$

$$h_4 = \frac{\sqrt{X_c^2 - L^2 \sin^2 \beta_2} - L \sin \beta_2}{2 \sin \beta_2} \qquad (2.5.8)$$

$$\beta_2 = \left|\frac{\pi}{4} - \alpha\right| \qquad (2.5.9)$$

$$\beta_3 = \frac{\pi}{2} - 2\alpha \qquad (2.5.10)$$

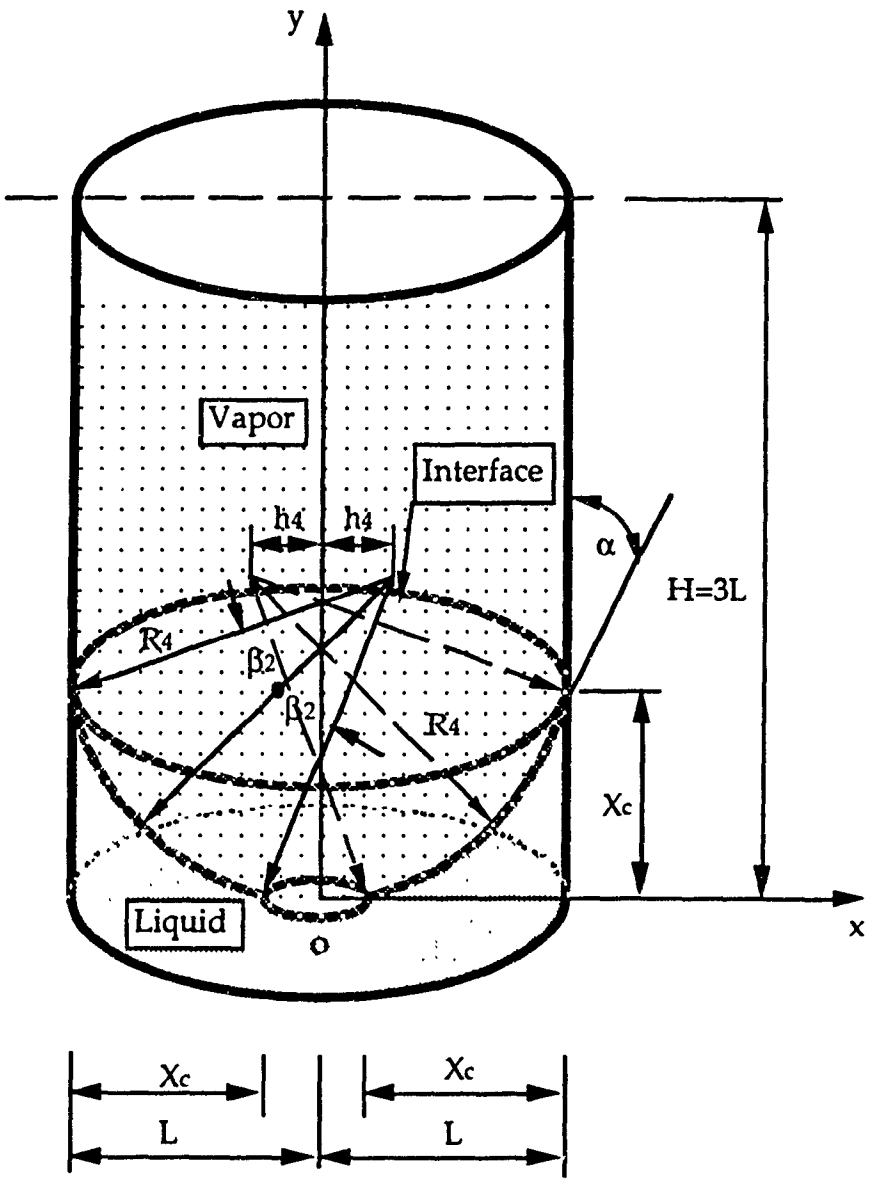

Fig.2.5.3 Wetting liquid configuration system 4 in a cylindrical tank with contact angle $0^o \leq \alpha < 45^o$ at zero-gravity

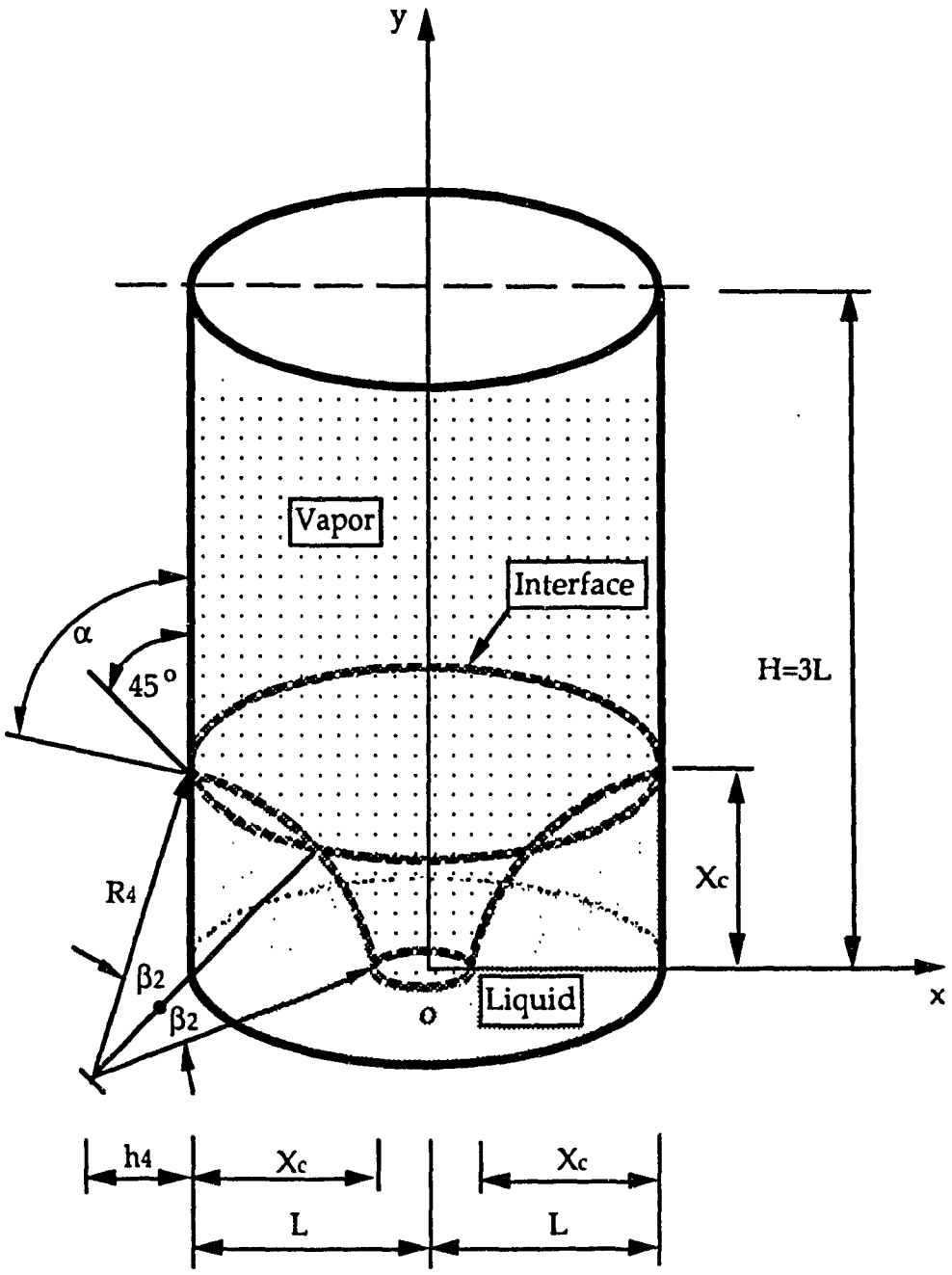

Fig.2.5.4 Wetting liquid configuration system 4 in a cylindrical tank with contact angle $45^{o} < \alpha < 90^{o}$ at zero-gravity

$$X_c = L - |x| \tag{2.5.11}$$

Inserting equations (2.5.7), (2.5.8), (2.5.10) and (2.5.11) to equations (2.5.5) and (2.5.6), gives the general expressions for the ratio of system 4:

$$\theta_{c4} = \frac{2\sqrt{2}X_c \sin\beta_2 \left\{2L\sin\beta_2 - \left[X' - L\sin\beta_2\right]\left(\frac{\pi}{2} - 2\alpha\right)\right\}}{\frac{16}{3}L^3\sin^3\beta_2 + \left[X' - L\sin\beta_2\right]\left[2L^2\sin^2\beta_2 - X_c^2\beta_3\right] - 2LX_c^2\sin\beta_2} \tag{2.5.12}$$

$$\left(0 \le \alpha < \frac{\pi}{4}\right)$$

$$\theta_{c4} = \frac{2\sqrt{2}\,X_c \sin\beta_2 \left\{\left[X' + L\sin\beta_2\right]\beta_3 - 2L\sin\beta_2\right\}}{\frac{4}{3}L^3\sin^3\beta_2 - 2LX_c^2\sin\beta_2 - 2L^2\sin^2\beta_2\left[X' - L\sin\beta_2\right] + \left[X' + L\sin\beta_2\right]X_c^2\beta_3} \tag{2.5.13}$$

$$\left(\frac{\pi}{4} < \alpha < \frac{\pi}{2}\right)$$

respectively. Where

$$X' = \sqrt{X_c^2 - L^2\sin^2\beta_2} \tag{2.5.14}$$

The value of the minimum $\theta_{c4,min}$ is reached when $X_c \rightarrow L$ in the dimensionless form:

$$\bar{\theta}_{c4,min} = \frac{2\sqrt{2}\sin\beta_2 \left\{2\sin\beta_2 - \left[\cos\beta_2 - \sin\beta_2\right]\left(\frac{\pi}{2} - 2\alpha\right)\right\}}{\frac{16}{3}\sin^3\beta_2 - 2\sin\beta_2 + \left[2\sin^2\beta_2 + \frac{\pi}{2} - 2\alpha\right]\left[\cos\beta_2 - \sin\beta_2\right]} \tag{2.5.15}$$

$$\left(0 \le \alpha < \frac{\pi}{4}\right)$$

$$\bar{\theta}_{c4,min} = \frac{2\sqrt{2}\sin\beta_2\left\{\left(\cos\beta_2+\sin\beta_2\right)\beta_3-2\sin\beta_2\right\}}{\frac{4}{3}\sin^3\beta_2-2\sin\beta_2-2\sin^2\beta_2\left(\cos\beta_2-\sin\beta_2\right)+\left(\cos\beta_2+\sin\beta_2\right)\beta_3}$$

$$\left(\frac{\pi}{4}<\alpha<\frac{\pi}{2}\right) \qquad (2.5.16)$$

2.6 Comparison Between Configuration System 3 and 4 in Cylindrical Tanks

The configuration system 3 with the minimum interface configuration ratio $\bar{\theta}_{c3,min}$ is shown in Fig.2.5.1 while the configuration system 4 with the minimum interface configuration ratio $\bar{\theta}_{c4,min}$ is shown in Figs.2.5.3 and 2.5.4 when $x_c \rightarrow L$.

The graphs of the equations (2.5.3), (2.5.4), (2.5.15) and (2.5.16) are given in Fig.2.6.1 and Fig.2.6.2 for a contact angle smaller or greater than 45^o, respectively. These results clearly show $\bar{\theta}_{c4,min}$ to be between $\bar{\theta}_{c3,min}$ and $\bar{\theta}_{c3,max}$ throughout the entire contact angle region of the wetting liquid. The following conclusion can be drawn:

$$\bar{\theta}_{c3,min} < \bar{\theta}_{c4,min} \leq \bar{\theta}_{c3,max} \qquad (2.6.1)$$

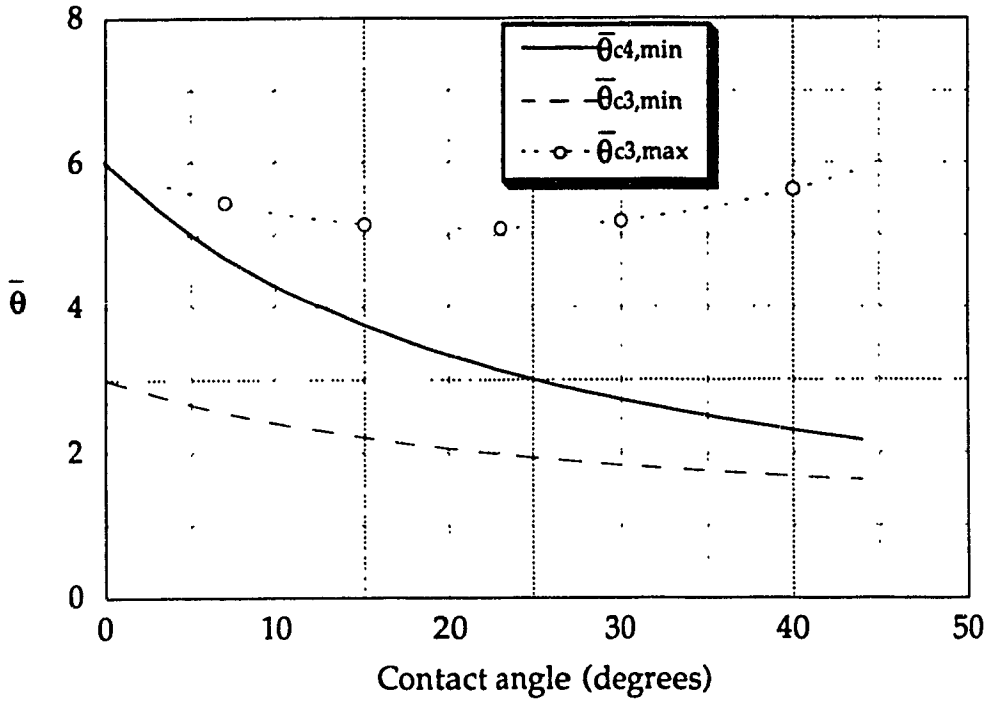

Fig.2.6.1 Interface configuration ratios of systems 3 and 4 in a cylindrical tank when contact angle $0^o \leq \alpha < 45^o$

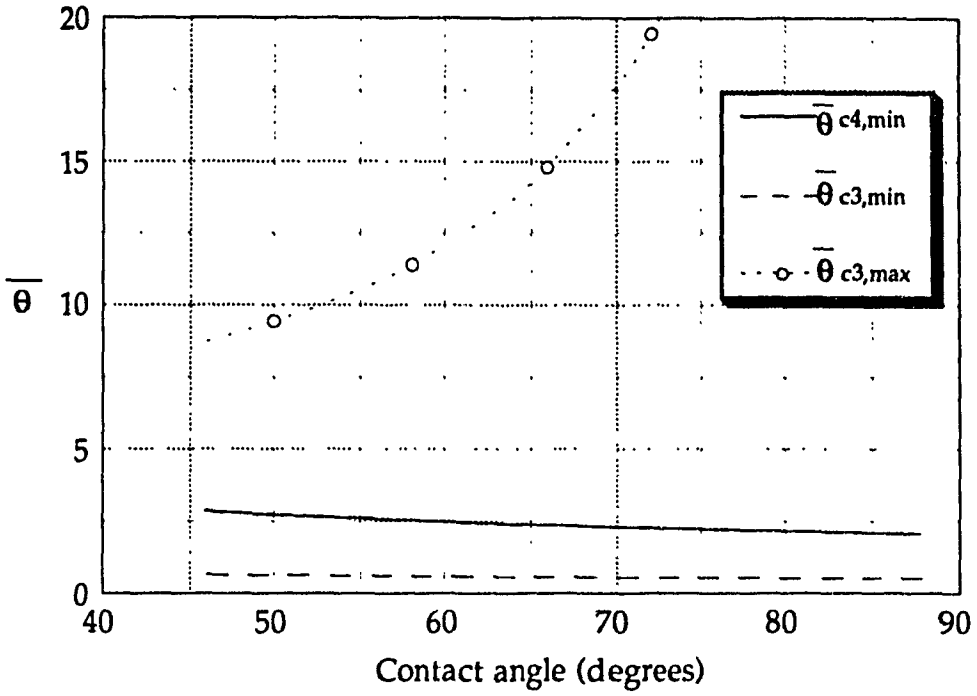

Fig.2.6.2 Interface configuration ratios of systems 3 and 4 in a cylindrical tank when contact angle $45^{o} < \alpha < 90^{o}$

2.7 Liquid Critical Depth

2.7.1 Liquid Critical Depth in Rectangular Tanks

Equations (2.3.7), (2.3.8), (2.3.12) and (2.3.7), (2.3.8), (2.3.13) are plotted in Figs.2.7.1 and 2.7.2, respectively. Similar to cylindrical containers, it is obvious that a similar conclusion is arrived at.

$$\bar{\theta}_{r1,min} < \bar{\theta}_{r2,min} \leq \bar{\theta}_{r1,max} \qquad (2.7.1)$$

When the liquid depth is large enough, the system will have the configuration of system 1, as shown in Fig.2.3.5; when the liquid level is low, the system will have the configuration of system 2 as shown in Figs.2.3.9 and 2.3.10.

Suppose the original configuration of a liquid with the contact angle of 20° is at almost full, where the configuration ratio is at $\bar{\theta}_{r1,min}$ of system 1, as indicated in Fig.2.7.3. As the liquid depth goes down due to volume decrease and $\bar{\theta}_{r1}$ increasing, the configuration of system 1 will remain unchanged until $\bar{\theta}_{r1}$ is equal to $\theta_{r2,min}$ where the configuration may change to that of system 2. When the liquid level reaches the critical depth, the ratio $\bar{\theta}_{r1}$ is larger than $\theta_{r2,min}$, the configuration will be at the system 2. There is a liquid critical depth where the configuration changes from one system to the other. At this particular depth (critical depth), the system can have either the configuration system 1 or 2. Below this depth, the configuration is that of system 2, and above that depth, the configuration is that of system 1. The dimensionless critical depth in a rectangular tank, $\bar{\gamma}_r$ is defined by

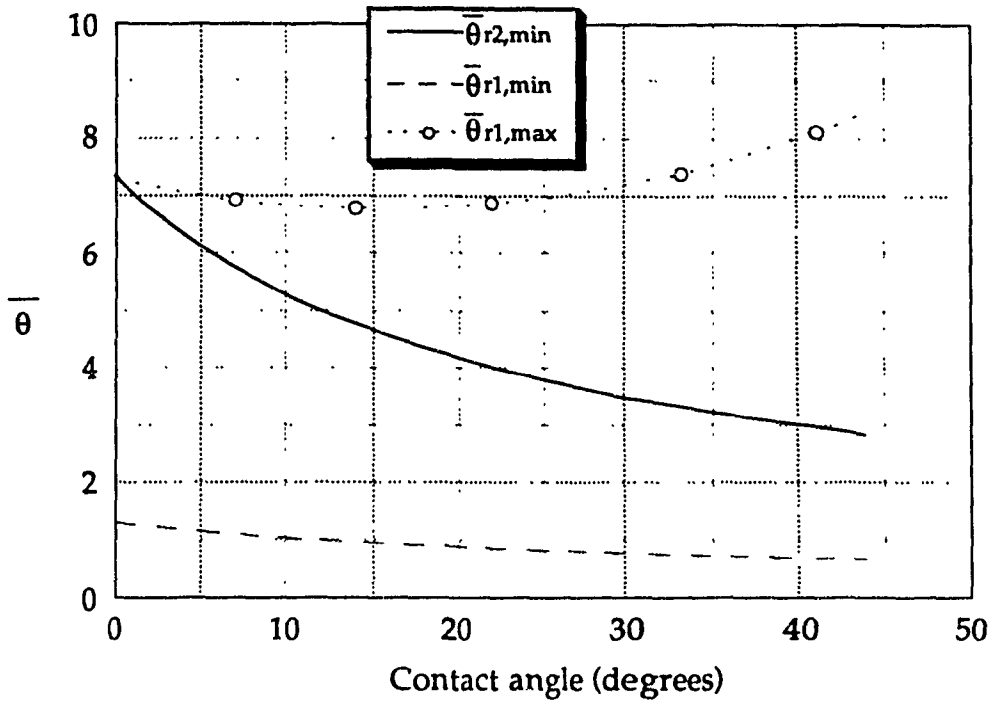

Fig.2.7.1 Interface configuration ratios of systems 1 and 2

at contact angle $0^0 \leq \alpha < 45^0$

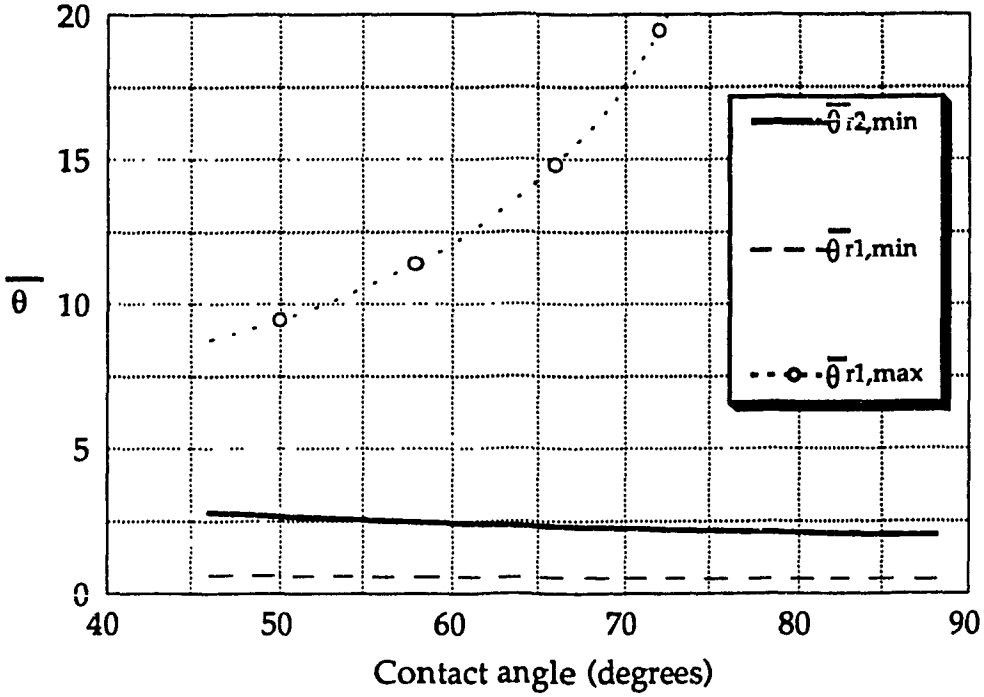

Fig.2.7.2 Interface configuration ratios of systems 1 and 2 at contact angle $45^o < \alpha < 90^o$

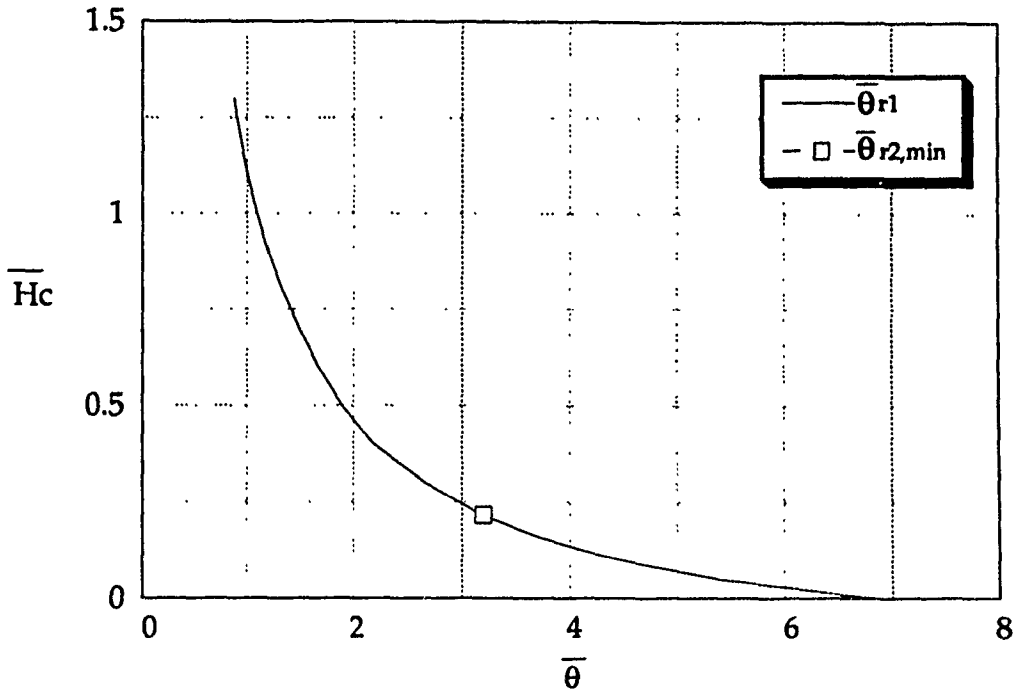

Fig.2.7.3 Interface configuration ratios versus liquid depth at the contact angle $\alpha = 20^{o}$ in a rectangular tank

$$\bar{\gamma}_r = \frac{\sqrt{2}\left(\frac{\pi}{2}-\alpha\right)\left\{2\sin^2\left(\frac{\pi}{4}-\alpha\right)+\sin\left[2\left(\frac{\pi}{4}-\alpha\right)\right]-2\left(\frac{\pi}{4}-\alpha\right)\right\}}{8\left(\frac{\pi}{4}-\alpha\right)\sin\left(\frac{\pi}{4}-\alpha\right)\cos(\alpha)} - \frac{1}{\cos(\alpha)} + \frac{\left[\sin(2\alpha)+2\left(\frac{\pi}{2}-\alpha\right)\right]}{4\cos^2(\alpha)} \qquad (2.7.2)$$

$$\left(0 \le \alpha < \frac{\pi}{4}\right)$$

$$\bar{\gamma}_r = \frac{\sqrt{2}\left(\frac{\pi}{2}-\alpha\right)\left\{2\sin^2\left(\alpha-\frac{\pi}{4}\right)-\sin\left[2\left(\alpha-\frac{\pi}{4}\right)\right]+2\left(\alpha-\frac{\pi}{4}\right)\right\}}{8\left(\alpha-\frac{\pi}{4}\right)\sin\left(\alpha-\frac{\pi}{4}\right)\cos(\alpha)} - \frac{1}{\cos(\alpha)} + \frac{\left[\sin(2\alpha)+2\left(\frac{\pi}{2}-\alpha\right)\right]}{4\cos^2(\alpha)} \qquad (2.7.3)$$

$$\left(\frac{\pi}{4} < \alpha < \frac{\pi}{2}\right)$$

where

$$\bar{\gamma}_r = \frac{\gamma_r}{L} \qquad (2.7.4)$$

If the liquid depth is greater than the critical depth, the interface configuration will remain at system 1; while the system 2 will be obtained if the liquid depth is lower than the critical depth. The experimental verification by photographic study at NASA (Petrash et al, 1963) confirmed the present analytical results and vice versa.

The critical depth can then be used to define which configuration of a system will acquire by comparing the liquid depth with the critical depth.

Figures 2.7.4 and 2.7.5 clearly demonstrates the region of configurations for a liquid system. It is a useful tool in predicting liquid location for the design of liquid tanks. The above analysis indicates that the critical depth has no relation to the height of the tank provided that the latter is higher than the critical depth, which is an important conclusion. The filling ratio of liquid volume to container volume used before might be inappropriate as an independent parameter.

The result obtained from the plots of the equation (2.7.2) and (2.7.3) indicates that the critical depth is increasing with the contact angle increase, as shown in Figs.2.7.6 and 2.7.7.

2.7.2 Liquid Critical Depth in Cylindrical Tanks

The equation (2.6.1) indicates that the $\bar{\theta}_{c4,min}$ curve is located between $\bar{\theta}_{c3,min}$ and $\bar{\theta}_{c3,max}$ curves. Thus, the configuration of system 3 will change to that of system 4 when the liquid depth is low.

The non-dimensional critical depth is

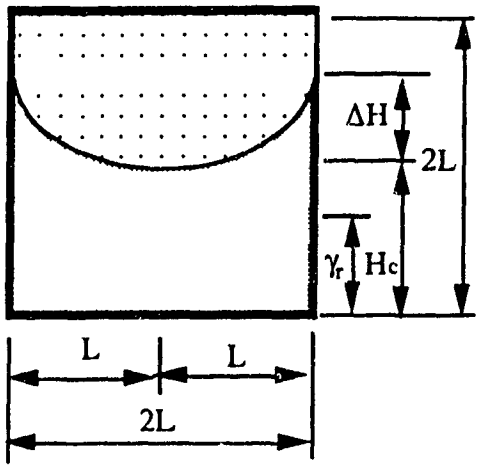

(a) Configuration system 1at liquid depth H_c > critical depth γ_r

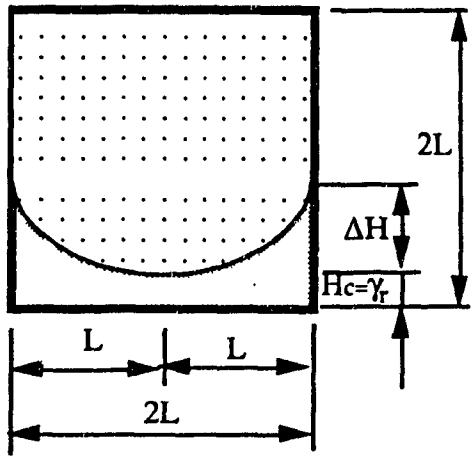

(b) Configuration system 1 at liquid depth H_c = critical depth γ_r

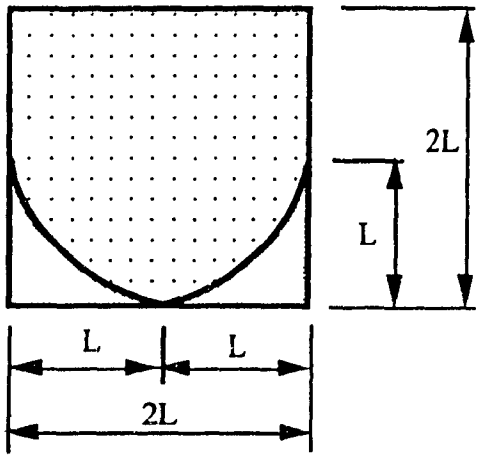

(c) Configuration system 2 at liquid depth H_c = critical depth γ_r

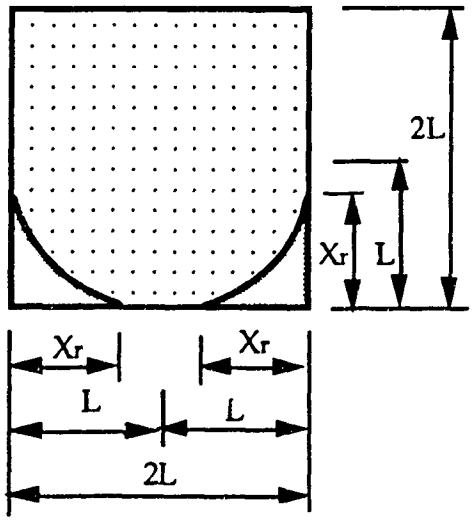

(d) Configuration system 2 at liquid depth H_c < critical depth γ_r

Fig.2.7.4 The interface configurations at different liquid depths compared with critical depth at contact angle $0^o \leq \alpha < 45^o$

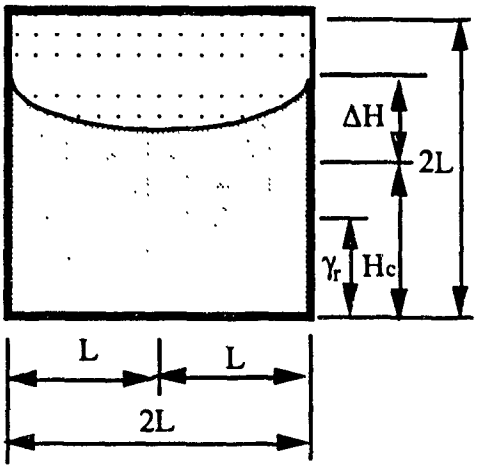

(a) Configuration system 1at liquid depth H_c > critical depth γ_r

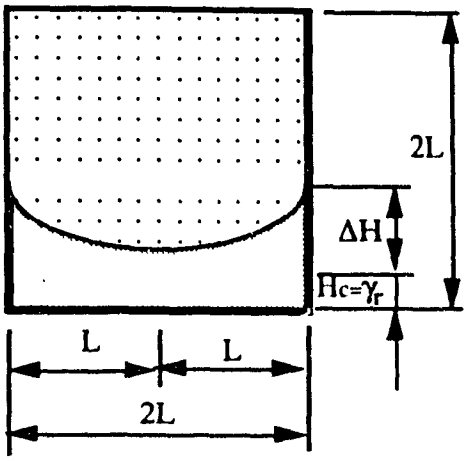

(b) Configuration system 1 at liquid depth H_c = critical depth γ_r

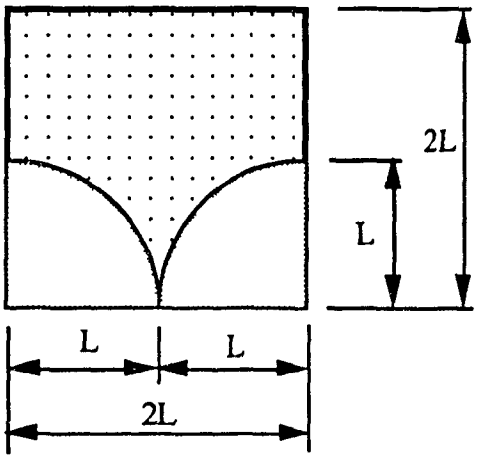

(c) Configuration system 2 at liquid depth H_c = critical depth γ_r

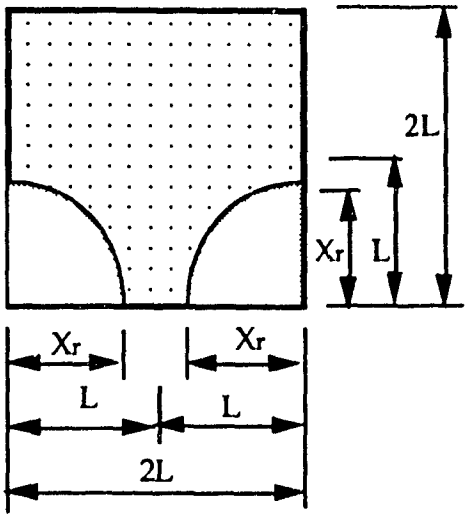

(d) Configuration system 2 at liquid depth H_c < critical depth γ_r

Fig.2.7.5 The interface configurations at different liquid depths compared with critical depth at contact angle $45^o < \alpha < 90^o$

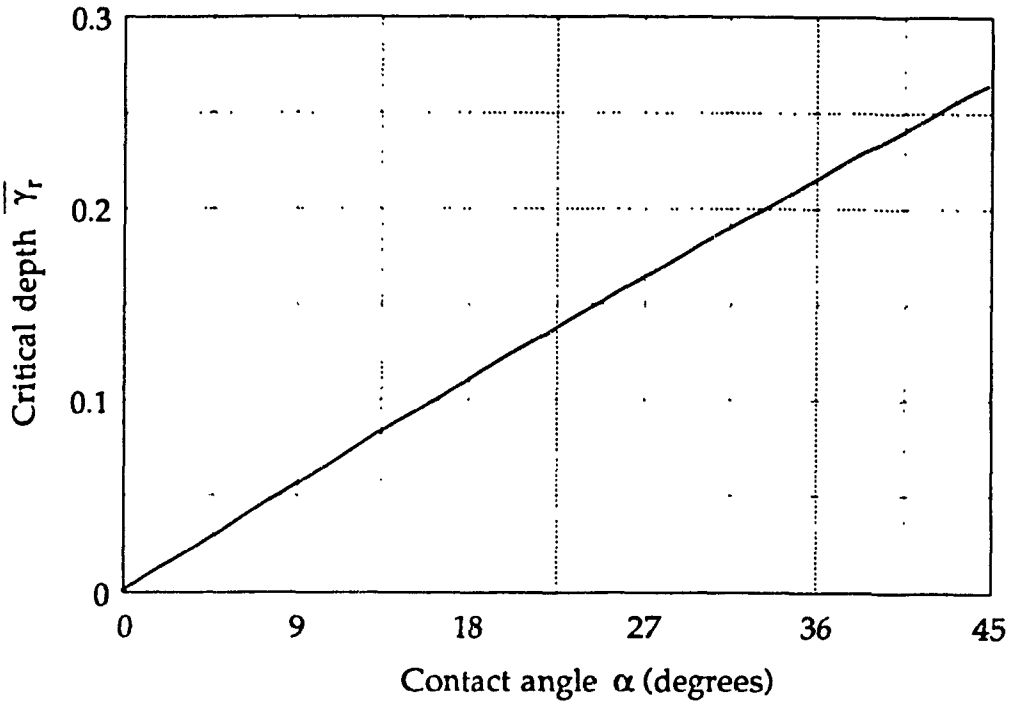

Fig.2.7.6 Liquid critical depth with the contact angle at $0^o \leq \alpha < 45^o$ in a rectangular tank

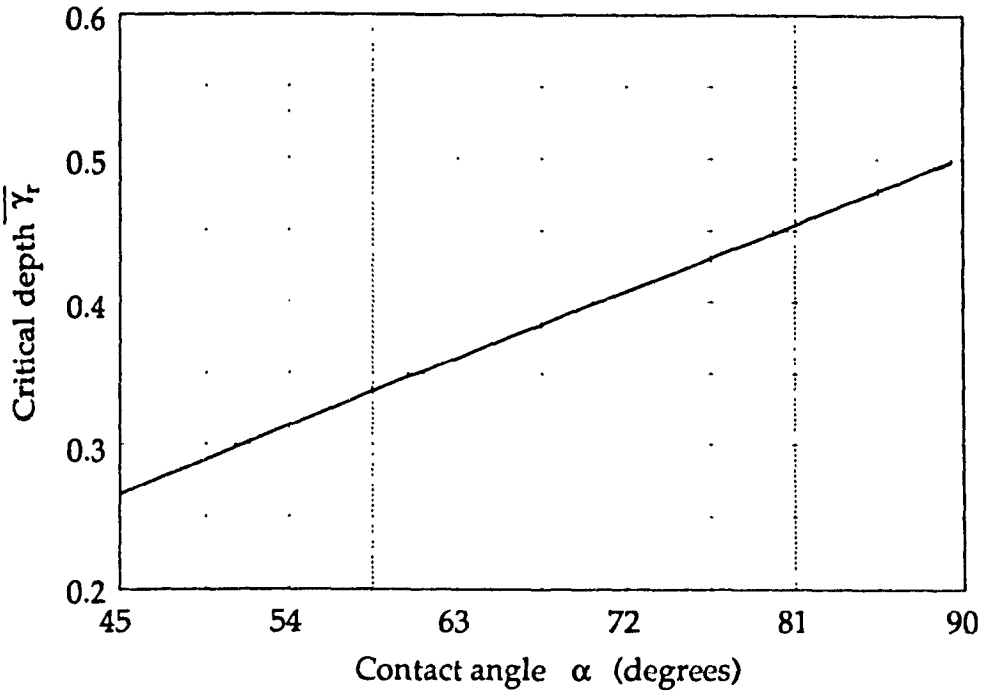

Fig.2.7.7 Liquid critical depth with the contact angle at $45^o < \alpha < 90^o$ in a rectangular tank

$$\bar{\gamma}_c = \frac{\sqrt{2}(1-\sin\alpha)\left[\frac{16}{3}\sin^3\beta_2 - 2\sin\beta_2 + \left(2\sin^2\beta_2 + \frac{\pi}{2} - 2\alpha\right)(\cos\beta_2 - \sin\beta_2)\right]}{2\sin\beta_2\cos^2\alpha\left[2\sin\beta_2 - (\cos\beta_2 - \sin\beta_2)\left(\frac{\pi}{2} - 2\alpha\right)\right]} - \frac{(1-\sin\alpha)(2\cos^2\alpha - 1 + \sin\alpha)}{3\cos^3\alpha} \qquad (2.7.6)$$

$$\left(0 \le \alpha < \frac{\pi}{4}\right)$$

$$\bar{\gamma}_c = \frac{\sqrt{2}(1-\sin\alpha)\left[\frac{4}{3}\sin^3\beta_2 - 2\sin\beta_2 - 2\sin^2\beta_2(\cos\beta_2 - \sin\beta_2)\right]}{2\sin\beta_2\cos^2\alpha\left[(\cos\beta_2 + \sin\beta_2)\left(2\alpha - \frac{\pi}{2}\right) - 2\sin\beta_2\right]} + \frac{\sqrt{2}(1-\sin\alpha)(\cos\beta_2 + \sin\beta_2)\left(2\alpha - \frac{\pi}{2}\right)}{2\sin\beta_2\cos^2\alpha\left[(\cos\beta_2 + \sin\beta_2)\left(2\alpha - \frac{\pi}{2}\right) - 2\sin\beta_2\right]} - \frac{(1-\sin\alpha)(2\cos^2\alpha - 1 + \sin\alpha)}{3\cos^3\alpha} \qquad (2.7.7)$$

$$\left(\frac{\pi}{4} < \alpha < \frac{\pi}{2}\right)$$

Below this critical depth, the configuration is at the system 4, and above that depth, the configuration is at the system 3. The results found from plotting equations (2.7.6) and (2.7.7) also illustrate that the critical depth increases when the contact angle is increased, as given in Figs.2.7.8 and 2.7.9.

The same procedures may be applied to other geometries to analyze the critical depth.

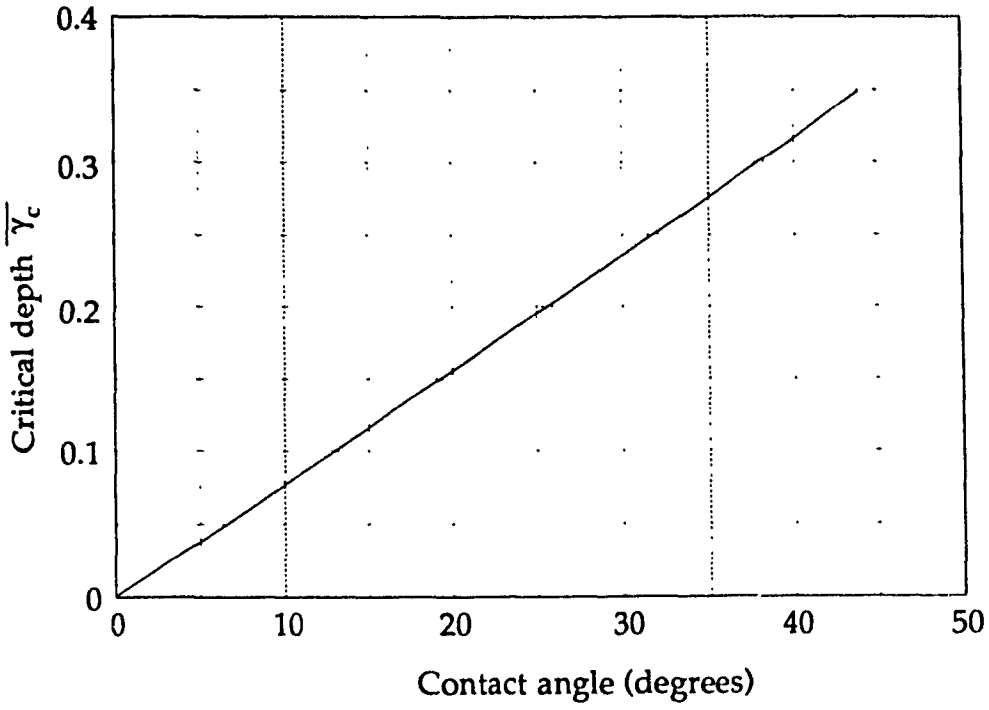

Fig.2.7.8 Liquid critical depth in a cylindrical tank with contact angles at $0^o \leq \alpha < 45^o$

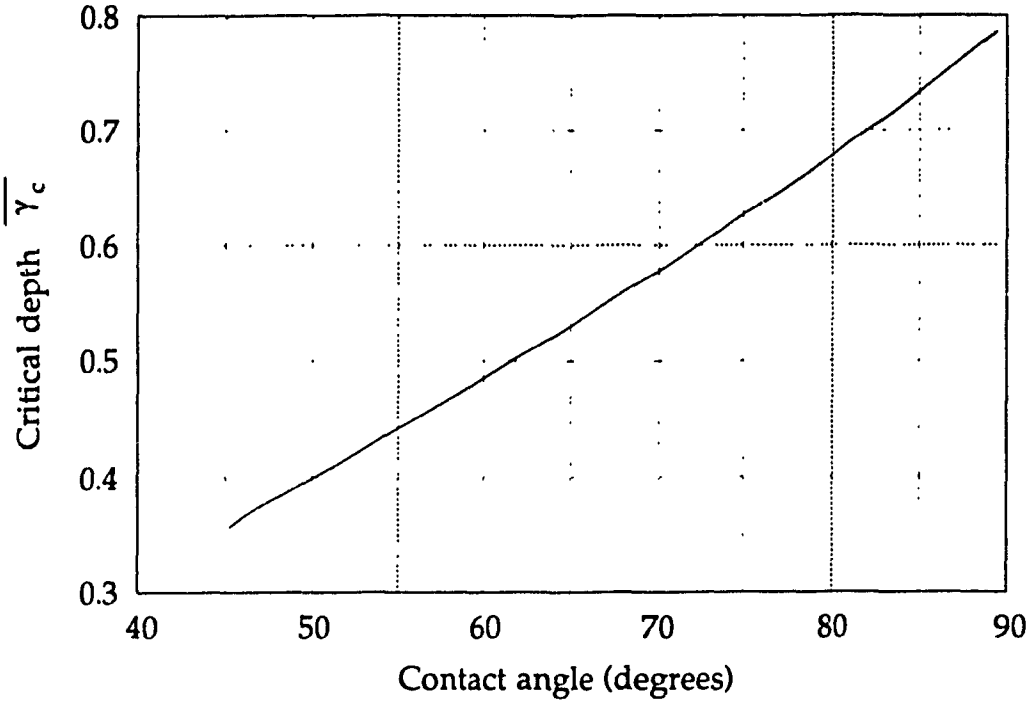

Fig.2.7.9 Liquid critical depth in a cylindrical tank with contact angles $45^o < \alpha < 90^o$

2.8 Non-wetting Liquid Interface Configuration and Comparison

Consider a rectangular tank partially filled with a non-wetting liquid where the contact angle is greater than 90 degrees. The equilibrium liquid configuration in a zero gravity environment is again a constant curvature liquid-vapor surface meeting the tank wall at the same contact angle as was observed in the terrestrial field. Sketches showing the configuration of a non-wetting liquid in a rectangular tank under zero gravity is presented in Figs.2.8.1. and 2.8.2 for configuration systems 5 and 6, respectively, depending on different liquid depths.

Following the same procedure of analysis, the interface configuration ratios are:

$$\bar{\theta}_{r5} = \frac{\beta_5}{\cos(\pi-\alpha)\left\{\bar{H} - \frac{[2-\sin(\pi-\alpha)]}{2\cos(\pi-\alpha)} + \frac{\beta_5}{2\cos^2(\pi-\alpha)}\right\}} \tag{2.8.1}$$

$$\bar{\theta}_{r5,min} = \frac{\beta_5}{\cos(\pi-\alpha)\left[2 - \frac{2-\sin(\pi-\alpha)}{2\cos(\pi-\alpha)} + \frac{\beta_5}{2\cos^2(\pi-\alpha)}\right]} \tag{2.8.2}$$

$$\bar{\theta}_{r5,max} = \frac{\beta_5}{\cos(\pi-\alpha)\left[\frac{\beta_5}{2\cos^2(\pi-\alpha)} - \frac{\sin(\pi-\alpha)}{2\cos(\pi-\alpha)}\right]} \tag{2.8.3}$$

$$\bar{\theta}_{r6,min} = \frac{2\beta_6\left[1+\sin\left(\alpha-\frac{\pi}{2}\right)\right]}{\beta_6 + \sin^2\beta_6 - \cos\beta_6\sin\beta_6} \tag{2.8.4}$$

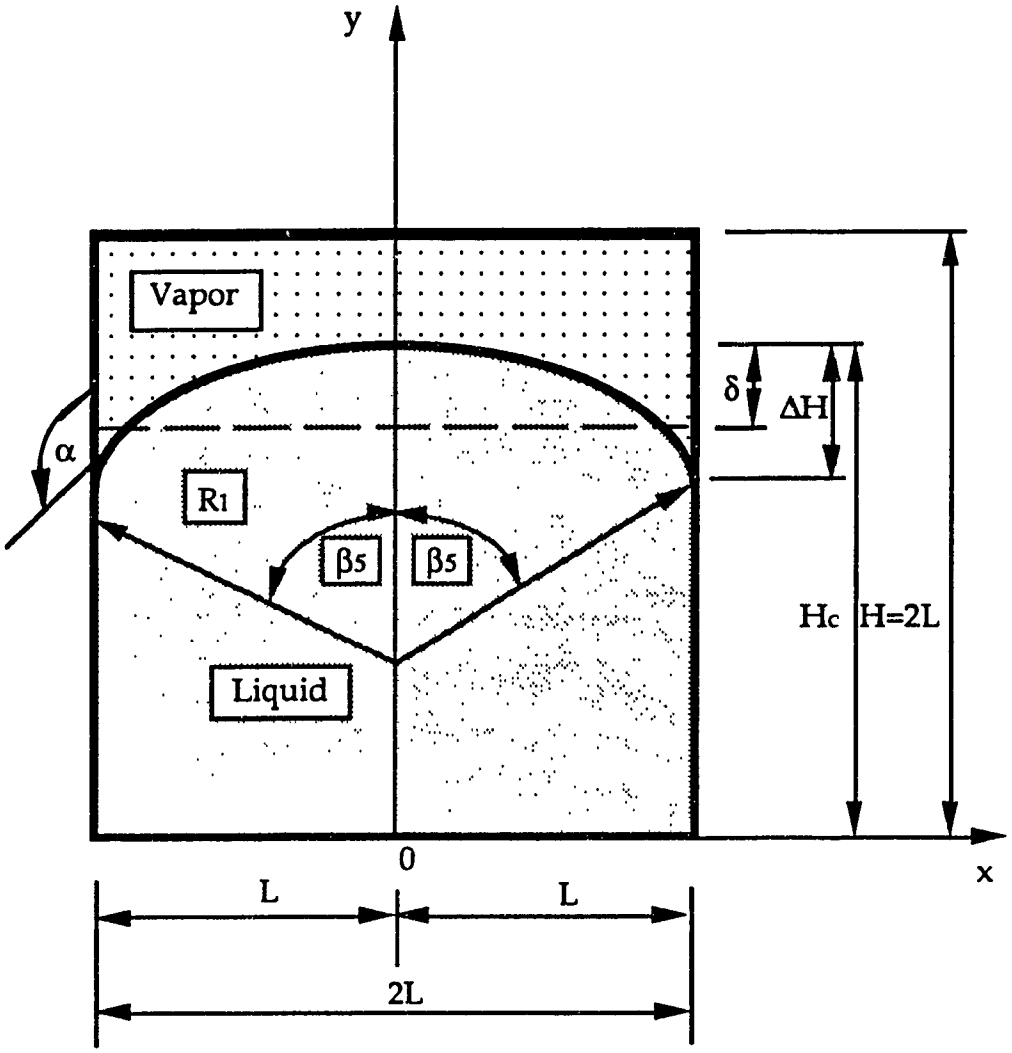

Fig.2.8.1 Non-wetting liquid configuration system 5 in a rectangular tank under zero-gravity

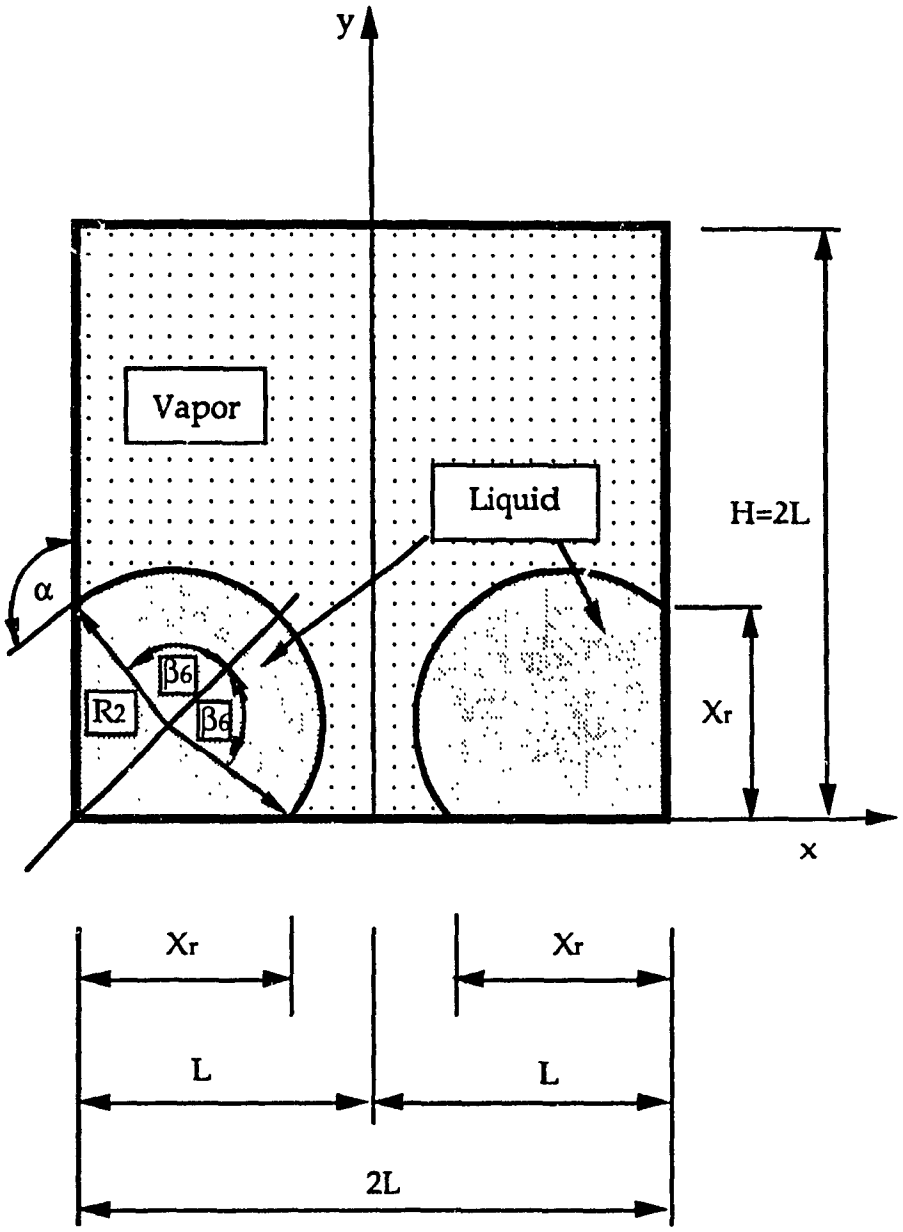

Fig.2.8.2 Non-wetting liquid configuration system 6 in a rectangular tank under zero-gravity

$$\beta_5 = \alpha - \frac{\pi}{2} \tag{2.8.5}$$

$$\beta_6 = \alpha - \frac{\pi}{4} \tag{2.8.6}$$

Fig.2.8.3 presents the plot of results of equations (2.8.2), (2.8.3) and (2.8.4). The mathematical form is

$$\bar{\theta}_{r5,min} < \bar{\theta}_{r6,min} < \bar{\theta}_{r5,max} \tag{2.8.7}$$

It indicates that a non-wetting liquid at contact angle smaller than 135 degrees has almost the same characteristics for configuration systems as of a wetting liquid, that is, when liquid depth is high enough, the configuration system is that of 5, otherwise, it is system 6.

The same principles of analytical method for non-wetting liquids at a rectangular tank system can also be extended to non-wetting liquids in a cylindrical tank system. Similar results can be predicted.

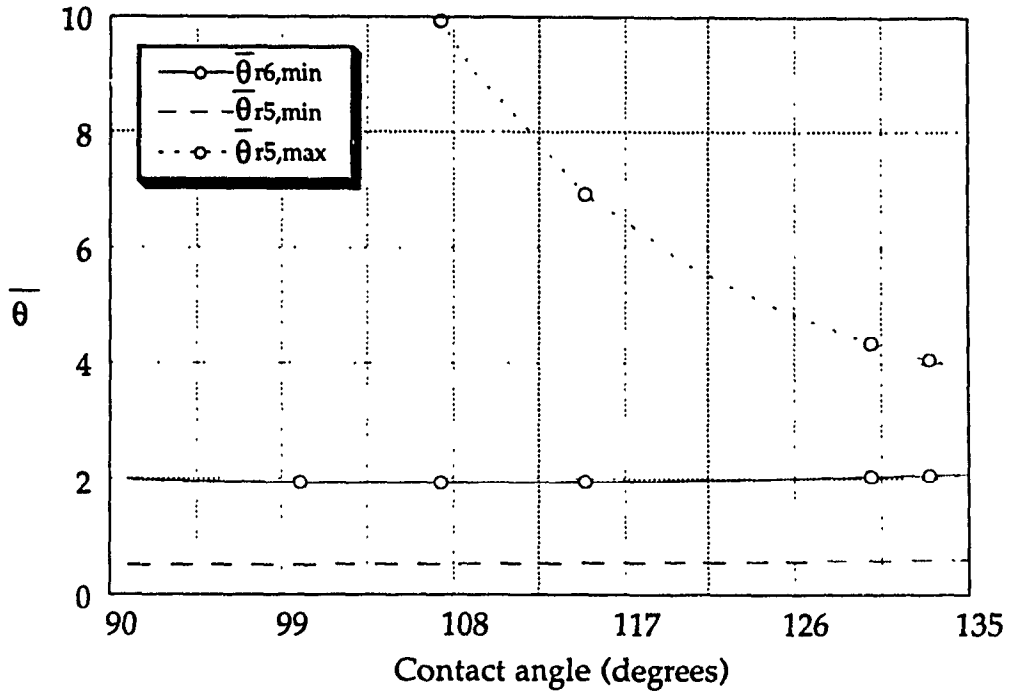

Fig.2.8.3 Comparison of interface configuration ratios between systems 5 and 6 for non-wetting liquid

CHAPTER 3

NUMERICAL SOLUTIONS

3.1 Introduction to the method

The dynamic behavior of liquids in space vehicles is a fascinating subject that has attracted the attention of researchers in recent years. When external forces are removed, the fluid mass will undergo a dynamic transition with the aim to establish a new equilibrium state. Forces and free liquid shape and position during and after the dynamic phase might dramatically affect the liquid management systems, pumping and venting, and the stability and control of the spacecraft.

Many techniques have been developed to determine liquid dynamics in zero-gravity environment. An exact solution to the general problem of liquid motion in a container on a spacecraft by the analytic method is extremely difficult. A very small fraction of a wide range of problems can be solved by classical solution methods. Since drastic simplifications with respect to the physics of the problem are required to achieve analytical solutions, the results are limited and often unrealistic. Earthbound experiments using drop towers or aircrafts suffer from an extremely low period of microgravity which is not sufficient to evaluate fluid response to dynamic disturbances. Orbital experiments provide excellent means to evaluate low-gravity fluid dynamic behavior. However at present, these are expensive and require a long lead time to carry out the tests.

The development of numerical methods and the availability of high speed computers has made possible simulations of the liquid free surface dynamics. Computational methods are characterized by a lower cost and providing sufficiently accurate information concerning the physics of the problem. For example, the computational cost is many orders of magnitude lower than the cost required for a similar experiment to be performed in orbit. It is not implied here that experimental work is not required. What is advocated is that the use of approximate solutions will give sufficient information about the problems to be encountered and will reduce the number of experiments that have to be performed in space. The computer code that will be presented here has been developed to predict liquid response characteristics for rather general conditions. The present analysis focuses the dynamic response of a liquid in rectangular and cylindrical containers, to a step transition from terrestrial to weightlessness conditions. The finite differences SOLA–VOF solution algorithm, developed by Nichols et al (1980) and Hirt (1981) was chosen to conduct the analysis. An important characteristic of this method is that it is strongly based on physical considerations, not just on mathematical manipulations. The employed numerical technique is able to successfully track the liquid-vapor interface configuration over a wide range of conditions using the fractional volume of fluid scheme and provide useful design data.

3.2 Governing Equations

The schematic of the wetting liquid problem to be studied is shown in Fig.2.1.1. Fluids to be investigated are assumed to be incompressible with constant kinematic viscosity ν. The differential equations to be solved are written in terms of Cartesian coordinates (x, y). For cylindrical (axisymmetrical) coordinates, x is the radial coordinate (represented by r), y the axial coordinate (represented by z). A coefficient ε is used to choose the coordinate system. A zero value of ε corresponds to a Cartesian geometry, whereas a value of one refers to a cylindrical geometry. The fractional volume of fluid scheme is represented by a function f(x, y, t). A unit value of f indicates a cell full of fluid while a zero value is for the cell containing no fluid. Cells with f values between zero and one contain a liquid-vapor interface.

The mass continuity equation is

$$\frac{\partial u}{\partial x} + \frac{\partial v}{\partial y} + \varepsilon \frac{u}{x} = 0 \qquad (3.2.1)$$

Momentum equations are:

x-direction or r-direction

$$\frac{\partial u}{\partial t} + u\frac{\partial u}{\partial x} + v\frac{\partial u}{\partial y} = -\frac{1}{\rho}\frac{\partial p}{\partial x} + A_x + \nu\left\{\frac{\partial^2 u}{\partial x^2} + \frac{\partial^2 u}{\partial y^2} + \varepsilon\left(\frac{1}{x}\frac{\partial u}{\partial x} - \frac{u}{x^2}\right)\right\} \qquad (3.2.2)$$

y-direction or z-direction

$$\frac{\partial v}{\partial t} + u\frac{\partial v}{\partial x} + v\frac{\partial v}{\partial y} = -\frac{1}{\rho}\frac{\partial p}{\partial y} + A_y + \nu\left\{\frac{\partial^2 v}{\partial x^2} + \frac{\partial^2 v}{\partial y^2} + \frac{\varepsilon}{x}\frac{\partial v}{\partial x}\right\} \tag{3.2.3}$$

The equation of the fractional volume of fluid is:

$$\frac{\partial f}{\partial t} + \frac{\partial fu}{\partial x} + \frac{\partial fv}{\partial y} + \varepsilon\frac{fu}{x} = 0 \tag{3.2.4}$$

Laplace's equation for surface tension effects is:

$$P_s = -\sigma\left\{\frac{d}{dx}\left[\frac{\frac{dy}{dx}}{\sqrt{1+\left(\frac{dy}{dx}\right)^2}}\right] + \frac{\varepsilon}{x}\left[\frac{\frac{dy}{dx}}{\sqrt{1+\left(\frac{dy}{dx}\right)^2}}\right]\right\} \tag{3.2.5}$$

The velocity components u, v are in the Cartesian coordinate directions x, y or cylindrical coordinate direction r, z, respectively. Body or gravitational accelerations are denoted by A_x, A_y. Fluid density is denoted by ρ. Surface tension is expressed by σ. P_s is the surface pressure.

3.3 Finite Difference of Momentum Equations

The finite difference mesh used for numerically solving the differential equations consists of uniform rectangular cells of width Δx and height Δy. Fluid velocities and pressures as well as the fractional volume of fluid are located at cell positions as shown in Fig.3.3.1. The u-velocity component is at the middle of the vertical sides of a cell. The v-velocity component is located at the middle of the horizontal sides. Pressure and fractional volume of fluid are at the cell center. The finite difference notation in Fig.3.3.1, subscripts i and j denote ith cell in the x-direction and jth cell in the y-direction at cell centers, $i+\frac{1}{2}$ denotes the right cell edge, and $j+\frac{1}{2}$ denotes the upper cell edge.

The finite difference of momentum equations are

$$u^{n+1}_{i+\frac{1}{2}j} = u_{i+\frac{1}{2}j} + \Delta t \left\{ \frac{p^{n+1}_{i,j} - p^{n+1}_{i+1,j}}{\frac{\rho \Delta x}{2}(f_{i,j} + f_{i+1,j})} + A_x - FLUX - FLUY + VISCX \right\} \tag{3.3.1}$$

$$v^{n+1}_{i,j+\frac{1}{2}} = v_{i,j+\frac{1}{2}} + \Delta t \left\{ \frac{p^{n+1}_{i,j} - p^{n+1}_{i,j+1}}{\frac{\rho \Delta y}{2}(f_{i,j} + f_{i,j+1})} + A_y - FLVX - FLVY + VISCY \right\} \tag{3.3.2}$$

where Δt is the time increment. The superscript on quantities evaluated at time $n\Delta t$ are omitted, while n+1 means the next time step. The advective and viscous terms in equations (3.3.1) and (3.3.2) are defined by the followings:

$$FLUX = \frac{u_{i+\frac{1}{2}j}}{2\Delta x}\left\{ u_{i+\frac{3}{2}j} - u_{i-\frac{1}{2}j} + \psi\left[sgn\left(u_{i+\frac{1}{2}j}\right)\right]\left(2\,u_{i+\frac{1}{2}j} - u_{i+\frac{3}{2}j} - u_{i-\frac{1}{2}j}\right)\right\} \tag{3.3.3}$$

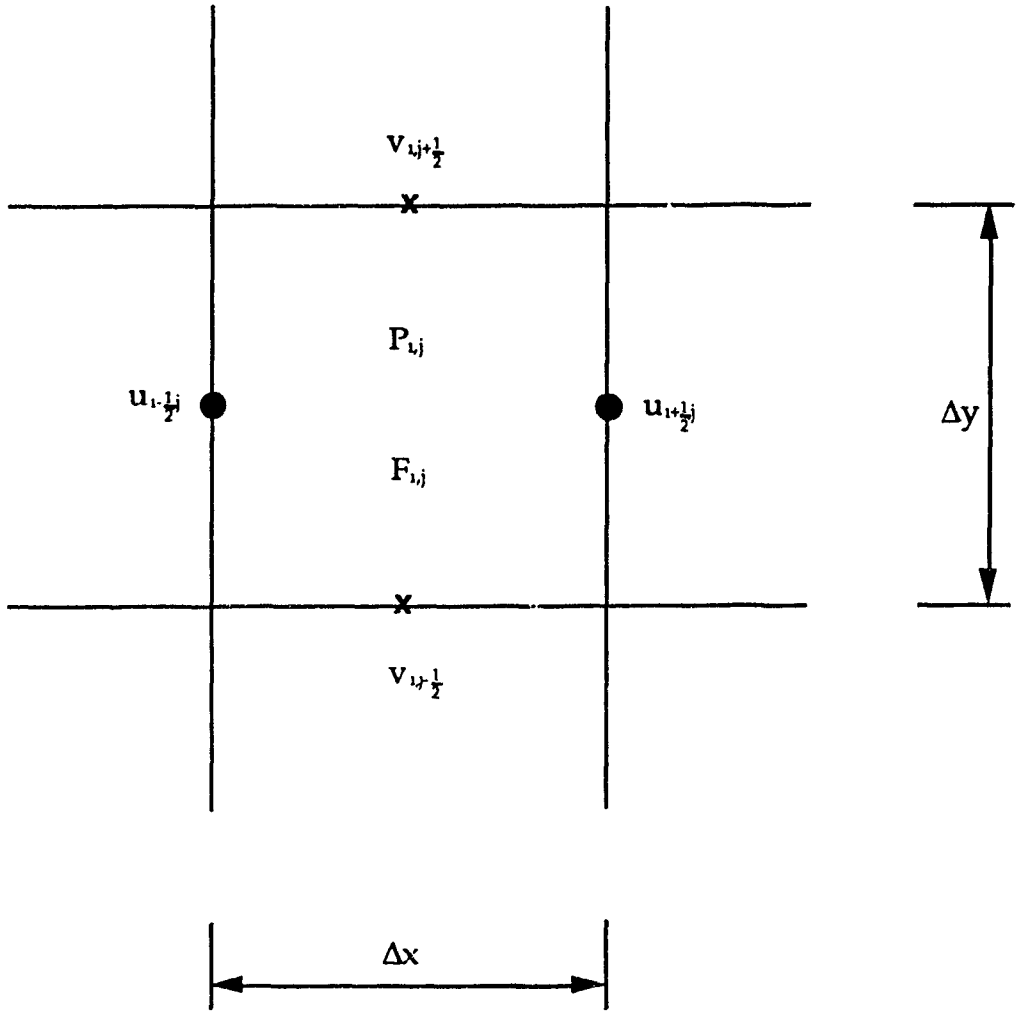

Fig.3.4.1 Location of variable components in a cell

$$FLUY = \frac{v_{av}}{2\Delta y}\left(u_{i+\frac{1}{2},j+1} - u_{i+\frac{1}{2},j-1} + \psi\left[\mathrm{sgn}\,(v_{av})\right]\left(2\,u_{i+\frac{1}{2},j} - u_{i+\frac{1}{2},j-1} - u_{i+\frac{1}{2},j+1}\right)\right) \tag{3.3.4}$$

$$v_{av} = \frac{1}{4}\left(v_{i+1,j-\frac{1}{2}} + v_{i,j+\frac{1}{2}} + v_{i,j-\frac{1}{2}} + v_{i+1,j+\frac{1}{2}}\right) \tag{3.3.5}$$

$$VISCX = \frac{\nu}{\Delta x^2}\left(u_{i+\frac{3}{2},j} - 2\,u_{i+\frac{1}{2},j} + u_{i-\frac{1}{2},j}\right) + \frac{\nu}{\Delta y^2}\left(u_{i+\frac{1}{2},j+1} - 2\,u_{i+\frac{1}{2},j} + u_{i+\frac{1}{2},j-1}\right) \tag{3.3.6}$$

$$+ \nu\,\varepsilon\left[\frac{u_{i+\frac{3}{2},j} - u_{i-\frac{1}{2},j}}{2\,\Delta x^2\,(i-1)} - \frac{u_{i+\frac{1}{2},j}}{\Delta x^2\,(i-1)^2}\right]$$

$$FLVX = \frac{u_{av}}{2\Delta x}\left(v_{i+1,j+\frac{1}{2}} - v_{i-1,j+\frac{1}{2}} + \psi\left[\mathrm{sgn}\,(u_{av})\right]\left(2\,v_{i,j+\frac{1}{2}} - v_{i-1,j+\frac{1}{2}} - v_{i+1,j+\frac{1}{2}}\right)\right) \tag{3.3.7}$$

$$FLVY = \frac{v_{i,j+\frac{1}{2}}}{2\,\Delta y}\left(v_{i,j+\frac{3}{2}} - v_{i,j-\frac{1}{2}} + \psi\left[\mathrm{sgn}\left(v_{i,j+\frac{1}{2}}\right)\right]\left(2\,v_{i,j+\frac{1}{2}} - v_{i,j-\frac{1}{2}} - v_{i,j+\frac{3}{2}}\right)\right) \tag{3.3.8}$$

$$u_{av} = \frac{1}{4}\left(u_{i-\frac{1}{2},j} + u_{i-\frac{1}{2},j+1} + u_{i+\frac{1}{2},j} + u_{i+\frac{1}{2},j+1}\right) \tag{3.3.9}$$

$$VISCY = \frac{\nu}{\Delta x^2}\left(v_{i+1,j+\frac{1}{2}} - 2\,v_{i,j+\frac{1}{2}} + v_{i-1,j+\frac{1}{2}}\right) + \frac{\nu}{\Delta y^2}\left(v_{i,j+\frac{3}{2}} - 2\,v_{i,j+\frac{1}{2}} + v_{i,j-\frac{1}{2}}\right) \tag{3.3.10}$$

$$+ \nu\,\varepsilon\left[\frac{v_{i+1,j+\frac{1}{2}} - v_{i-1,j+\frac{1}{2}}}{2\,\Delta x^2\,(i-1.5)}\right]$$

where $\mathrm{sgn}(u_{av})$ represents the sign of u_{av}. A parameter Ψ governs the choice of the donor-cell or centered-difference approximations. The second order centered-difference approximation is indicated by a zero value of Ψ. When Ψ is equal to unity, the first order donor-cell form is obtained. A Ψ value between zero and one corresponds to the approximation between first order and second order, which can be easily adjusted to satisfy both numerical stability and accuracy requirement.

3.4 Finite Difference of Continuity Equation

The velocities computed from equations (3.3.1) and (3.3.2) will not, in general, satisfy the continuity equation. The pressure must be adjusted in each computational cell to arrive at the required values of velocities. The finite difference form for continuity equation is:

$$D_{i,j}^{n+1} = \frac{u_{i+\frac{1}{2},j}^{n+1} - u_{i-\frac{1}{2},j}^{n+1}}{\Delta x} + \frac{v_{i,j+\frac{1}{2}}^{n+1} - v_{i,j-\frac{1}{2}}^{n+1}}{\Delta y} + \varepsilon \frac{\left(u_{i+\frac{1}{2},j}^{n+1} - u_{i-\frac{1}{2},j}^{n+1}\right)}{2\,(i - 1.5)\,\Delta x} = 0 \qquad (3.4.1)$$

If the divergence of a cell, $D_{i,j}^{n+1}$, is negative value indicating a net flow of mass into the cell, the cell pressure is needed to be increased to eliminate the inflow. Likewise, the pressure is decreased to draw a flow back when there is the net flow out of the cell. Because there is one pressure variable for each cell, the divergence for each cell can be driven to zero in this way. The pressure change Δp to drive $D_{i,j}^{n+1}$ to zero for an interior cell containing fluid and for a free surface cell is described by equations (3.4.2) and (3.4.3), respectively.

$$\Delta p = -\frac{D_{i,j}^{n+1}}{2\,\Delta t\left[\frac{1}{(\Delta x)^2} + \frac{1}{(\Delta y)^2}\right]} \qquad (3.4.2)$$

$$\Delta p = (1 - \eta)\, P_n + \eta P_s - P_{i,j} \qquad (3.4.3)$$

where P_s is a pressure at the surface, P_n is a pressure inside the fluid and $P_{i,j}$ is the surface cell pressure. η is the ratio of the distance between the cell centers and the distance between the free surface and the center of the interpolation cell.

The new cell pressure is then adjusted to

$$P_{i,j} + \Delta p \tag{3.4.4}$$

and thus new velocity components located on the sides of the cell are adjusted to reflect this change.

$$u_{i+\frac{1}{2},j} \Rightarrow u_{i+\frac{1}{2},j} + \frac{\Delta t\, \Delta p}{\Delta x} \tag{3.4.5}$$

$$u_{i-\frac{1}{2},j} \Rightarrow u_{i-\frac{1}{2},j} - \frac{\Delta t\, \Delta p}{\Delta x} \tag{3.4.6}$$

$$v_{i,j+\frac{1}{2}} \Rightarrow v_{i,j+\frac{1}{2}} + \frac{\Delta t\, \Delta p}{\Delta y} \tag{3.4.7}$$

$$v_{i,j-\frac{1}{2}} \Rightarrow v_{i,j-\frac{1}{2}} - \frac{\Delta t\, \Delta p}{\Delta y} \tag{3.4.8}$$

The iteration of the pressure adjustment usually is required because its neighbors are affected when one cell is adjusted. The iteration proceeds by sweeping the computational mesh row by row starting with the bottom and working upward. For each cell, the divergence, $D_{i,j}^{n+1}$, is computed using the

most current velocity values available. If D values in all cells reach a very small number, typically of order 10^{-3} or smaller, the iteration is considered to arrive at convergence. Multiplication of Δp by a coefficient ω can be used to accelerate the convergence of the iteration. The value of ω in this solution is set to 1.7.

3.5 Fractional Volume of Fluid and Surface Tension

The function of fractional volume of fluid is governed by equation (3.2.4). A straight line cutting through a cell can be assumed as an approximate interface. The interface slope is determined using a function $Y(x)$ or $X(y)$, depending on its orientation. When the interface is described by $Y(x)$, it is approximated to

$$Y_i = Y(x_i) = [f(i, j-1) + f(i, j) + f(i, j+1)]\,\Delta y \qquad (3.5.1)$$

then

$$\left(\frac{dY}{dx}\right)_i = \frac{Y_{i+1} - Y_{i-1}}{2\Delta x} \qquad (3.5.2)$$

dX/dy can also be obtained in the same way.

The smaller value between the $\left|\frac{dY}{dx}\right|$ and $\left|\frac{dX}{dy}\right|$ is chosen to be the approximation of the slope. After determining the slope of this line, it can

then be constructed in the cell with the known amount of f volume lying on the f fluid side. This line provides the information for the application of free surface pressure boundary conditions. Once the curvature in each free surface cell is obtained from the function $Y(x)$ or $X(y)$, the surface tension pressure can be found.

3.6 Boundary Conditions

Boundary conditions are satisfied by setting appropriate velocities in the fictitious cells surrounding the mesh. The left boundary will be discussed as follows while the boundary conditions at other walls are analogous. If this is a no-slip rigid wall, for all jth row,

$$u_{1,j} = 0 \tag{3.6.1}$$

$$v_{1,j} = - v_{2,j} \tag{3.6.2}$$

If it is a rigid free-slip wall, for all jth row,

$$u_{1,j} = 0 \tag{3.6.3}$$

$$v_{1,j} = v_{2,j} \tag{3.6.4}$$

The continuative boundary conditions used at the left wall for all jth row are

$$u_{1,j} = u_{2,j} \tag{3.6.5}$$

$$v_{1,j} = v_{2,j} \tag{3.6.6}$$

No-slip and free-slip conditions are imposed on the velocities computed from the momentum equations and after each time cycle of pressure iteration through the mesh. These continuative boundary conditions, however, are only imposed after applying the momentum equations and not after each cycle through the pressure iteration. P and f given in the following equations are imposed to no-slip, free-slip and continuative conditions.

$$P_{1,j} = P_{2,j} \tag{3.6.7}$$

$$f_{1,j} = f_{2,j} \tag{3.6.8}$$

For the free surface boundary conditions, velocities are set to vanish the divergence on every cell boundary between a surface cell and an empty one. Zero values for $\frac{\partial u}{\partial y}$ or $\frac{\partial v}{\partial x}$ are also used to set exterior tangent velocities to a free surface on boundaries between empty cells adjacent to a surface cell. The free surface boundary condition for normal stress is also satisfied by the equation (3.4.3).

3.7 Computational Procedure

The fluid computation is advanced through a series of time cycles. Each time cycle at one increment in time, Δt, consists of three steps:

(a) Finite difference approximations of the Navier-Stokes equations are used to compute the first guess for new time level velocities using the initial conditions or previous time cycle values for all advective, pressure, and viscous terms.

(b) Pressures are iteratively adjusted in each cell and then the velocity changes induced by each pressure change are added to the previous velocities obtained from the last step in order to satisfy the continuity equation. Iterations usually are necessary because the pressure variation required in one cell to satisfy equation (3.2.1) will affect the four adjacent cells.

(c) The function of fractional volume of fluid defining fluid regions is calculated accordingly to give the new fluid configuration.

At each step, suitable boundary conditions must be imposed at all mesh and free surface boundary cells. Repetition of these steps will arrive at a solution through any desired time period.

The computational code is mostly run on the Digital Equipment VAX 6510 computer (VMS system), called VAX2; while the result data processes and vector plots are performed on SUN STATION computers, called

MAXWELL (UNIX system) at the Concordia University. From 5X16 to 20X24 cells are usually used for the analysis. The CPU time used for running the program varies mostly from 15 minutes to 3 hours on VAX 6510, depending on the problem to be dealt with.

3.8 Discussion of Conservative and Non-conservative Form

The substitution of the continuity equation (3.2.1) into momentum equation (3.2.2) and (3.2.3), yields the conservative form of momentum, which is widely used in the past (Welch et al, 1966; Hirt et al, 1975). For this form, the divergence D is required to be vanished. However, in the numerical method, it is sometimes hard to insure the exact zero value of the divergences in the continuity and momentum equations because of the errors resulting from the pressure iteration, the inherent errors in finite differences and roundoff errors by the computer. The computational results obtained from the comparison of conservative with non-conservative forms confirm that the non-conservative form might be advantageous.

CHAPTER 4

RESULTS OF THE NUMERICAL SIMULATIONS

4.1 Liquid-vapor Interface Dynamics and Configurations

The dynamic behavior of the liquid-vapor during a step transition from terrestrial conditions to weightlessness and its configuration when all the transient effects have died down are the subject of the present investigations. The hypothesis concerning the most probable liquid-vapor interface position for heights less than the critical depth will be also verified by solving the complete set of fluid equations. Since only limited experimental data in microgravity environment from the literature are available, they are used as reference for studying the deviation of the dynamic behavior obtained from the numerical analysis. The validation of the numerical technique is also made by comparisons with the steady state solutions derived from the analytical methods.

A rigid container partially filled with a wetting liquid, as shown in Fig.2.1.1, is considered to undertake a step transition from terrestrial conditions to weightlessness. Originally at time t = 0, the system is under the influence of one gravity. At time $t = 0^+$, the system is subjected to zero-gravity. During the transition period, the system is assumed to preserve the contact angle. The equations of momenta, continuity, fractional volume and surface

tension pressure are marched in time using the previously presented numerical technique. The velocity components, free surface shape etc. are recorded at a chosen time level.

The dimensionless time and the normalized interface formation time will be used as the measuring parameters in the transition process. In order to derive a non-dimensional form of time, the characteristic time given by Abramson (1966):

$$t_o = \sqrt{\frac{L^3\rho}{\sigma}} \tag{4.1.1}$$

is used, where t_o = the characteristic time; ρ = density of the fluid; L = the half width or radius of a container; σ = surface tension. Thus, the time level in dimensionless form is defined as

$$\bar{t} = \frac{t}{t_o} \tag{4.1.2}$$

The dimensionless interface formation time, τ, is represented by

$$\tau = \frac{t_{0.5}}{t_o} \tag{4.1.3}$$

where $t_{0.5}$ is the time required for the liquid-vapor interface oscillations to decay to 0.5 % of the original amplitude. All the linear dimensions are normalized by using the half width or radius of a tank, L.

The dynamic interface response and velocity vectors to the gravity change in a rectangular tank are demonstrated in the four frames, as shown in Fig.4.1.1.

(A). At time $\bar{t} = 0$, the fluid is in 1-g field. The existence of large body forces restrains the free surface to generate a large depression arising from the surface tension forces. The velocity components are zero and the pressure is hydrostatic.

(B). At $\bar{t} = 9$, the gravitational forces have long been removed at zero-gravity and the surface tension forces are a dominant factor. The interface at central line is moving down and that at walls is moving up. The velocity components are not zero.

(C). At $\bar{t} = 19$, the fluid is still moving while the amplitudes of liquid velocities are smaller than that at $\bar{t} = 9$. The profile of liquid-vapor interface is primarily formed. The velocity components certainly remain non-zero.

(D). The liquid stops moving and oscillation at $\bar{t} = 38$ when the liquid system reaches the equilibrium state under zero-gravity. The liquid-vapor interface becomes a surface of constant curvature intersecting the wall at the contact angle. The steady state configuration of system 1 indicated by the analytic approach is obtained.

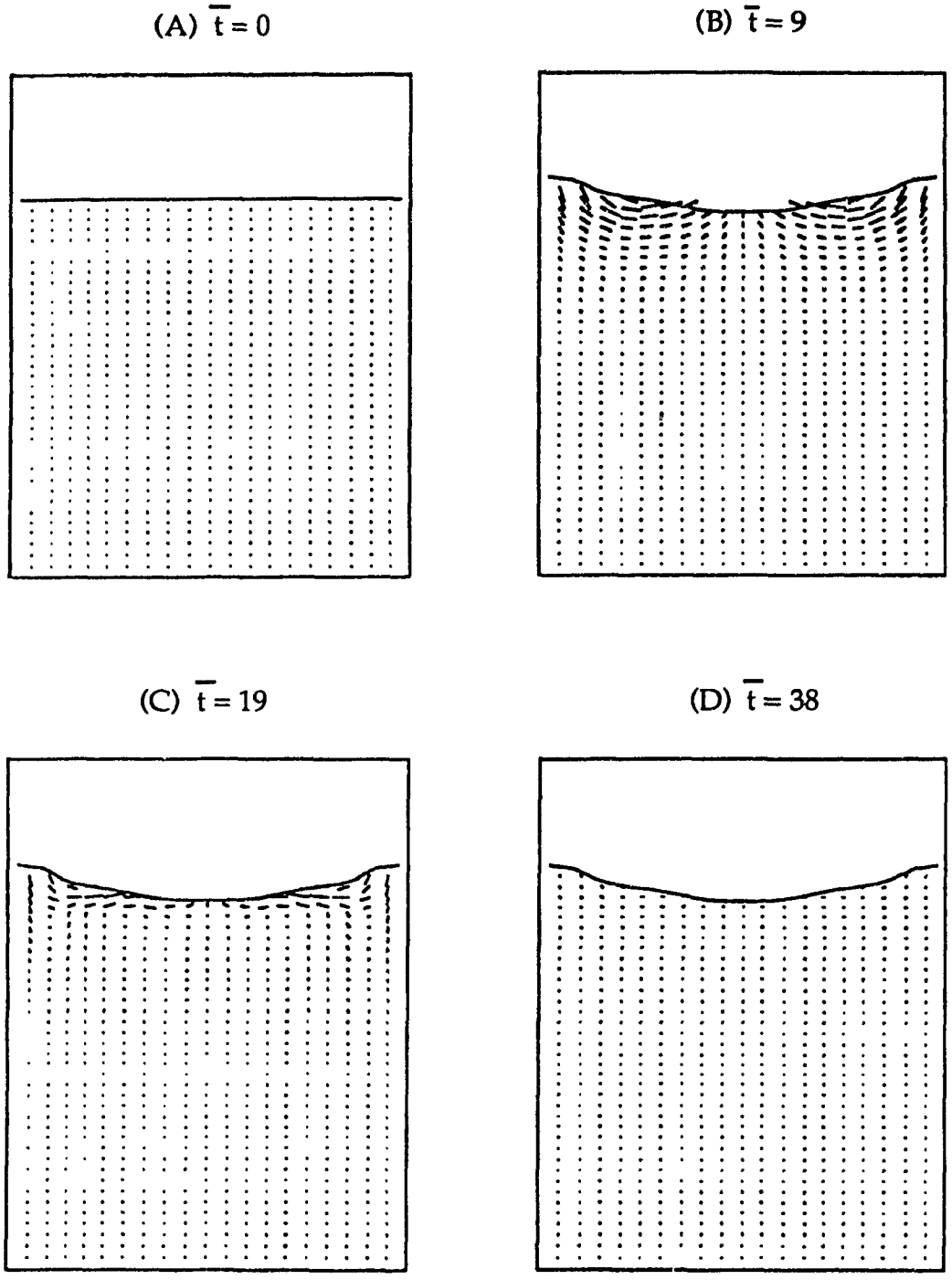

Fig.4.1.1 Liquid dynamic response to a step transition from 1-g to 0-g in a rectangular tank at high initial liquid depth

Figure.4.1.2 also demonstrates the dynamic processes of liquid in a rectangular tank during the transition period from 1-g to 0-g when the initial liquid depth is lower than the critical depth. Frame (A) is under 1-g gravity field. At frame (B), $\bar{t} = 0.5$, the movement of liquid is severe. At frame (C), the liquid is separated into two parts as the result of liquid movement. The liquid is still moving and the interface is not steady whereas the amplitudes are rather smaller than that at previous phase. Frame (D) shows the configuration of the system at the steady state, when the interface becomes stable and velocity components are zero again. The plot of this phase is as expected by the analytic method to be configuration of system 2.

Similar calculations for a cylindrical tank are presented in Figs.4.1.3 and 4.1.4. The results illustrate the same characteristics as that in a rectangular tank. The graphs from the numerical analysis agree with that derived from the analytic method. The configuration systems 3 and 4 are confirmed by plots of (D) in both figures. Furthermore, plots of frames (B) and (c) are confirm the photographic studies in the drop tower experiments although the complete steady state condition was not achieved in all drop tests (Otto, 1966). These satisfactory correlations with experiments inspire confidence in the use of the computational model to predict the liquid response in space vehicle tanks due to gravity change.

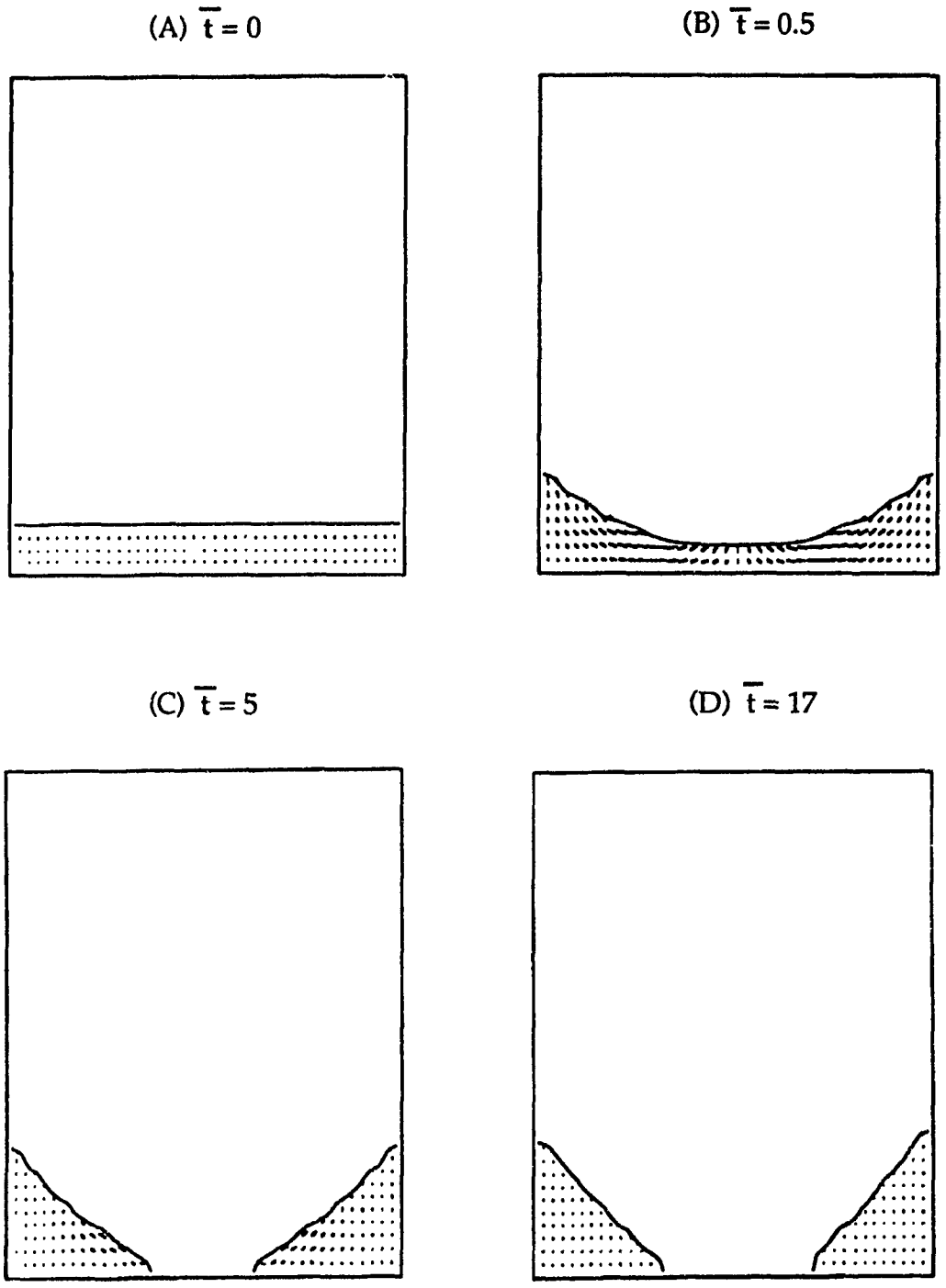

Fig.4.1.2 Liquid dynamic response to a step transition from 1-g to 0-g in a rectangular tank at low initial liquid depth

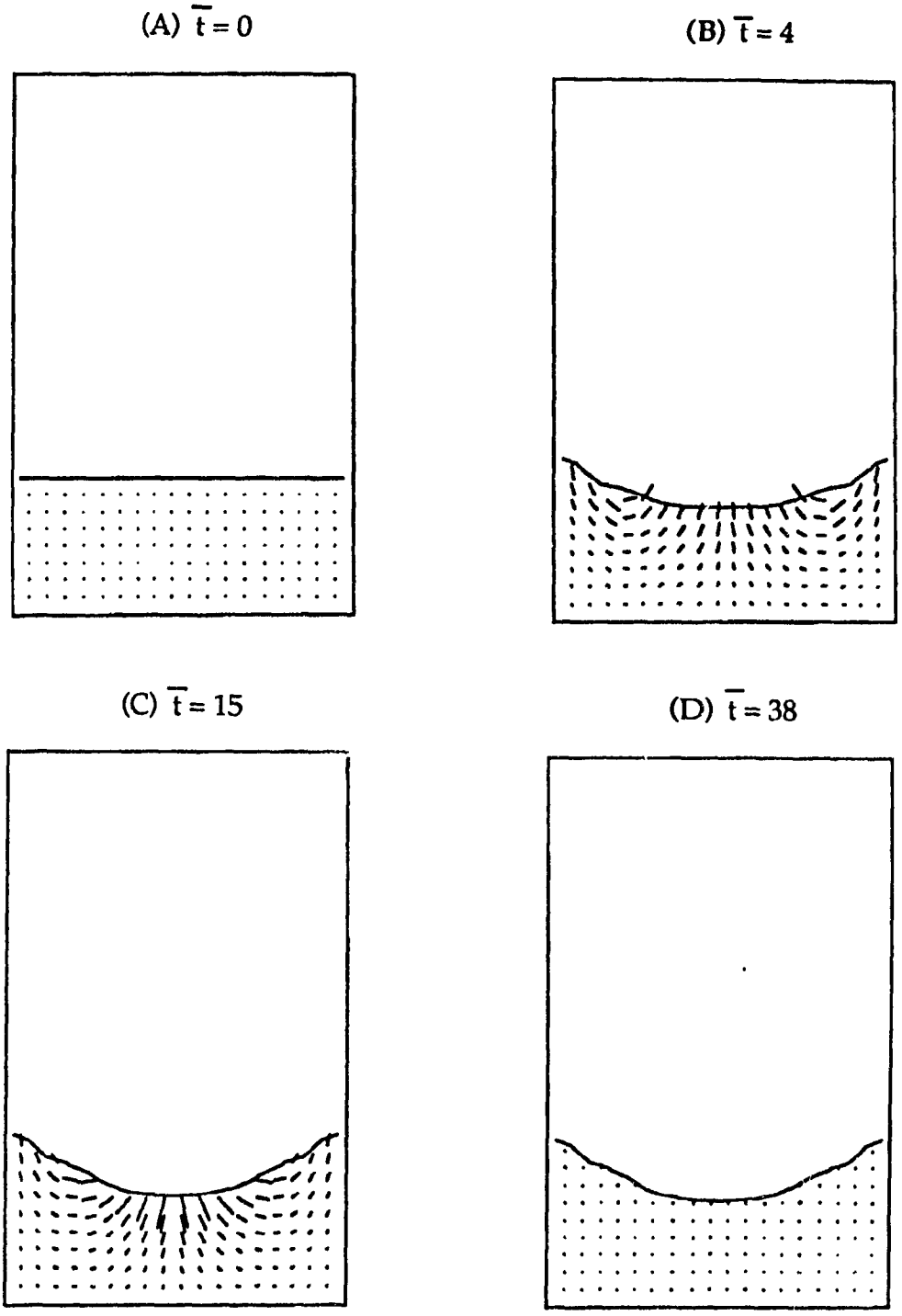

Fig.4.1.3 Liquid dynamic response to a step transition from 1-g to 0-g in a cylindrical tank at high initial liquid depth

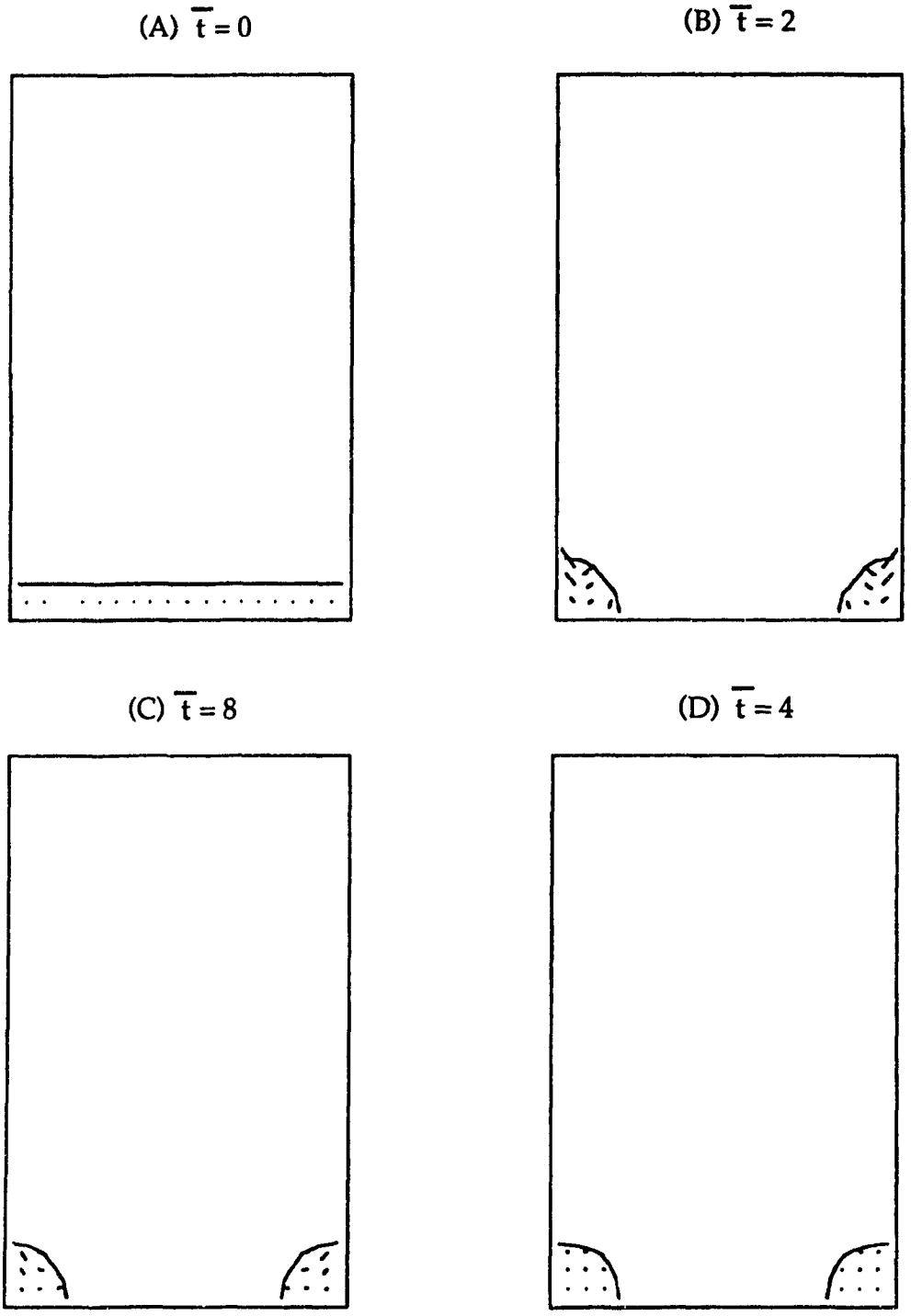

Fig.4.1.4 Liquid dynamic response to a step transition from 1-g to 0-g in a cylindrical tank at low initial liquid depth

Stable interface configurations are expected when no kinetic energy exists in the liquid. When the system switches from the 1-g to 0-g, the interface will change from a flat to an up or down concave depending on the contact angle. During this t. ansient period, a periodic oscillation might result depending on the internal damping forces. As the kinetic energy is dissipated by viscous forces, the liquid eventually reverts to the equilibrium configuration.

Figure 4.1.5 shows a comparison of the numerical results for different initial liquid depth with the critical depth at contact angle of 44.9^{o} for a rectangular tank. One is for above the critical depth while the other is for below the critical depth. The one above the critical depth approaches the steady state of the configuration of system 1 as predicted by the analytic method. When the initial liquid depth is below the critical depth the liquid is going to be two separated parts once gravity is removed, which agrees well with the configuration of system 2 presented by the analytic approach. Comparison of numerical results for different initial liquid depth with the critical depth at contact angle of 44.9^{o} in a cylindrical tank is shown in Fig.4.1.6. Four sets of data are chosen, two for liquid heights above the critical depth and two below the critical depth. They reach the configuration systems 3 and 4, respectively.

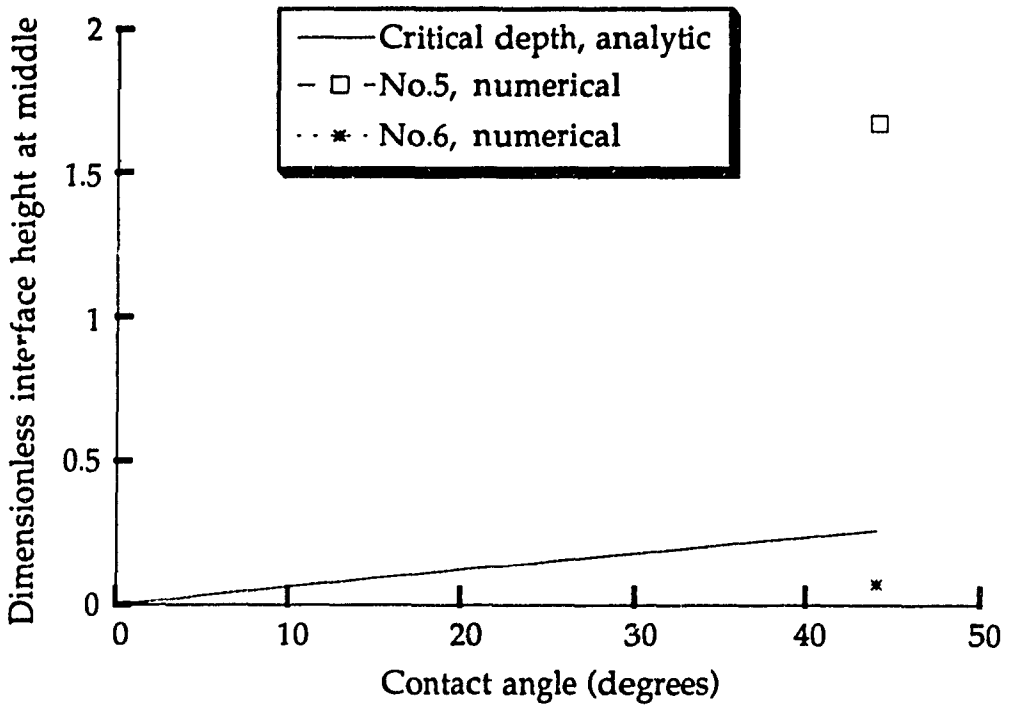

Fig.4.1.5 Comparison of liquid depth obtained from numerical analysis with the critical depth at contact angle of 44.9^{0} in a rectangular tank

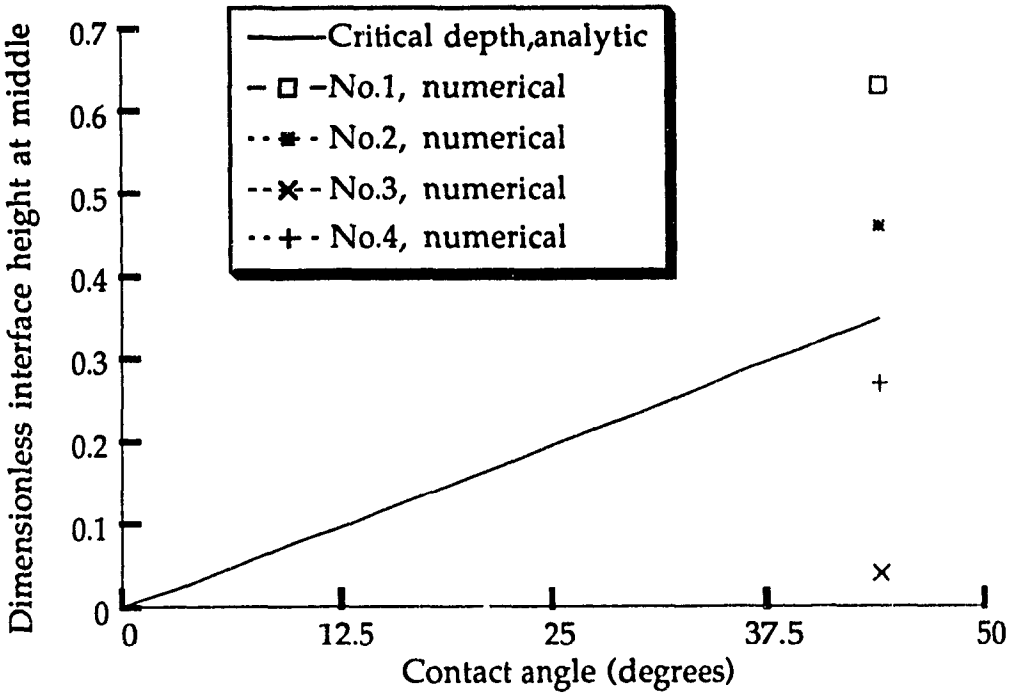

Fig.4.1.6 Comparison of liquid depth obtained from numerical analysis with the critical depth at contact angle of 44.9^{o} in a cylindrical tank

4.2 Interface Oscillations

When the gravitational force is suddenly removed, the potential energy of the system is considerably in excess of its 0-g equilibrium value. Upon entering the zero-gravity field, the liquid mass then oscillates about the equilibrium liquid configuration until viscous forces in the liquid damp out the oscillation and bring the liquid to rest.

During the transition period for contact angle equal to 44.9^{o} the interface is found to exhibit the distinct characteristics of an under damped system, as shown in Figs.4.2.1. and 4.2.2 for rectangular and cylindrical geometries, respectively. A dominant damped natural frequency is clearly present. The amplitudes of oscillations and the time required to reach the steady state are significantly affected by Re number, as can be seen in Fig.4.2.3. If the Re number is large, the amplitude decay is small with time while the time to reach the steady state is going to be much longer. For smaller contact angles, such as 30^{o} and 12^{o}, the chaotic undulations depicted in Figs.4.2.4 and 4.2.5. are always apparent. Nevertheless, for all cases studied the interface reached the corresponding steady capillary dominated shape, when all the transients had died down. The interface oscillations in a cylindrical tank at contact angle of 60^{o} also represent the characteristics of an under damped system, as shown in Fig.4.2.6.

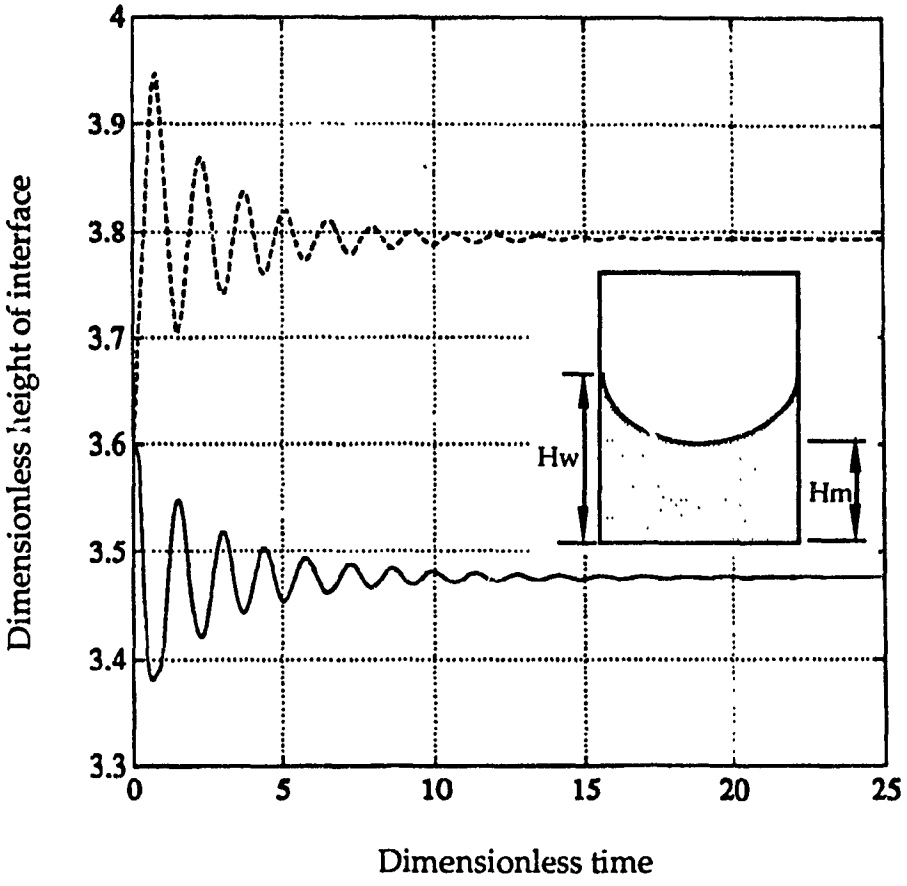

Fig.4.2.1 Interface oscillations at contact angle=44.9^{o} in a rectangular tank

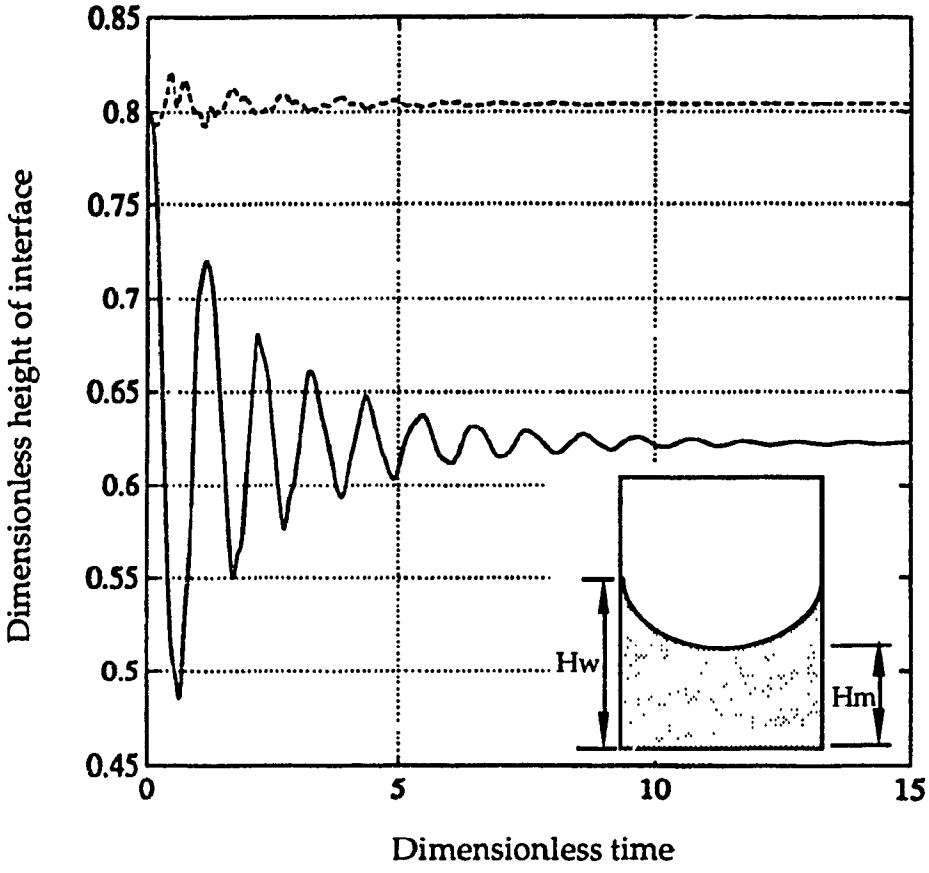

Fig.4.2.2 Interface oscillations at contact angle=44.9^{o} in a cylindrical tank

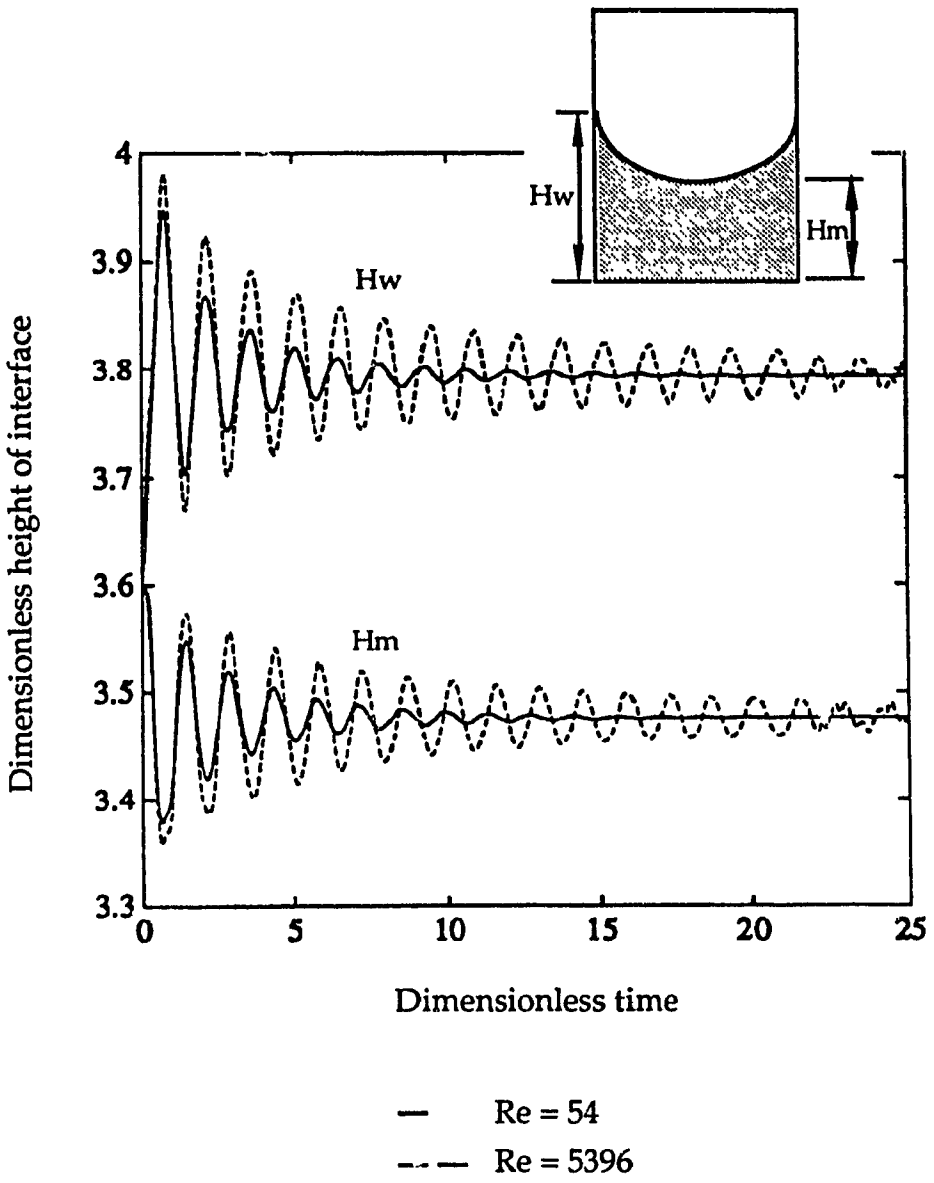

Fig.4.2.3 Interface oscillations with different Re number

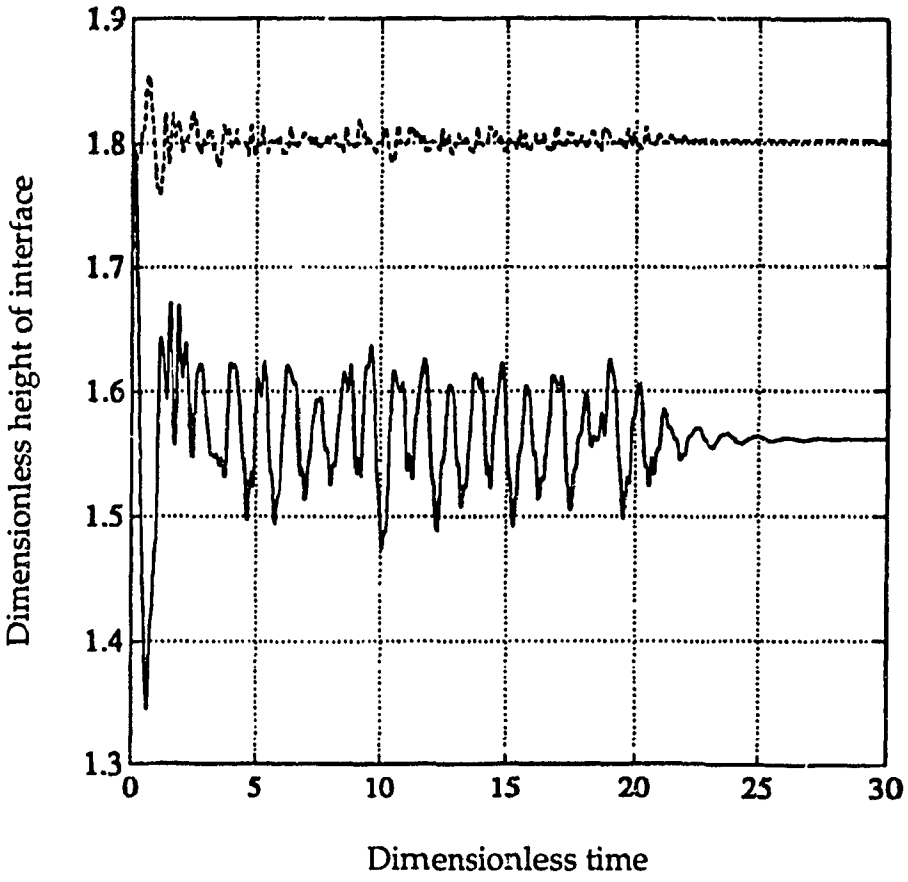

Fig.4.2.4 Interface oscillations at contact angle=30^{o} in a cylindrical tank

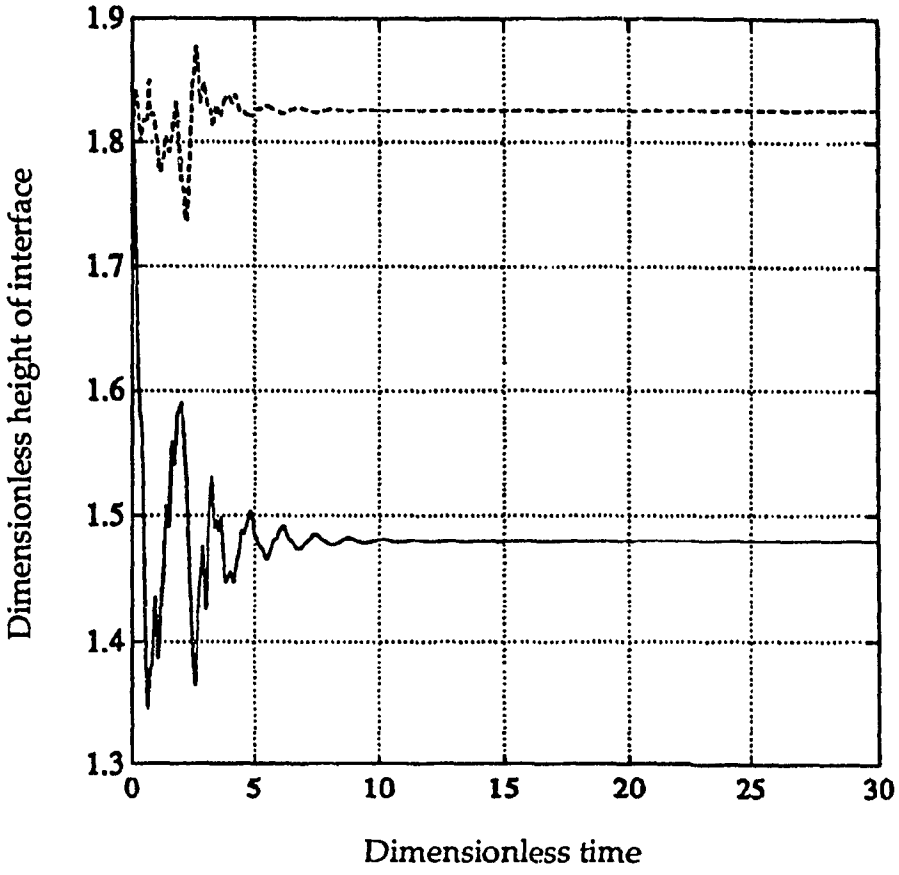

Fig.4.2.5 Interface oscillations at contact angle=12^{o} in a cylindrical tank

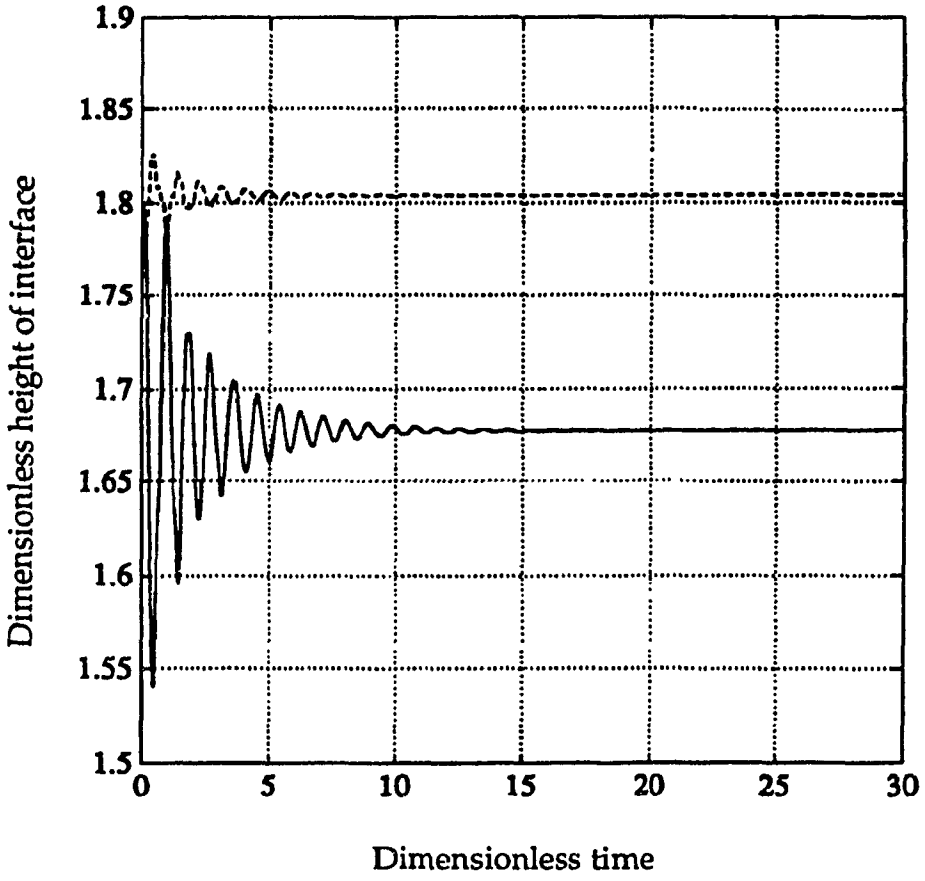

Fig.4.2.6 Interface oscillations at contact angle=60^{o} in a cylindrical tank

Comparison of Fig.4.2.2 with Fig.4.2.7 shows that there is little difference in oscillation amplitudes and frequencies when the initial interface heights in the two cases are only slightly different. Further comparison for initial interface heights are made, as presented in Figs.4.2.8 and 4.2.9. Although the initial heights are different, the oscillation modes are similar.

4.3 Interface Formation Time

One of the important parameters under study is the time required for the interface to form its zero gravity configuration after release from a normal gravity field. The time necessary for the interface to form its equilibrium shape after entering zero gravity can be represented by the time required for the liquid-vapor interface oscillations to decay to 0.5% of the original amplitude, $t_{0.5}$. The dimensionless interface formation time is obtained by normalizing the time $t_{0.5}$ using the characteristic time.

Numerical studies have shown that the time $t_{0.5}$, depends strongly on the fluid density ρ, surface tension σ, viscosity ν, the half width or radius of a container L, and the contact angle α. Mathematically

$$f_n(t_{0.5}, \rho, \sigma, \nu, L, \alpha) = 0 \qquad (4.3.1)$$

From the dimensional analysis, the following dimensionless parameters can be obtained.

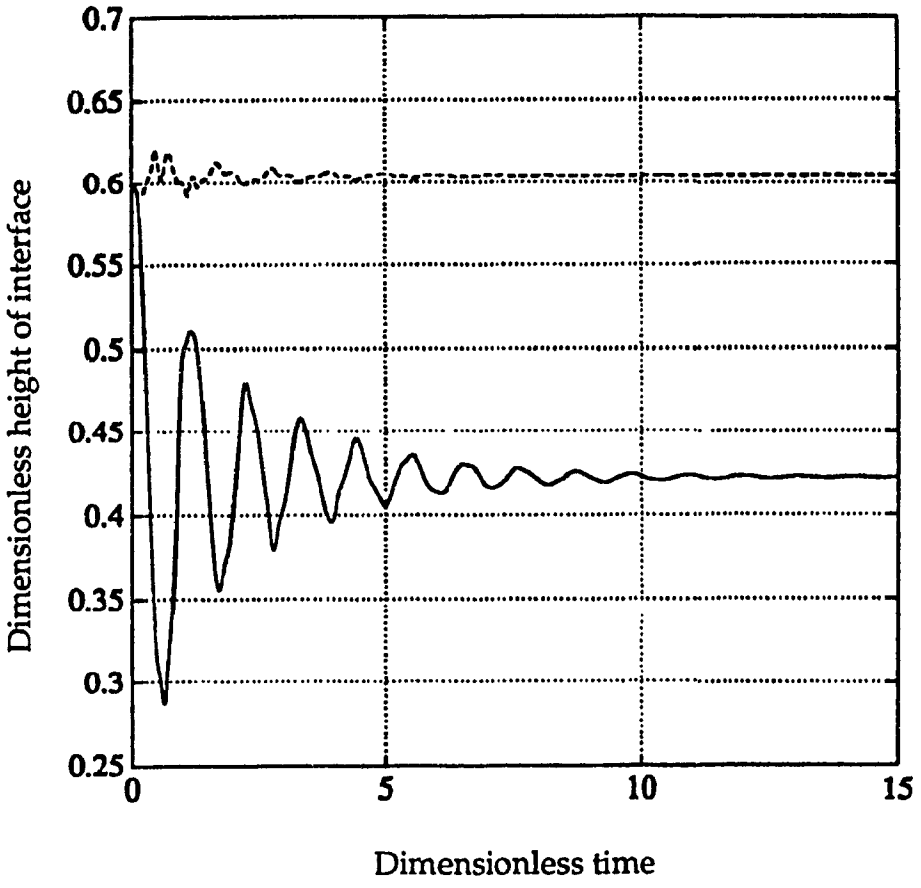

Fig.4.2.7 Initial interface height of 0.6 at contact angle =44.9^{o} in a cylindrical tank

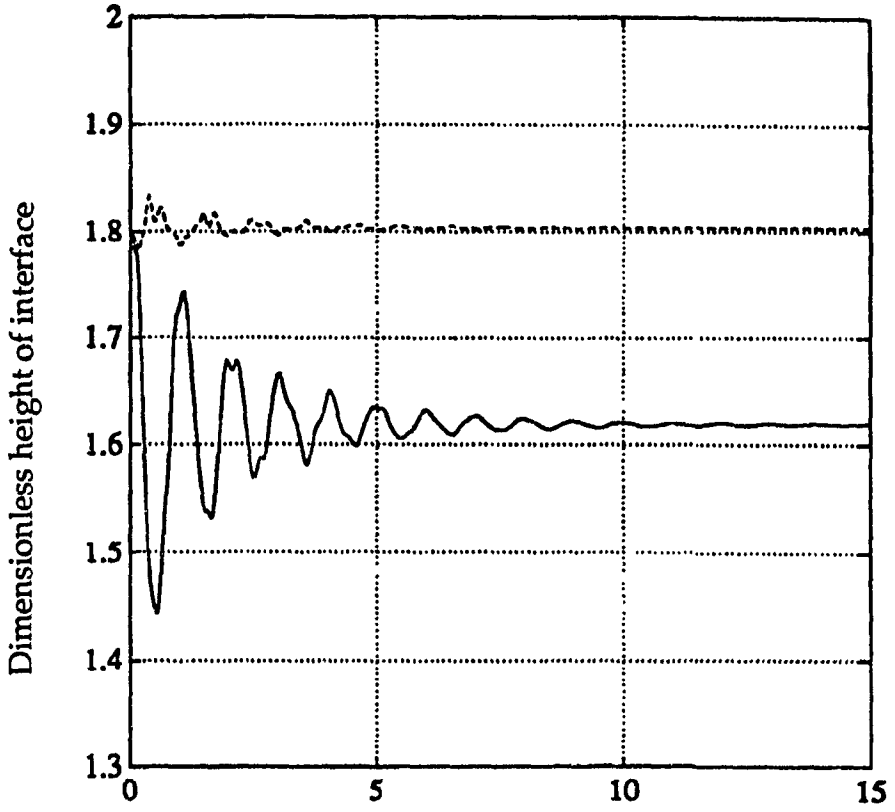

Fig.4.2.8 Initial interface height at 1.8

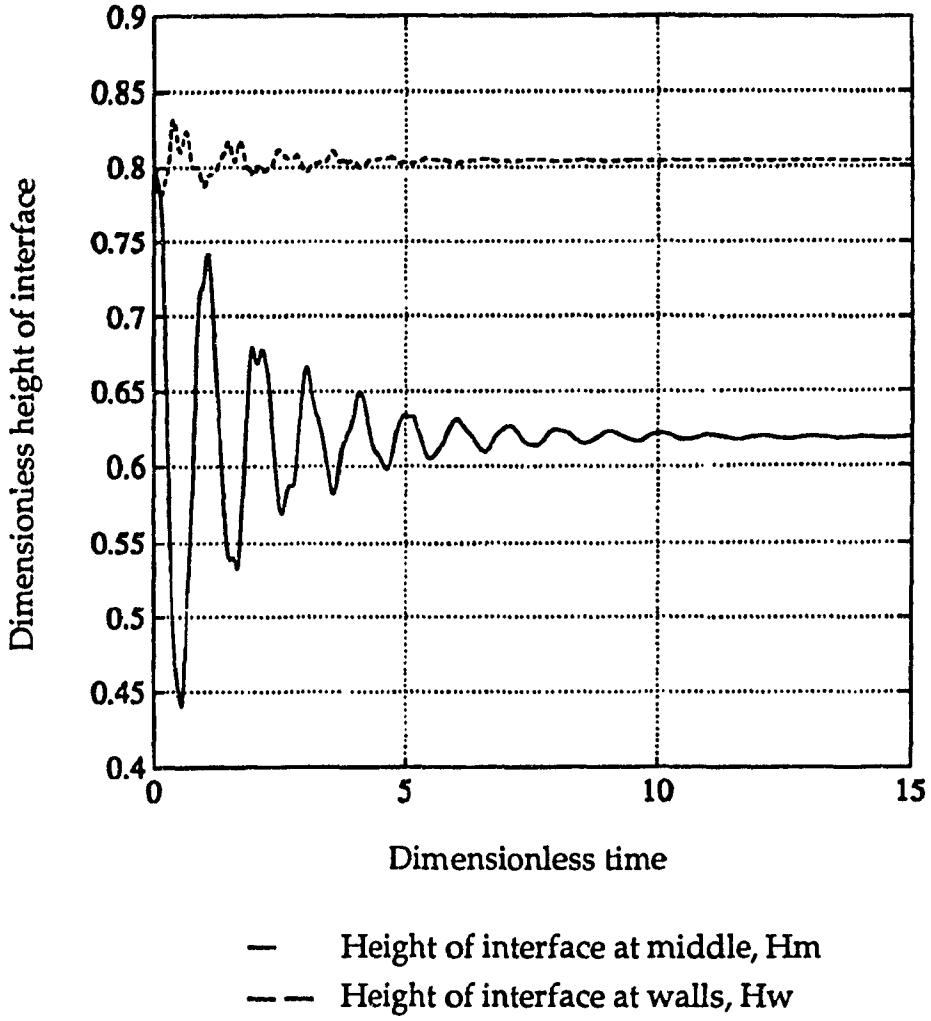

Fig.4.2.9 Initial interface height at 0.8

$$\pi_1 = \mathrm{Re} = \frac{1}{\nu}\sqrt{\frac{\sigma L}{\rho}} \tag{4.3.2}$$

$$\pi_2 = \tau = \frac{t_{0.5}}{\sqrt{\frac{L^3 \rho}{\sigma}}} \tag{4.3.3}$$

$$\pi_3 = \alpha \tag{4.3.4}$$

The general expression for the formation time as a function of Re number and the contact angle is rearranged as follows:

$$\tau = f_n\,(\mathrm{Re}, \alpha) \tag{4.3.5}$$

For a given contact angle,

$$\tau = f_n\,(\mathrm{Re}) \tag{4.3.6}$$

It is expected that Re numbers will be of significance in describing dynamic behavior because it incorporates the effects of viscosity, tank geometry, density and surface energy. Reynolds number defines the conditions required to obtain similar flow characteristics in different sized systems and defines regimes of different behavior.

Numerical results for the dimensionless interface formation time τ as a function of the Re number in a rectangular and a cylindrical tank are given in Figs.4.3.1 and 4.3.2, respectively. The slope of curve at the beginning is steep, then it tends to be nearly horizontal, which means that the required time

increases steeply at considerably small Re numbers while the time increases quite slowly at large Re numbers. It is obvious from the graphs that the transition time required for the previous interface under one-g to reach steady state conditions increases as the damping forces decrease.

The effect of the parameter, contact angle α, on the time required to form the steady state interface when Re number is constant is shown in Fig.4.3.3. The time increases with increasing α.

4.4 Interface Height

Although the values of fluid properties, such as viscosity, surface tension and density, have a profound influence on the numerical solution during the dynamic transition from terrestrial conditions to weightlessness, they have no effect on the liquid-vapor interface heights at the secondary static state. Therefore, from dimensional analysis at zero-gravity, the dimensionless interface height

$$\bar{y} = f_n(\bar{x}, \alpha) \tag{4.5.1}$$

Similarly, the dimensionless distance of the vertex at the central line from the original one-gravity liquid level has the form of

$$\bar{\delta} = f_n(\alpha) \tag{4.5.2}$$

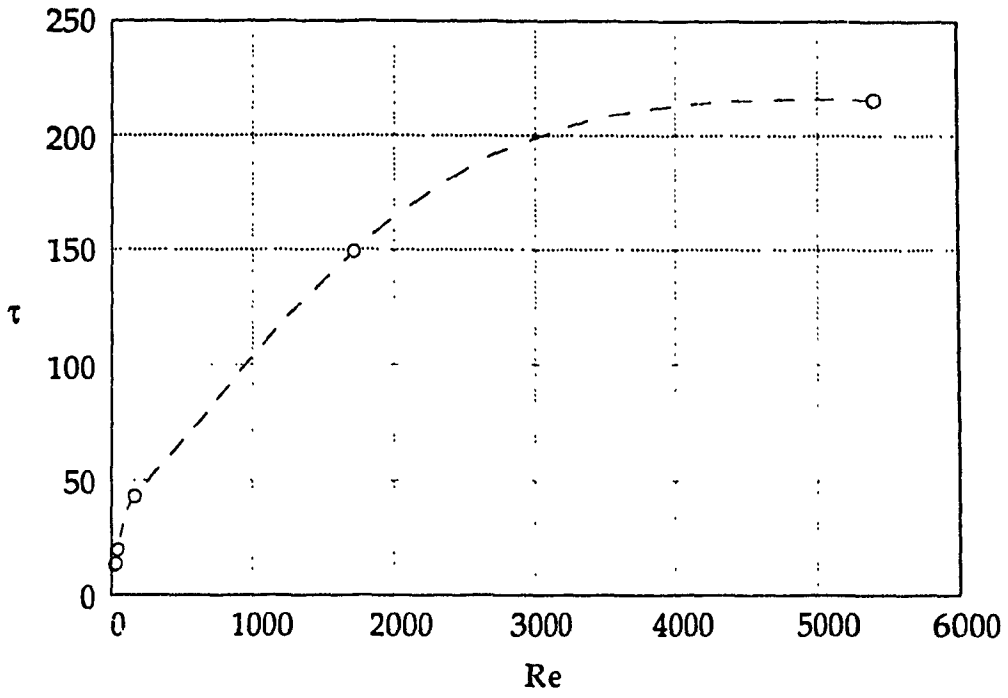

Fig.4.3.1 Dimensionless interface formation time as a function of Re number at contact angle = 44.9^{o} in a rectangular tank

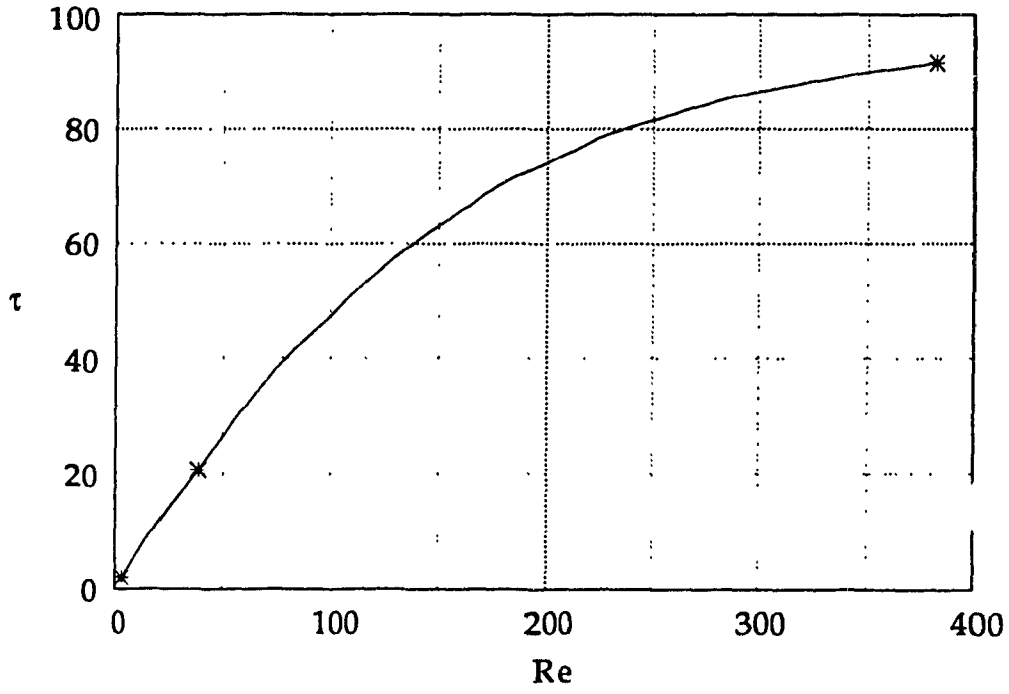

Fig.4.3.2 Dimensionless interface formation time as a function of Re number at contact angle of 44.9° in a cylindrical tank

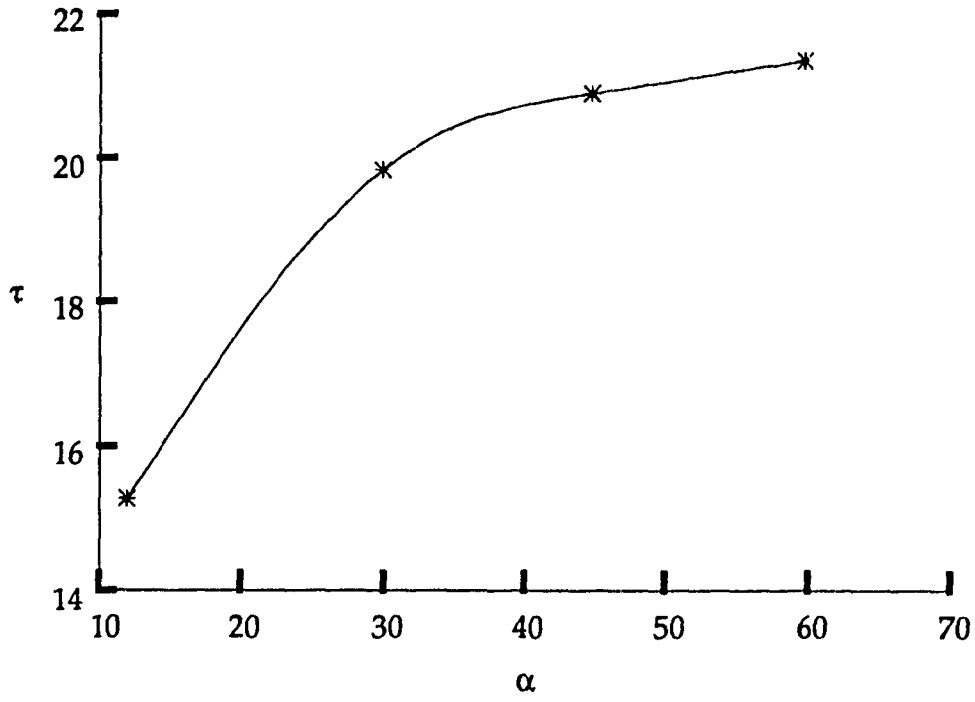

Fig.4.3.3 Dimensionless interface formation time τ versus contact angle at Re = 38.2

Equations (4.5.1) and (4.5.2) are the general form of equations (2.1.11), (2.1.12) and (2.1.15), (2.1.16), respectively. The variations of $\bar{\delta}$ with the contact angle in a rectangular and a cylindrical tank are shown graphically in Figs.4.4.1 and Fig.4.4.2, respectively. It can be seen that the numerically obtained values of $\bar{\delta}$ for different contact angles agree well with the values calculated from the analytic method.

4.5 Shapes of Interface at the Equilibrium State

The liquid-vapor interface will reach the steady state after certain time period switching from 1-g to 0-g field. The interface shapes are obtainable from the numerical analysis at different contact angles. Figs.4.5.1, 4.5.2, 4.5.3 and 4.5.4 show the comparison of interface shapes at equilibrium state calculated from both analytic and numerical methods in a rectangular tank at the contact angle of 12^{o}, 30^{o}, 44.9^{o} and 60^{o}, respectively. Both analytic and numerical results, generally, agree well.

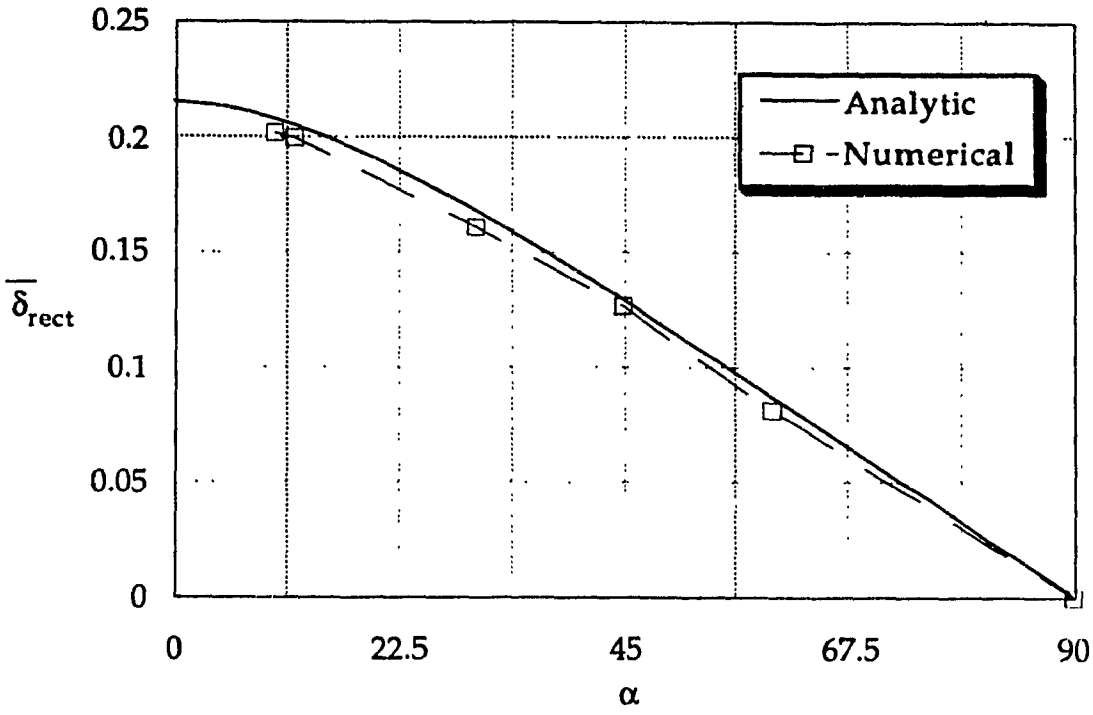

Fig.4.4.1 Dimensionless distances of vertex at the central line from the original 1-g level versus contact angles in a rectangular tank

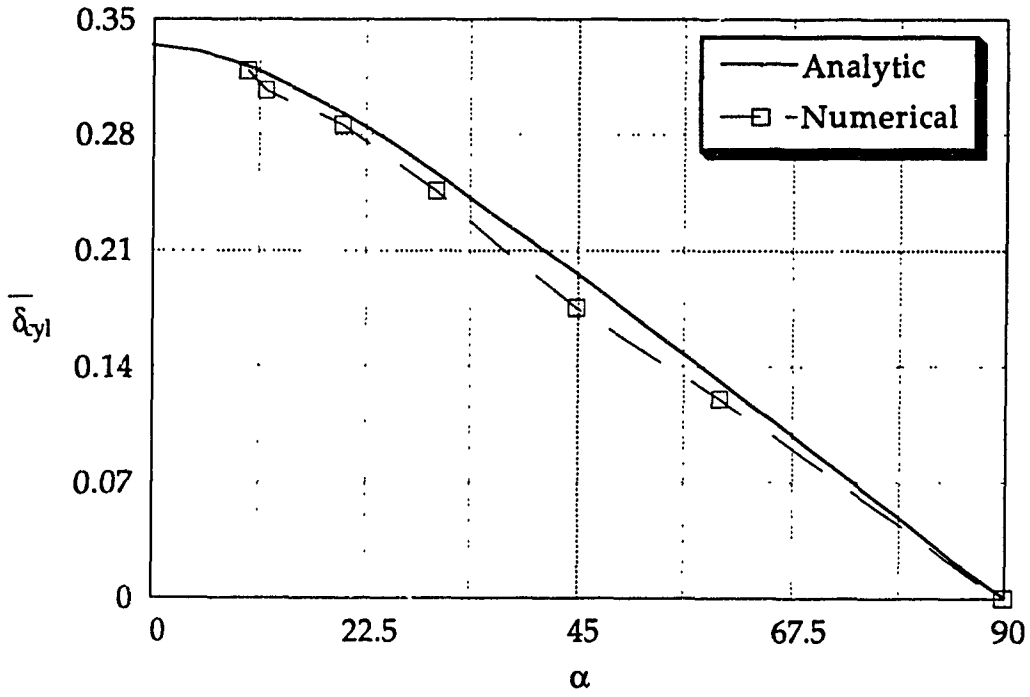

Fig.4.4.2 Dimensionless distances of vertex at the central line from the original 1-g level versus contact angles in a cylindrical tank

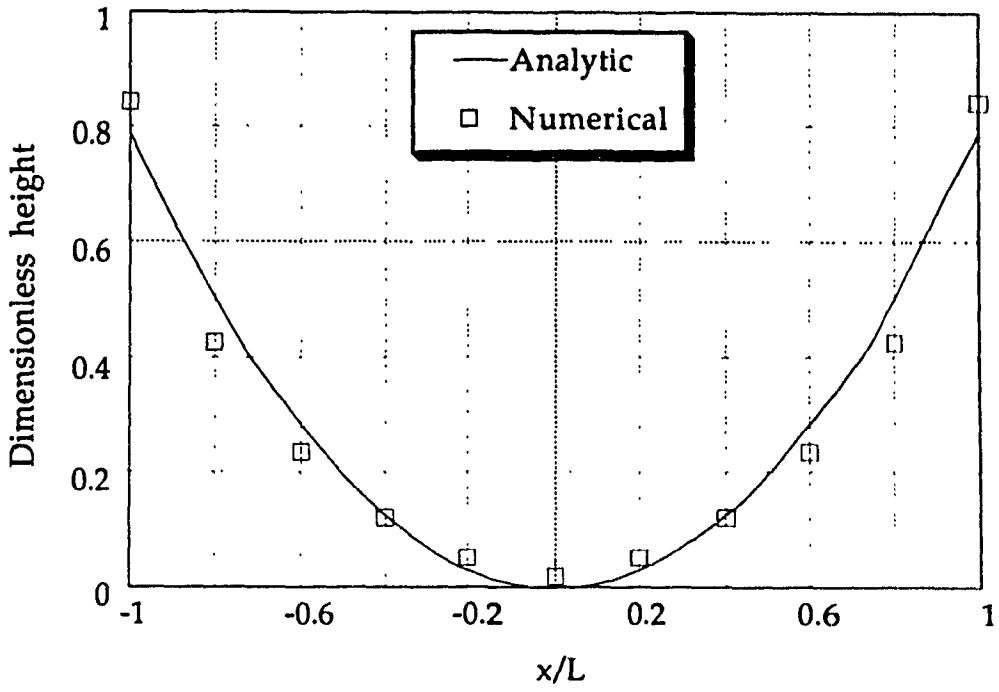

Fig.4.5.1 Liquid-vapor interface shape obtained from both analytic and numerical methods in a rectangular tank at contact angle of 12^{o}

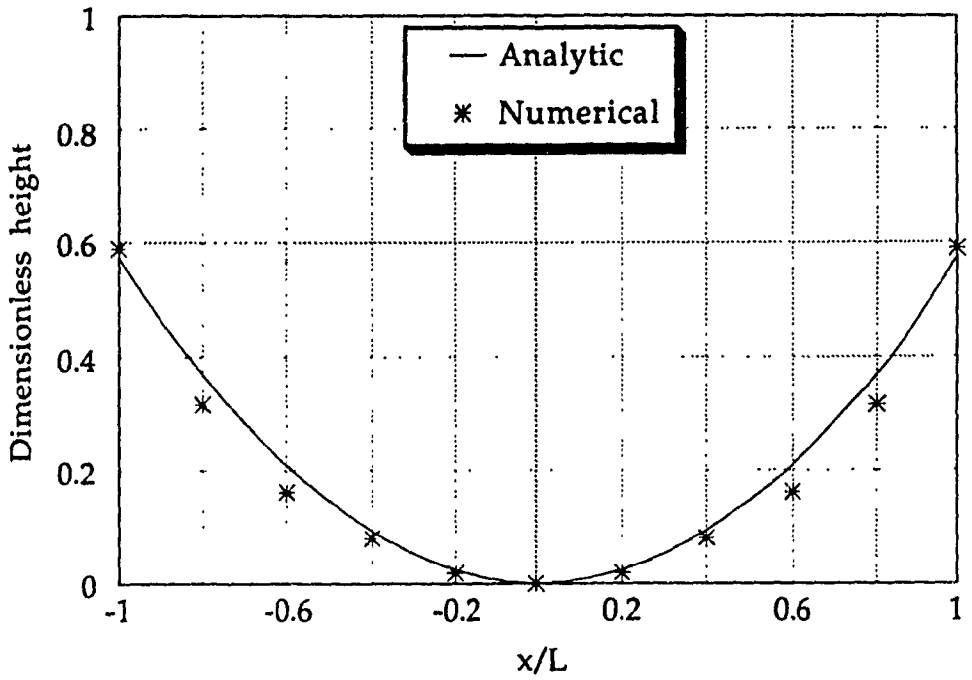

Fig.4.5.2 Liquid-vapor interface shape obtained from both analytic and numerical methods in a rectangular tank at contact angle of 30^{o}

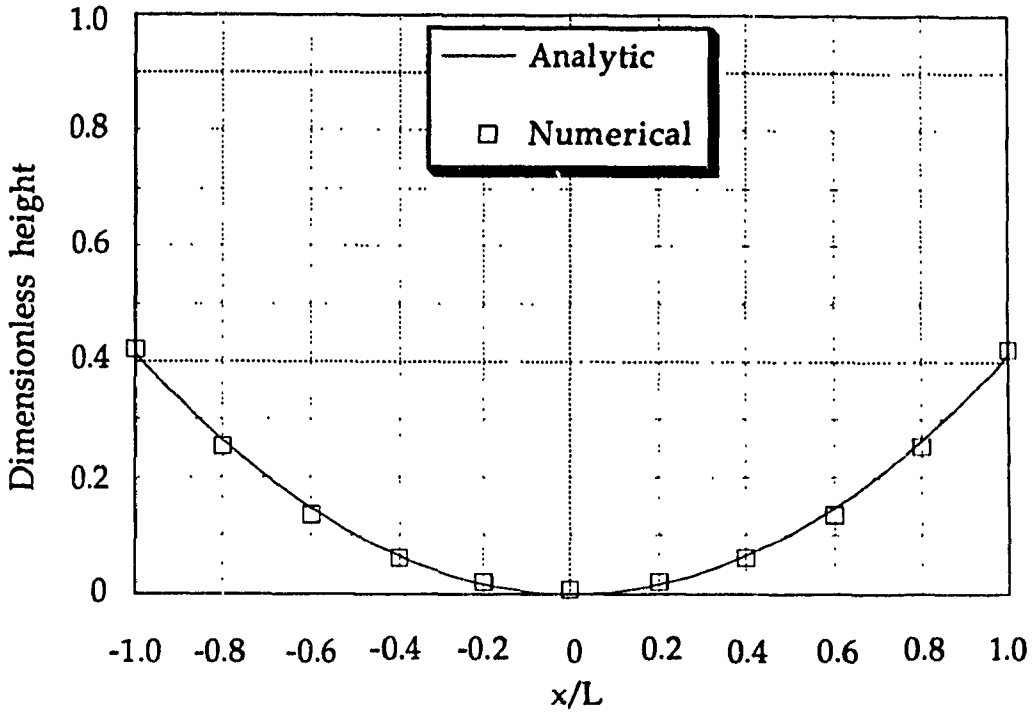

Fig.4.5.3 Liquid-vapor interface shape obtained from both analytic and numerical methods in a rectangular tank at contact angle of 44.9^{o}

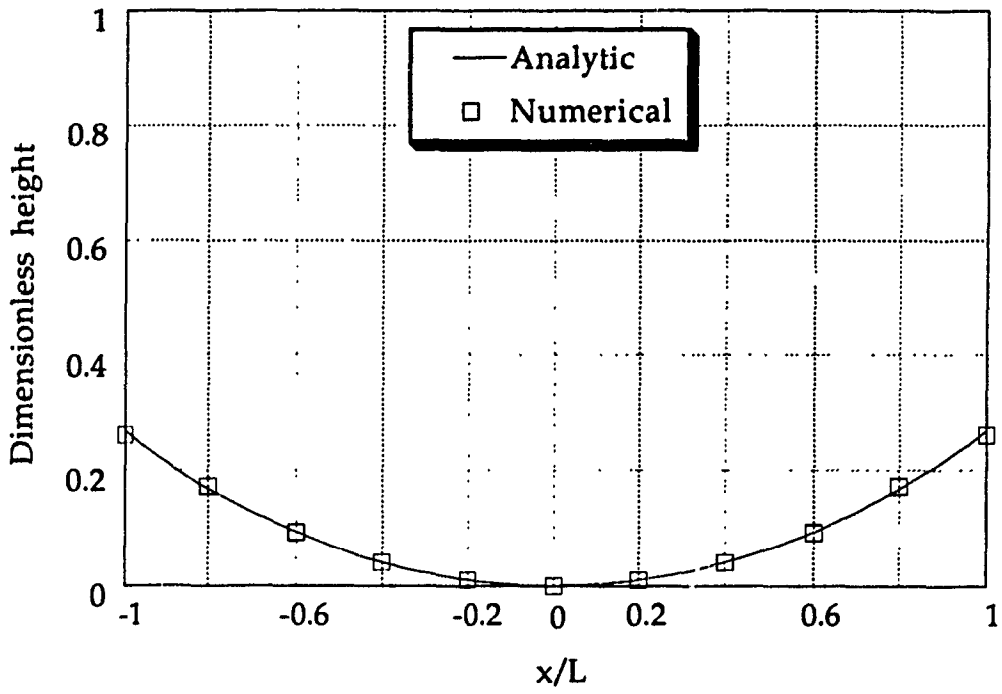

Fig.4.5.4 Liquid-vapor interface shape obtained from both analytic and numerical methods in a rectangular tank at contact angle of 60^{o}

4.6 Damping of Liquid Oscillation

Liquid damping is the other factor to be considered in the solution of the liquid motion problem as the magnitudes of these oscillations depend on the amount of liquid damping present. An investigation of the primary variables which may contribute to damping factor is required. Of particular importance are the surface tension, container size, kinematic viscosity and amplitude of oscillation. After entering the zero-gravity field, the liquid is oscillating along the equilibrium interface with the decay of the interface oscillating amplitude. The logarithmic rate of decay of this amplitude is considered as a damping factor δ_d.

Fig.4.6.1 shows the relationship between the damping factor and Re number in a rectangular tank. With the increase of Re number, the rate of decay of oscillation is decreased due to the reduction of viscous damping. The damping factor varies rapidly at small Re number while it does not change significantly at large Re number. Re number equal to 170 at δ_d of 0.4 appears to be a changing point, which may be used for the classification of small or large Re number region. A similar relation is observed in a cylindrical tank, as shown in Fig.4.6.2. However, the changing point is around Re number of 50, which is less than that in the rectangular tank. This may conclusively show that the geometry of a container is related to the functional relationship between Re number and the damping factor.

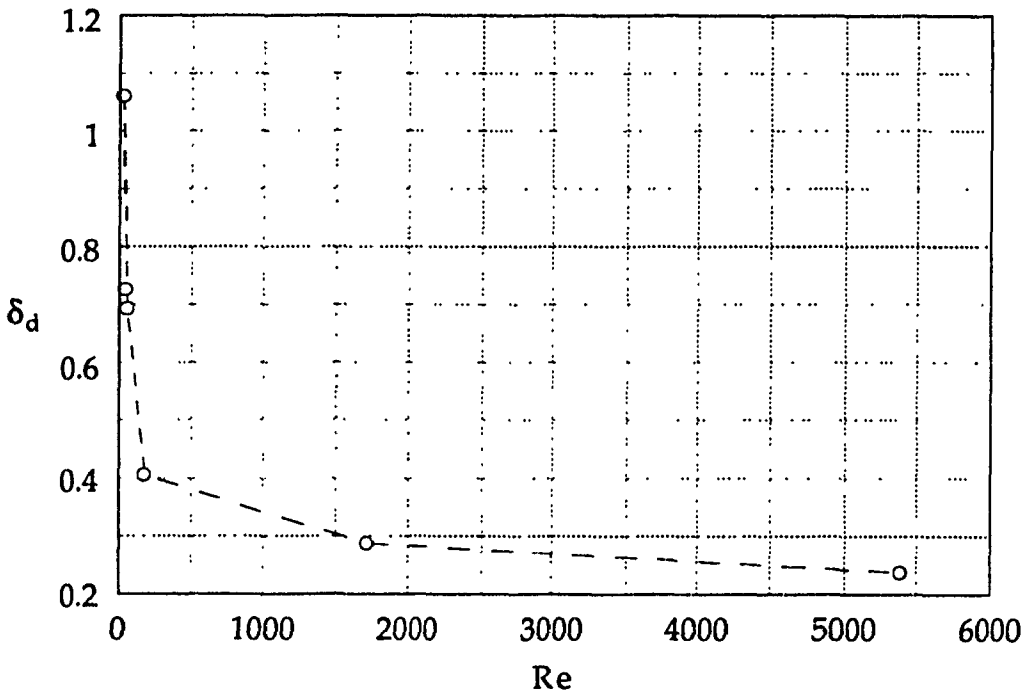

Fig.4.6.1 Damping factor versus Re number in a rectangular tank

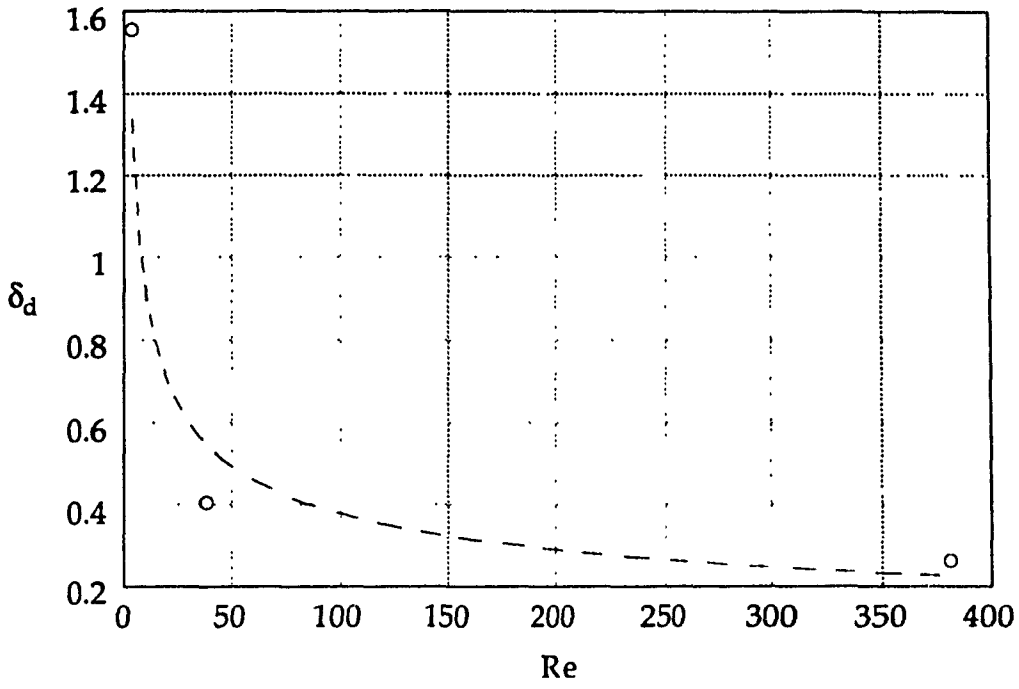

Fig.4.6.2 Damping factor versus Re number in a cylindrical tank

CHAPTER 5

CONCLUSIONS

Analytical and numerical studies concerning the liquid free-surface equilibrium configuration in a zero gravity environment and its dynamic behavior during tr sition from one gravity to zero gravity fields in both rectangular and cylindrical tanks have been presented.

Based on the Dupré-Young and Laplace-Young equations, solutions for the equilibrium liquid-vapor interface have been obtained over a wide range of physical and geometrical parameters. The analysis based on the previous corollary, has shown conclusively that the critical depth dictates whether the free-surface of the liquid will either cover completely the lower plate of the container or not. Numerical results have also confirmed the above mentioned finding. In the past, a filling ratio (a measure of the amount of fluid present in the container) has been used as an independent variable. This, however, can not define uniquely the liquid-vapor interface condition. For a given filling ratio the interface may attain two distinct configurations. Although both are extrema of the potential function one is a local minimum while the other is an absolute one. A new independent variable, the interface configuration ratio, is proposed herein instead of the previously used filling ratio. It has been shown that in zero-gravity environment given several minimum potential energy states of a mechanical system consisting from liquid-vapor-solid vessel,

the state with absolute minimum is the one with the smallest liquid-vapor interface.

A transient numerical solution for the equations describing the motion of a liquid with a free-surface under the influence of capillary forces in a two-dimensional geometry has also been presented. These numerical simulations describe the dynamic response of the free-surface during a step transition from one gravity to weightlessness. The numerical results show that in all cases the second equilibrium state (0-g) is attained asymptotically as the transient effects diminish. The investigations reveal that the dimensionless interface formation time increases with the Reynolds number and the contact angle. The second bifurcation, obtained analytically when the liquid height is less than the critical depth, has also been confirmed numerically.

Under the present condition, the computational results can be generally obtained in a reasonable time using the VAX2 mainframe computer. However, the calculation using finer grids will increase the requirement with respect to computer storage and speed.

Experimental studies on liquid behavior in zero gravity should be considered at the next stage. Investigations with the aim to obtain the interface behaviour in other container geometries as well as sloshing, draining and refilling in the zero gravity environment are required.

REFERENCES

Abramson, H.N. (editor), The Dynamic Behavior of Liquids in Moving Containers, NASA SP-106, 1966.

Benedikt, E.T., General behavior of a liquid in a zero or near-zero gravity environment, Weightlessness-Physical Phenomena and Biological Effects, edited by E.T.Benedikt, Plenum Press, New York, pp. 3-32, 1961.

Benedikt, E.T., Scale of separation phenomena in liquids under conditions of nearly free fall, ARS J.29, 150, 1959.

Canadian Press, Federal minister Benoit Bouchard tests a Canadarm simulator at the Spar Aerospace facility in Mississauga, Ont., Spar gets federal contract for space station, the Gazette, Montreal, Canada, March 8, 1991.

Clodfelter, R.G. and Lewis, R.C., Fluid studies in a zero gravity environment, Astronaut. Systems Div. TN 61-84, Wright-Patterson AFB, Ohio, June, 1961.

Clodfelter, R.G., Rept. ASD-TDR-63-506, Air Force System Command, Wright-Patterson Air Force Base, Ohio, September, 1963.

Concus, P., Equilibrium Fluid Interfaces in the Absence of Gravity, Symposium on Microgravity Fluid Mechanics, Fed-Vol.42, the Winter Annual Meeting of ASME, California, December 7-12, 1986.

Hirt, C.W., Nichols, B.D. and Romero, N.C., SOLA-A numerical solution algorithm for transient fluid flows, Los Alamos Scientific Laboratory report LA-5852, 1975.

Hirt, C.W., and Nichols, B.D., Volume of fluid (VOF) method for the dynamics for free boundaries, Journal of Computational Physics, Vol.39, 1981.

Li, T., Preliminary studies of liquid behavior in a low-g field, Rept. ERR-AN-036, Convair Astronautics, March, 1961.

Li, T., Hydrostatics in various gravitational fields, J.Chem.Phys. 36, April, 1962.

Myshkis, A.D., V.G.Babskii, N.D.Kopachevskii, L.A.Slobozhanin and A.D.Tyuptsov, translated by R.S.Wadhwa, Low-gravity Fluid Mechanics, Springer-Verlag, 1987.

Neiner, J.J., The effect of zero gravity on fluid behavior and system design, Wright Air Dev. Center TN 59-149, Armed Services Tech. Info. Agency AD 228810, April, 1959.

Nichols, D.B., C.W. Hirt and R.S. Hotchkiss, SOLA-VOF: A Solution Algorithm for Transient Fluid Flow with Multiple Free Boundaries, Los Alamos Scientific Laboratory Report LA-8355, Los Alamos, New Mexico, August, 1980.

Otto, E.W., Static and Dynamic Behavior of the Liquid-Vapor Interface during Weightlessness, Aerospace Chemical Engineering, No.61, Vol.62, 1966, pp.158-177.

Paynter, H.L., Time for Totally Wetting Liquid to Deform from a Gravity Dominated to a Nulled-Gravity Equilibrium State, AIAA Journal, Vol.2, No.9, September, 1964, pp. 1627-1630.

Petrash, D.A., Zappa, R.F. and Otto, E.W., Experimental Study of the Effects of Weightlessness on the Configuration of Mercury and Alcohol in Spherical Tanks, NASA TN D-1197, April 1962.

Petrash, D.A. and T.M. Nelson, Effect of Surface Energy on the Liquid-Vapor Interface Configuration during Weightlessness, NASA TN D-1582, January 1963.

Petrash, D.A., Nusle, R.C. and Otto, E. W., Effect of Contact Angle and Tank Geometry on the Configuration of the Liquid-vapor Interface During Weightlessness, Natl.Aeronaut. Space Admin.Tech. Note D-2075, 1963.

Reynolds, W.C., Behavior of liquids in free fall, J.Aerospace Sci., 26, 847, 1959.

Reynolds, W.C., Hydrodynamic considerations for the design of systems for very low gravity environments, TR LG-1, Dept.Mech.Eng., Stanford University, Sept., 1961.

Siegel, R., Transient Capillary Rise in Reduced and Zero-Gravity Fields, Journal of Applied Mechanics, June 1961, pp. 165-170.

Siegert, C.E., Petrash, D.A. and Otto, E.W., Time Response of Liquid-vapor Interface after Entering Weightlessness, NASA TN D-2458, August, 1964.

Trusela, R.A. and Clodfelter, R.C., Heat transfer problems of space vehicle power systems. Soc. Automotive Engrs. Paper 154 C, April, 1960.

Unterberg, W. and Congelliere, J., Zero Gravity Problems in Space Powerplants: A Status Survey, ARS Journal, June 1962, pp 862-872.

Vatistas, G.H., V.Kozel, W.Yan and T.S.Sankar, Liquid Free Surface Response to a Step Change from Terrestrial Conditions to Zero Gravity, 1990 proceedings of ASME International Computers in Engineering Conference and Exhibition, Boston, U.S.A., August 1990.

Vatistas, G.H., V.Kozel, W.Yan and T.S.Sankar, The Dynamic Behaviors of Liquids Contained in Cylinders During Transition to Weightlessness, A Changing World — The Challenge for Space, Proceedings of the Sixth Conference on Astronautics, Canadian Aeronautics and Space Institute, Ottawa, Canada, November 1990.

Vatistas, G.H., V.Kozel, W.Yan and T.S.Sankar, Investigations of Liquid Motion in Rigid Containers Under Microgravity Conditions, 1991 proceedings of ASME International Computers in Engineering Conference and Exhibition, Santa Clara, California, U.S.A., August 19, 1991.

Welch, J.Eddie, Harlow, F.H., Shannon, J.P. and Daly, B.J., The MAC Method-A Computing Technique for Solving Viscous, Incompressible, Transient Fluid-flow Problems Involving Free Surfaces, Los Alamos Scientific Laboratory report UC-32 and TID-4500, 1966.

Young,T., Essay on the Cohesion of fluids, Phil Trans.Roy.Soc. (London), 95, 65, 1805.

APPENDICES

I. Calculations of Interface Configuration Ratio in a Rectangular Tank

A.1 Configuration System 1

(A) Area

From Fig.A.1, for a unit thickness, the liquid-vapor interface area A_{r1} is defined by

$$A_{r1} = 2\,\beta_1\,R_1 \tag{A.1.1}$$

where

$$\beta_1 = \left(\frac{\pi}{2} - \alpha\right) \tag{A.1.2}$$

$$\cos\beta_1 = \sin\alpha \tag{A.1.3}$$

$$R_1 = \frac{L}{\cos\alpha} \tag{A.1.4}$$

$$\xi = R_1 \sin\alpha \tag{A.1.5}$$

$$A_{r1} = 2\left(\frac{\pi}{2} - \alpha\right)\frac{L}{\cos\alpha} \tag{A.1.6}$$

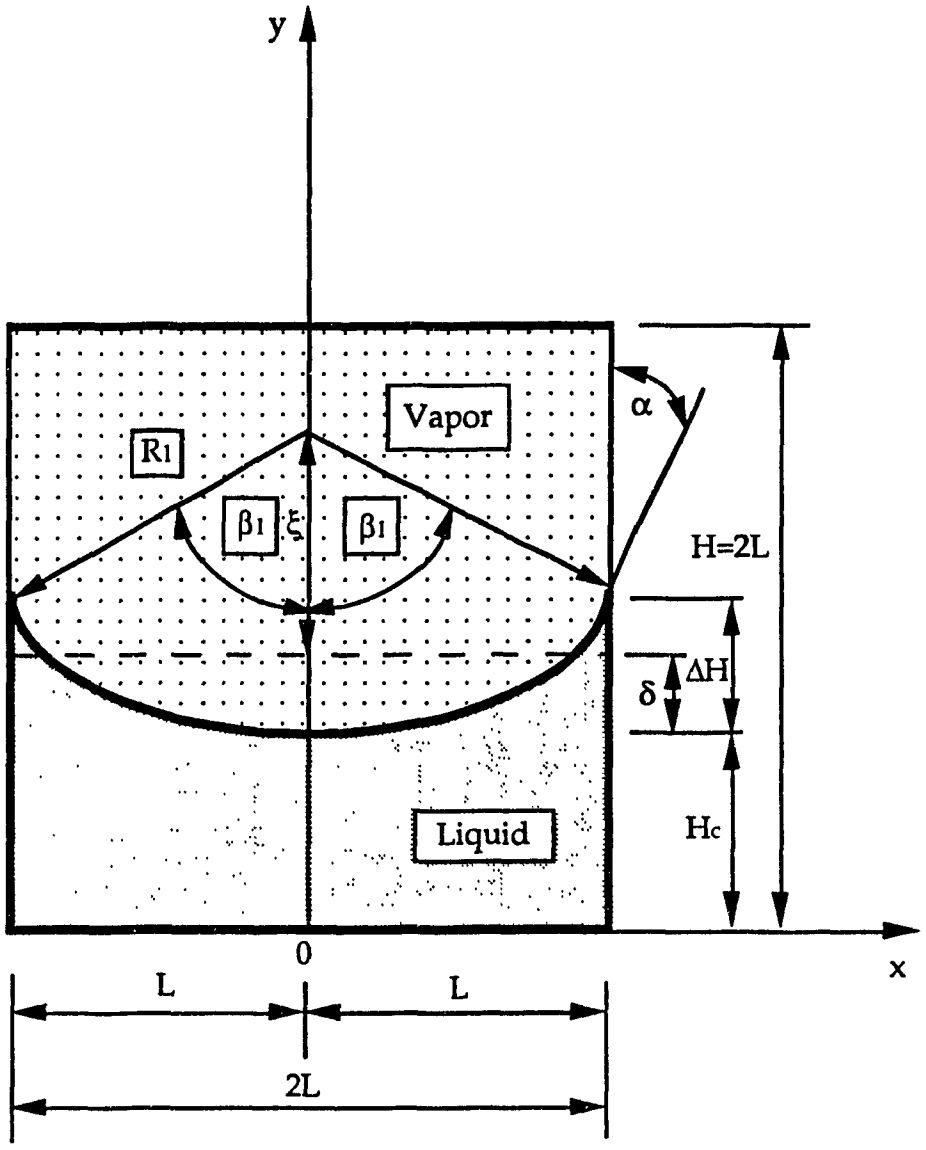

Fig.A.1 Configuration system 1 in a rectangular tank

$$\Delta H = R_1 - \xi = \frac{L\,(1 - \sin\alpha)}{\cos\alpha} \tag{A.1.7}$$

$$\Delta\overline{H} = \frac{1 - \sin\alpha}{\cos\alpha} \tag{A.1.8}$$

(B) Volume

For a unit thickness, the liquid volume V_{r1} is defined by

$$V_{r1} = V_{a1} + V_{b1} \tag{A.1.9}$$

where

$$V_{a1} = 2\,L\,H_c \tag{A.1.10}$$

$$\begin{aligned} V_{b1} &= 2L\,\Delta H - \beta_1 R_1^2 + L\xi \\ &= 2\,L\,\Delta H - \frac{\beta_1 L^2}{\cos^2\alpha} + L^2 \tan\alpha \\ &= 2\,L^2\left(\frac{1 - \sin\alpha}{\cos\alpha} - \frac{\beta_1}{\cos^2\alpha} + \frac{\tan\alpha}{2}\right) \end{aligned} \tag{A.1.11}$$

The liquid volume V_{r1} is

$$V_{r1} = 2\,L\,H_c + 2\,L^2\left(\frac{1 - \sin\alpha}{\cos\alpha} - \frac{\beta_1}{\cos^2\alpha} + \frac{\tan\alpha}{2}\right) \tag{A.1.12}$$

(C) Configuration Ratio of the System 1

The configuration ratio of the system 1 is as follows

$$\theta_{r1} = \frac{A_{r1}}{V_{r1}}$$

$$= \frac{2\,\beta_1 \frac{L}{\cos\alpha}}{2L\left\{H_c - L\left[\frac{1-\sin(\alpha)}{\cos(\alpha)} - \frac{\beta_1}{2\cos^2(\alpha)} + \frac{1}{2}\tan(\alpha)\right]\right\}}$$

$$= \frac{\beta_1}{\cos(\alpha)\left\{H_c + L\left[\frac{1-\sin(\alpha)}{\cos(\alpha)} - \frac{\beta_1}{2\cos^2(\alpha)} + \frac{1}{2}\tan(\alpha)\right]\right\}} \qquad \text{(A.1.13)}$$

The equation (A.1.13) is the same as the equation (2.3.3).

(D) Parameter δ

The liquid mass conservation shows

$$2L\,\delta = 2L\,\Delta H - \frac{\beta_1 L^2}{\cos^2\alpha} + L^2\tan\alpha \qquad \text{(A.1.14)}$$

rearrange the equation (A.1.14)

$$\delta = \delta_{rect} = \Delta H - \frac{\beta_1 L}{2\cos^2\alpha} + \frac{L}{2}\tan\alpha \qquad \text{(A.1.15)}$$

$$\bar{\delta}_{rect} = \frac{1}{2\cos^2(\alpha)}\left\{\cos(\alpha)\,[2-\sin(\alpha)] - \left(\frac{\pi}{2} - \alpha\right)\right\} \qquad \text{(A.1.15)}$$

A.2 Configuration System 2

(A) Area

From Fig.A.2, for a unit thickness in z-direction, the liquid-vapor interface area A_{r2} for left side part is defined by

$$A_{r2} = 2\,\beta_2\,R_2 \tag{A.2.1}$$

where

$$R_2 = \frac{\sqrt{2}}{2\sin\beta_2}\,X_r \tag{A.2.2}$$

$$\beta_2 = \left|\frac{\pi}{4} - \alpha\right| \tag{A.2.3}$$

$$X_2 = R_2 \sin\beta_2 \tag{A.2.4}$$

$$\zeta_2 = R_2 \cos\beta_2 \tag{A.2.5}$$

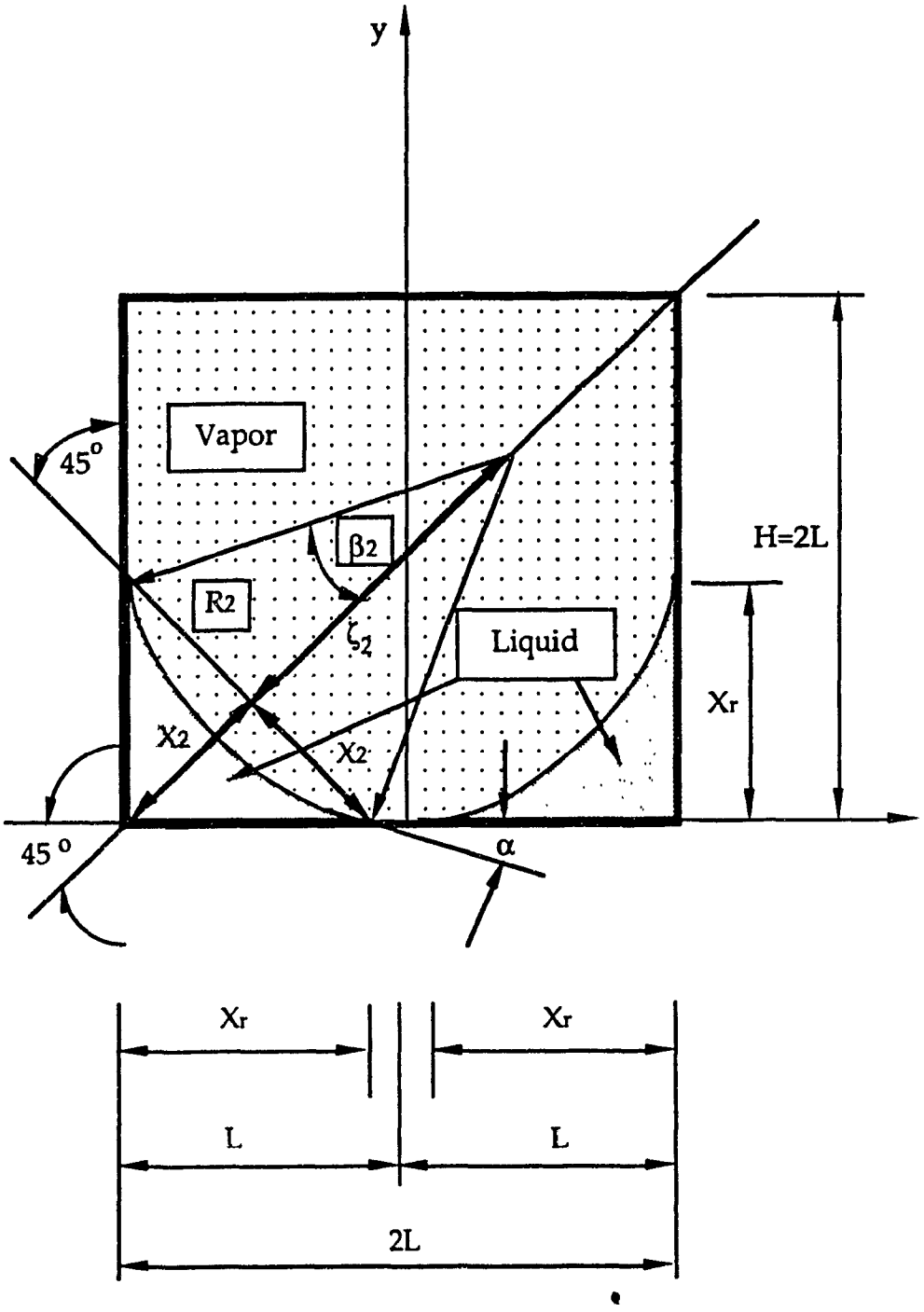

Fig.A.2 Configuration system 2 in a rectangular tank

(B) Volume

The liquid volume for left side part is calculated by

$$
\begin{aligned}
V_{r2} &= X_2^2 + X_2 \zeta_2 - \beta_2 R_2^2 \\
&= R_2^2 \sin^2\beta_2 + R_2^2 \sin\beta_2 \cos\beta_2 - \beta_2 R_2^2 \\
&= \frac{X_r^2}{2 \sin^2\beta_2}\left(\sin^2\beta_2 + \sin\beta_2 \cos\beta_2 - \beta_2\right)
\end{aligned}
\tag{A.2.6}
$$

(C) Configuration Ratio of the System 2

$$
\begin{aligned}
\theta_{r2} &= \frac{A_{r2}}{V_{r2}} \\
&= \frac{\dfrac{\beta_2 \sqrt{2}}{\sin\beta_2} X_r}{\dfrac{X_r^2}{2 \sin^2\beta_2}\left(\sin^2\beta_2 + \sin\beta_2 \cos\beta_2 - \beta_2\right)} \\
&= \frac{2\sqrt{2}\,\beta_2 \sin\beta_2}{X_r\left(\sin^2\beta_2 + \sin\beta_2 \cos\beta_2 - \beta_2\right)}
\end{aligned}
\tag{A.2.7}
$$

The equation (A.2.7) is the same form of the equation (2.3.9).

II. Calculations of Interface Configuration Ratio in a Cylindrical Tank

A.3 Configuration System 3

(A) Area

The schematic diagram is shown in Fig.A.3.1. The liquid-vapor interface area is calculated

$$A_{c3} = 2\pi R_3 \Delta H$$
$$= 2\pi L^2 \frac{(1 - \sin\alpha)}{\cos^2\alpha} \qquad \text{(A.3.1)}$$

(B) Volume

The liquid volume is

$$V_{c3} = V_{a3} + V_{d3} \qquad \text{(.A.3.2)}$$

where

$$V_{a3} = \pi L^2 \Delta H - V_{b3} \qquad \text{(A.3.3)}$$

The volume V_{b3} is calculated. The equation of the interface shown in Fig.A.3.2 is

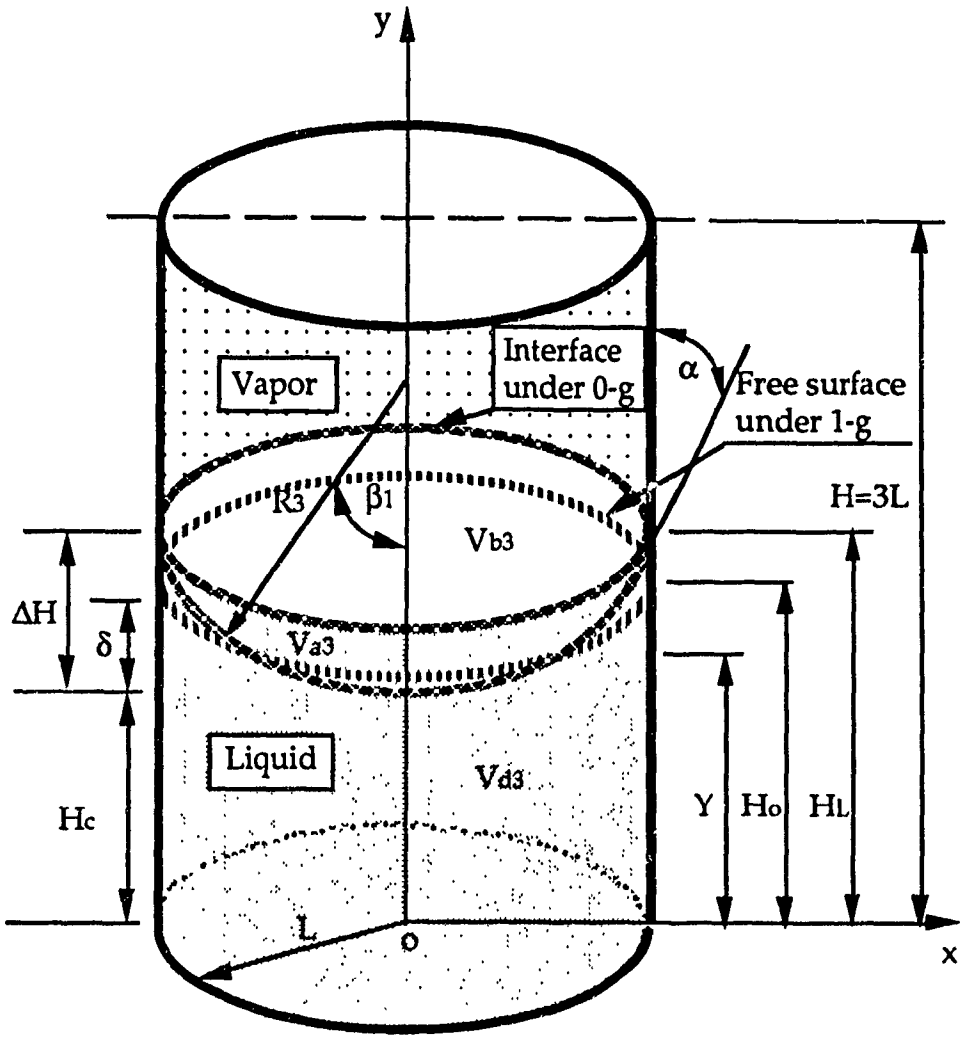

Fig.A.3.1 Configuration system 3 in a cylindrical tank

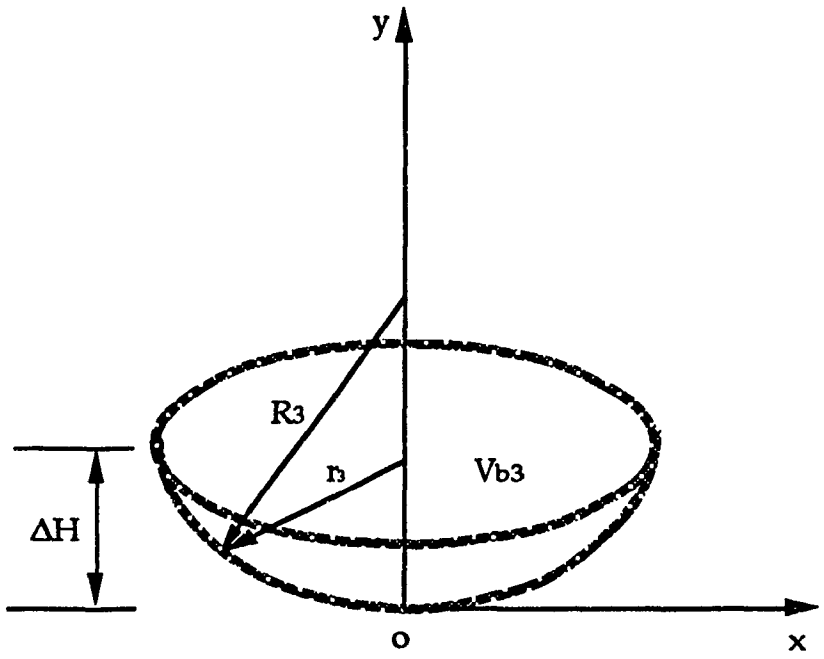

Fig.A.3.2 Calculation of the volume V_{b3}

$$R_3^2 = r_3^2 + (R_3 - y)^2 \tag{A.3.4}$$

or

$$r_3 = \sqrt{2 R_3 y - y^2} \tag{A.3.5}$$

$$\begin{aligned} V_{b3} &= \int_0^{2\pi} d\varnothing \int_0^{\sqrt{2R_3 y - y^2}} r_3 \, dr_3 \int_0^{\Delta h} dy \\ &= \pi \left(R_3 \Delta H^2 - \frac{1}{3} \Delta H^3 \right) \end{aligned} \tag{A.3.6}$$

or

$$V_{b3} = \frac{1}{6} \pi \Delta H \left(3 L^2 + \Delta H^2 \right) \tag{A.3.7}$$

$$V_{a3} = \frac{1}{6} \pi \Delta H \left(3 L^2 - \Delta H^2 \right) \tag{A.3.8}$$

$$V_{d3} = \pi L^2 H_c \tag{A.3.9}$$

$$\begin{aligned} V_{c3} &= V_{a3} + V_{d3} \\ &= \frac{1}{6} \pi \Delta H \left(3 L^2 - \Delta H^2 \right) + \pi L^2 H_c \\ &= \pi L^2 \left\{ \frac{L (1 - \sin \alpha)}{3 \cos \alpha} \left(\frac{2 \cos^2 \alpha - 1 + \sin \alpha}{\cos^2 \alpha} \right) + H_c \right\} \end{aligned} \tag{A.3.10}$$

(C) Configuration Ratio of the System 3

The configuration ratio for the system 3 is given

$$\theta_{c3} = \frac{A_{c3}}{V_{c3}}$$

$$= \frac{2\pi L^2 \frac{(1-\sin\alpha)}{\cos^2\alpha}}{\pi L^2 \left\{ \frac{L(1-\sin\alpha)}{3\cos\alpha} \left(\frac{2\cos^2\alpha - 1 + \sin\alpha}{\cos^2\alpha} \right) + H_c \right\}}$$

$$= \frac{2(1-\sin\alpha)}{\cos^2\alpha \left\{ \frac{L(1-\sin\alpha)}{3\cos\alpha} \left(\frac{2\cos^2\alpha - 1 + \sin\alpha}{\cos^2\alpha} \right) + H_c \right\}} \qquad \text{(A.3.11)}$$

The equation (A.3.11) is the same as the equation (2.5.1).

A.4 Configuration System 4

Configuration system 4 is shown in Fig.A.4.

(A) Area

The interface has the function as follows

$$(x + h_4)^2 + (y + r_4)^2 = R_4^2 \qquad \text{(A.4.1)}$$

since

$$h_4 = r_4 \qquad \text{(A.4.2)}$$

$$x = \sqrt{R_4^2 - (y + h_4)^2} - h_4 \qquad \text{(A.4.3)}$$

The surface area can be defined (where $X_c \rightarrow L$) by the following equation

$$A_{c4} = \int_0^L 2\pi f(y) \sqrt{1 + [f'(y)]^2}\, dy \qquad \text{(A.4.4)}$$

where

$$f(y) = x = \sqrt{R_4^2 - (y + h_4)^2} - h_4 \qquad \text{(A.4.5)}$$

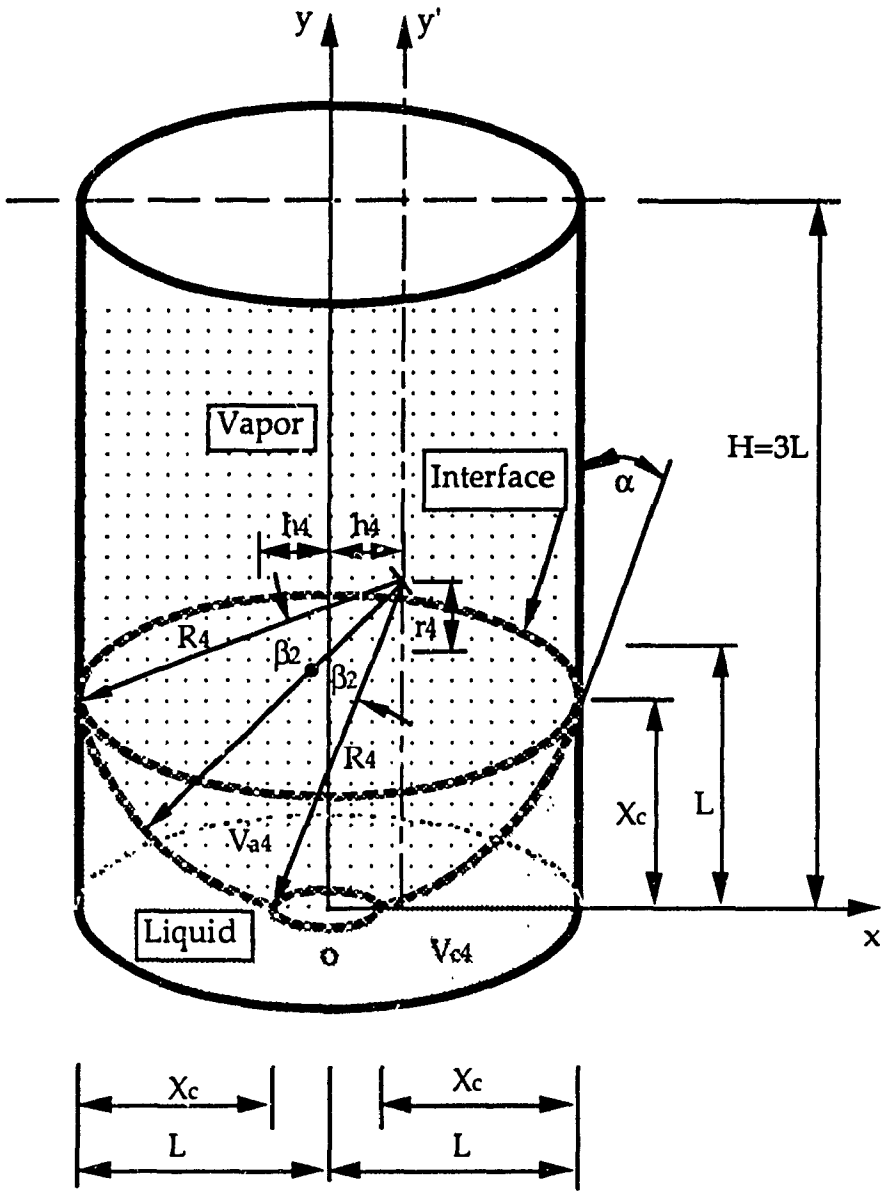

Fig.A.4 Configuration system 4 in a cylindrical tank

$$f'(y) = -\frac{h_4 + y}{\sqrt{R_4^2 - (h_4 + y)^2}} \tag{A.4.6}$$

$$1 + [f'(y)]^2 = \frac{R_4^2}{R_4^2 - (h_4 + y)^2} \tag{A.4.7}$$

$$f(y)\sqrt{1 + [f'(y)]^2} = R_4 \left\{ 1 - \frac{h_4}{R_4^2 - (h_4 + y)^2} \right\} \tag{A.4.8}$$

$$\begin{aligned} A_{c4} &= \int_0^L 2\pi f(y)\sqrt{1 + [f'(y)]^2}\, dy \\ &= 2\pi \int_0^L R_4 \left\{ 1 - \frac{h_4}{R_4^2 - (h_4 + y)^2} \right\} dy \\ &= 2\pi R_4 L - \int_0^L \frac{h_4}{R_4^2 - (h_4 + y)^2}\, dy \\ &= 2\pi R_4 L - h_4 \left[\sin^{-1}\left(\frac{h_4 + y}{R_4}\right) - \sin^{-1}\left(\frac{h_4}{R_4}\right) \right] \end{aligned} \tag{A.4.9}$$

since

$$\sin^{-1}\left(\frac{h_4 + y}{R_4}\right) = \frac{\pi}{2} - \alpha \tag{A.4.10}$$

$$\sin^{-1}\left(\frac{h_4}{R_4}\right) = \alpha \tag{A.4.11}$$

$$A_{c4} = 2\pi R_4 \left\{ L - h_4 \left(\frac{\pi}{2} - 2\alpha \right) \right\} \tag{A.4.12}$$

(B) Volume

The liquid volume is

$$V_{c4} = V_{b4} - V_{a4} \tag{A.4.13}$$

where

$$V_{b4} = \pi L^2 L = \pi L^3 \tag{A.4.14}$$

and

$$V_{a4} = \int_0^L S(y)\, dy \tag{A.4.15}$$

$$S(y) = \pi x^2 \tag{A.4.16}$$

$$x = \sqrt{R_4^2 - (y + h_4)^2} - h_4 \tag{A.4.17}$$

$$\begin{aligned} V_{a4} &= \int_0^L \pi x^2\, dy \\ &= \pi \int_0^L \left[\sqrt{R_4^2 - (y + h_4)^2} - h_4\right]^2 dy \\ &= \pi \left(R_4^2 L - h_4 L^2 - \frac{1}{3} L^3\right) - 2\pi h_4 \int_0^L \sqrt{R_4^2 - (y + h_4)^2}\, dy \end{aligned} \tag{A.4.18}$$

where

$$\int_0^L \sqrt{R_4^2 - (y + h_4)^2}\, dy = \frac{1}{2}\left[(h_4 + y)\sqrt{R_4^2 - (y + h_4)^2} + R_4^2 \sin^{-1}\left(\frac{h_4 + y}{R_4}\right)\right]_0^L$$

$$= \frac{1}{2}\left[(h_4 + L)\sqrt{R_4^2 - (L + h_4)^2} + R_4^2 \sin^{-1}\left(\frac{h_4 + L}{R_4}\right)\right]$$

$$- \left[(h_4)\sqrt{R_4^2 - h_4^2} + R_4^2 \sin^{-1}\left(\frac{h_4}{R_4}\right)\right] \qquad \text{(A.4.19)}$$

since

$$\sqrt{R_4^2 - (L + h_4)^2} = h_4 \qquad \text{(A.4.20)}$$

$$\sqrt{R_4^2 - h_4^2} = L + h_4 \qquad \text{(A.4.21)}$$

$$\sin^{-1}\left(\frac{h_4 + y}{R_4}\right) = \frac{\pi}{2} - \alpha \qquad \text{(A.4.22)}$$

$$\sin^{-1}\left(\frac{h_4}{R_4}\right) = \alpha \qquad \text{(A.4.23)}$$

Therefore

$$V_{a4} = \pi\left(R_4^2 L - h_1 L^2 - \frac{1}{3} L^3 - h_4 R_4^2\left(\frac{\pi}{2} - 2\alpha\right)\right) \qquad \text{(A.4.24)}$$

$$V_{c4} = V_{b4} - V_{a4}$$

$$= \pi L^3 - \pi\left(R_4^2 L - h_1 L^2 - \frac{1}{3} L^3 - h_4 R_4^2\left(\frac{\pi}{2} - 2\alpha\right)\right)$$

$$= \pi\left(\frac{4}{3} L^3 - R_4^2 L + h_4 L^2 + h_4 R_4^2\left(\frac{\pi}{2} - 2\alpha\right)\right) \qquad \text{(A.4.25)}$$

(C) Configuration Ratio of the System 4

$$\theta_{c4} = \frac{A_{c4}}{V_{c4}}$$

$$= \frac{2\,\pi\,R_4\left\{L - h_4\left(\frac{\pi}{2} - 2\,\alpha\right)\right\}}{\pi\left\{\frac{4}{3}L^3 - R_4^2\,L + h_4\,L^2 + h_4\,R_4^2\left(\frac{\pi}{2} - 2\,\alpha\right)\right\}}$$

$$= \frac{2\,R_4\left\{L - h_4\left(\frac{\pi}{2} - 2\,\alpha\right)\right\}}{\frac{4}{3}L^3 + h_4\,L^2 - R_4^2\left\{L - h_4\left(\frac{\pi}{2} - 2\,\alpha\right)\right\}} \qquad \text{(A.4.26)}$$

The equation (2.5.5) is obtained by substituting $\beta_3 = \frac{\pi}{2} - 2\,\alpha$ into the equation (A.4.26).